Report No. 2469 NASA CR-112216

EXCITATION, RESPONSE, AND FATIGUE LIFE ESTIMATION METHODS FOR THE STRUCTURAL DESIGN OF EXTERNALLY BLOWN FLAPS

Eric E. Ungar
K. L. Chandiramani
J. E. Barger

October 1972

Contract No. NAS1-9559-67

Submitted to:

National Aeronautics and Space Administration
Langley Research Center
Mail Stop 139
Langley Station
Hampton, Virginia 23365

ABSTRACT

Means for predicting the fluctuating pressures acting on externally blown flap surfaces are developed on the basis of generalizations derived from non-dimensionalized empirical data. Approaches for estimation of the fatigue lives of skin-stringer and honeycomb-core sandwich flap structures are derived from vibration response analyses and panel fatigue data. Approximate expressions for fluctuating pressures, structural response, and fatigue life are combined to reveal the important parametric dependences.

The two-dimensional equations of motion of multi-element flap systems are derived in general form, so that they can be specialized readily for any particular system. An introduction is presented of an approach to characterizing the excitation pressures and structural responses which makes use of space-time spectral density concepts and promises to provide useful insights, as well as experimental and analytical savings.

TABLE OF CONTENTS

Mostaccio

EXCITATION, RESPONSE, AND FATIGUE LIFE ESTIMATION METHODS FOR THE STRUCTURAL DESIGN OF EXTERNALLY BLOWN FLAPS

INTRODUCTION

Short take-off and landing (STOL) aircraft concepts have been attracting much attention in the past several years, because of their potential operational advantages over more conventional aircraft. Of the several STOL configurations that have been given very serious consideration, those incorporating "externally blown" flaps (e.g., see Fig. 1) have recently found increasing favor, and EBF aircraft technology currently is the subject of extensive study and evaluation.

Because the flaps of EBF aircraft are exposed to the direct impingement of the engine exhaust streams, as well as to the intense noise field that exists near the engines, the effects of the associated fluctuating pressures must be taken into account in the design of the flap structures. These effects are primarily of two kinds: (1) "sonic" fatigue of the flap airfoil structures, and (2) severe overall vibrations of the flap elements, with the associated high oscillatory loads in the structures (and actuators) that interconnect and support the flap elements. The present report is intended to provide some preliminary analytical approaches to assessing these effects, to revealing the important parameters, and to suggesting improved approaches.

The Sonic Fatigue Problem

The complex problems of sonic fatigue life prediction and corresponding structural design fortunately may be simplified by considering them in terms of a sequence of sub-problems. These sub-problems consist of: (1) characterization of the fluctuating pressure excitation, (2) determination of the structural responses to this excitation, (3) evaluation of the most significant associated oscillatory stresses, and (4) estimation of the corresponding fatigue life.

FLUCTUATING PRESSURES ON EBF SURFACES

Jet Configuration

At several core-nozzle diameters aft of the nozzle exit plane, the flow field produced by fan-jet engines appears to be dominated by that due to the core jet (see Appendix A). It is reasonable therefore to estimate the fluctuating pressures produced by the exhaust from a fan-jet engine on the basis of the pressures associated with the core jet, and to make use of the extensive information available concerning ideal circular jets.

The configuration of an ideal circular jet is sketched in Fig. 2. This shows a converging conical "potential flow region", surrounded by a diverging concial "mixing region". The total angle 2α subtended by the jet boundary typically is between 25 and 30 degrees (Ref. 3). The length of the potential core is given (Ref. 2) by

$$X_c = 3.45\ D(1 + 0.38\ M)^2\ , \qquad (1)$$

where D denotes the diameter of the (engine core) nozzle and M represents the Mach number of the exhaust stream.

Velocity Fluctuations in Jets

For estimation purposes it is also convenient to assume that the velocity fluctuations that are present in the jet in absence of an inserted flap are not altered substantially in the presence of the flap, and one may then interpret available velocity fluctuation data in terms of the pressure fluctuation information one requires. Figure 3 indicates how the axial turbulence intensity

$$I = \sqrt{u^2}/U_o \qquad (2)$$

Characterization of the fluctuating pressures on EBF surfaces for design and estimation purposes is summarized in the first of the following sections and is discussed in some detail in Appendix A. The next of the major sections of this report deals with estimation of structural responses, of the associated stresses, and of the fatigue life of EBF structures (based on previously published information and on extensions of previously employed approaches), both for skin-stringer and for honeycomb-core sandwich structures. The assumptions underlying these estimations, and their limitations, are also pointed out in these sections; a general,potentially extremely useful, approach toward characterizing the excitations and estimating responses is described in Appendix D.

The Buffeting Problem

This problem, which tends to be most significant at frequencies that are substantially lower than those of primary importance for sonic fatigue, also may be considered in terms of a sequence of sub-problems, namely: (1) characterization of the excitation, (2) determination of the associated vibratory responses, (3) evaluation of the most significant deflections and substructural loads, and (4) evaluation of these oscillations, deflections, and loads in terms of ride quality and substructural design requirements.

In contrast to the treatment of the sonic fatigue problem, this report deals with the buffeting problem in only a very preliminary manner. The final major section of this report presents the two-dimensional equations of motion of a general EBF system, in which the airfoil components are considered as rigid bodies interconnected by linear springs. These equations display the important parameters and provide a basis for carrying out natural-frequency and response calculations for specific EBF designs.

FATIGUE LIFE OF SKIN-STRINGER STRUCTURES

Overview of Estimation Approach

Conventional aircraft structures consist of skins, reinforced by stringers, frames, and bulkheads (Fig. 7). Fluctuating pressures acting on the skins tend to induce complex vibratory deflections in the entire assembly, resulting in associated stresses, which – in turn – lead to structural fatigue.

Because of the complexities of the excitations and responses, currently available "sonic fatigue" design methods* are based on analyses developed on the basis of simplifying assumptions, coupled with empirically derived relations. These analyses in essence focus on one bay (i.e., one skin panel) at a time, ignore the complex spatial and temporal distribution of the exciting pressure by assuming the pressure always to be completely in phase over the entire panel, and compute the mean-square displacement response of the panel (mode by mode) to this spatially uniform, but time-wise random, pressure. They then calculate the maximum stresses from the panel modal displacements, and finally relate these calculated stresses to experimentally measured stresses and fatigue data.

The panel boundary conditions clearly play an important role; they not only affect the natural frequencies of the panel (which determine the parts of the excitation spectrum that dominate the response), but also the mode-shapes and therefore the relation between modal deflection and stress. Thus, previous investigators have expended considerable effort on methods for predicting the natural frequencies.

In dealing with the panel responses and stresses, the reinforcing structures (i.e., stringers and frames) are considered essentially only as boundary conditions. They are in effect assumed to deflect very little – an assumption that is likely to

---

*Although these methods were developed to cope with the problem of fatigue induced by acoustic excitation, they may be expected also to be applicable (at least approximately) in many other cases of fluctuating-pressure excitation, including generally that due to impinging jets and tangential flows. In all cases, of course, the quality of the estimate depends on how well the actual situation matches the various underlying assumptions.

In view of Eqs. (7) and (17), then,

$$L_S = L_{OA} + 10 \log \frac{2T_f \cdot Hz}{1 + T_f^2 \omega^2} . \qquad (22)$$

Making use of Eq. (8), one may find the peak spectrum level, corresponding to Φ_{max}, to be given by

$$L_{s,peak} = L_{OA} + 10 \log \left(\frac{X}{X_{ref}}\right) - 10 \log \left(\frac{U_o}{U_{ref}}\right) + C_1 \qquad (23)$$

with

$$C_1 = 10 \log \left(\frac{0.2\ X_{ref} \cdot Hz}{U_{ref}}\right) \approx - 25.7 \text{ dB} , \qquad (24)$$

where X_{ref} represents a reference axial distance. To arrive at the above numerical value for C_1, X_{ref} was taken as 10 ft, and the previously cited value of U_{ref} = 750 ft/sec was used. By combining Eqs.(20), (23), and (24) one finds

$$L_{s,peak} \approx 152 + 30 \log \left(\frac{U_o}{U_{ref}}\right) + 10 \log \left(\frac{X}{X_{ref}}\right) - 20 \log \frac{T_o + 460}{520} \qquad (25)$$

One similarly finds that the high-frequency spectrum level, corresponding to the high-frequency approximation $\Phi_{hi\ freq}(f)$ of Eq. (16), is given by

$$L_{s,hi\ freq} = L_{OA} + 10 \log \left(\frac{U_o}{U_{ref}}\right) - 10 \log \left(\frac{X}{X_{ref}}\right) - 20 \log \left(\frac{f}{f_{ref}}\right) + C_2 , \qquad (26)$$

where

$$C_2 = 10 \log \left(\frac{U_{ref} \cdot Hz}{0.2\pi^2\ X_{ref} f_{ref}^2}\right) \approx - 24 \text{ dB} \qquad (27)$$

With this value of I, Eqs. (5) and (6) reduce to

$$\overline{p^2} = (0.24\ \rho_o U_o^2)^2; \tag{13}$$

this then may be used to estimate the pressures on surfaces on which a jet impinges normally.

From Figs. 5 and 6 one may similarly deduce that for surfaces on which jets impinge more nearly tangentially, $\sqrt{\overline{p^2}}/q \leq 0.12$, so that for conservative estimation purposes one may take

$$\overline{p^2} = (0.12\ q)^2 = (0.06\ \rho_o U_o^2)^2 \ . \tag{14}$$

Clearly, the assumption of normal incidence leads to mean-square pressures that are higher by a factor of 16 than the pressures one obtains for more tangential incidence, and structures that can withstand the normal incidence pressures for a given period may be expected in general to survive the tangential incidence pressures for a longer period.

Pressure spectrum (spectral density). — The frequency spectral density $\Phi_p(\omega)$ of the fluctuating pressures, for both the normal and tangential incidence cases, as has been stated, is given by Eqs. (7) and (8). The maximum value of the spectral density, which value is obtained for $T_f\omega << 1$, obeys

$$\Phi_{max}(f) = 2\overline{p^2}T_f = \frac{0.2X}{U_o}\,\overline{p^2} \approx 0.0115\ X\rho_o^2 U_o^3 \ , \tag{15}$$

where the last expression has been obtained by substitution of Eq. (13).

For high frequencies, on the other hand, — that is, for $T_f\omega >> 1$, — Eqs. (7), (8), and (13) yield

$$\Phi_{hi\ freq}(f) \approx \frac{\overline{p^2}}{2\pi^2 T_f f^2} = \frac{U_o\overline{p^2}}{0.2\pi^2 X f^2} = 0.029\ \frac{\rho_o^2 U_o^5}{Xf^2} \tag{16}$$

where $f = \omega/2\pi$ denotes the cyclic frequency.

$$q = \frac{1}{2} \rho_o U_o^2 \approx \frac{1}{2} \rho U^2 \tag{6}$$

represents the dynamic pressure at the exit.

The frequency-spectral density $\Phi_p(\omega)$ of the fluctuating pressure is shown in Appendix A to be of the same form as that of the fluctuating velocity component, and to obey*

$$\Phi_p(\omega) = \frac{1}{2\pi} \Phi_p(f) \approx \overline{p^2} \frac{T_f/\pi}{1 + T_f^2 \omega^2} \tag{7}$$

where T_f represents a typical time scale (or inverse frequency) of the pressure or velocity fluctuations and obeys

$$T_f \approx 0.1 \, X/U_o \, , \tag{8}$$

and where ω denotes the radian frequency.

From Appendix A one also finds that the pressure cross-correlation function $\phi_{p_1 p_2}(s,\tau)$ for two points on the flap surface near the jet axis, separated by a distance s, obeys

$$\phi_{p_1 p_2}(s,\tau) = \overline{p^2} \, e^{-s/L} \, e^{-|\tau|/T_f} \tag{9}$$

where L denotes a length scale, called the correlation length, and is given by

$$L \approx 0.025 \, X \, . \tag{10}$$

Near-Tangentially Impinging Jets. – For flap surfaces along which the engine exhaust flows essentially tangentially, the assumption of momentum flux annihilation would tend to overestimate the mean-square fluctuating pressure. From Figs. 5 and 6,

*The spectral density $\Phi_p(\omega)$ represents the mean-square pressure per rad/sec, whereas the spectral density $\Phi_p(f)$, expressed in cyclic rather than radian frequency, represents the mean-square pressure per Hertz.

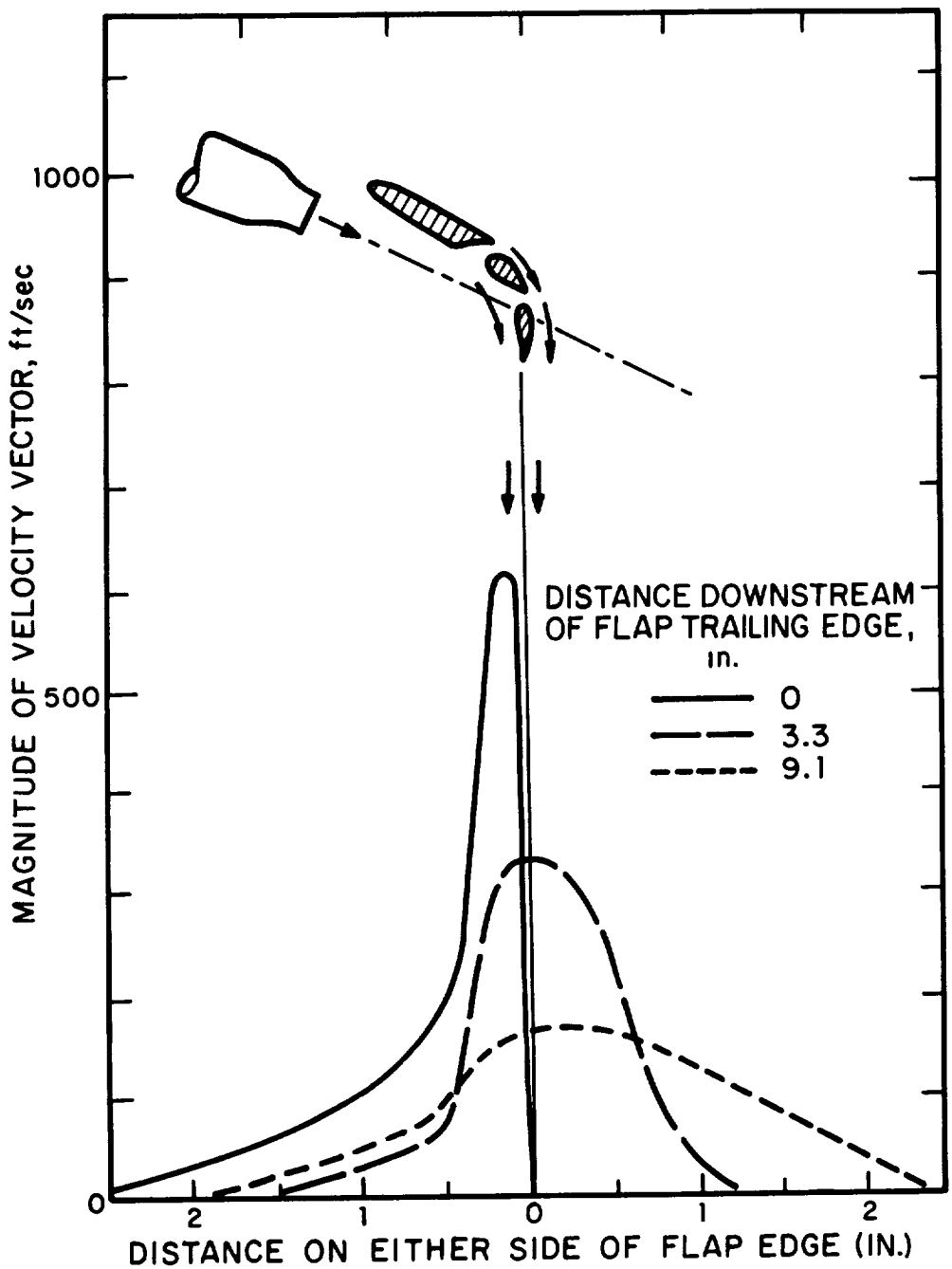

FIG. 17 FLOW FIELD FOR 30°-60° FLAP OF BASIC CONFIGURATION (REF. 31), FOR 625 ft/sec NOZZLE EXHAUST VELOCITY, 1.25 PRESSURE RATIO.

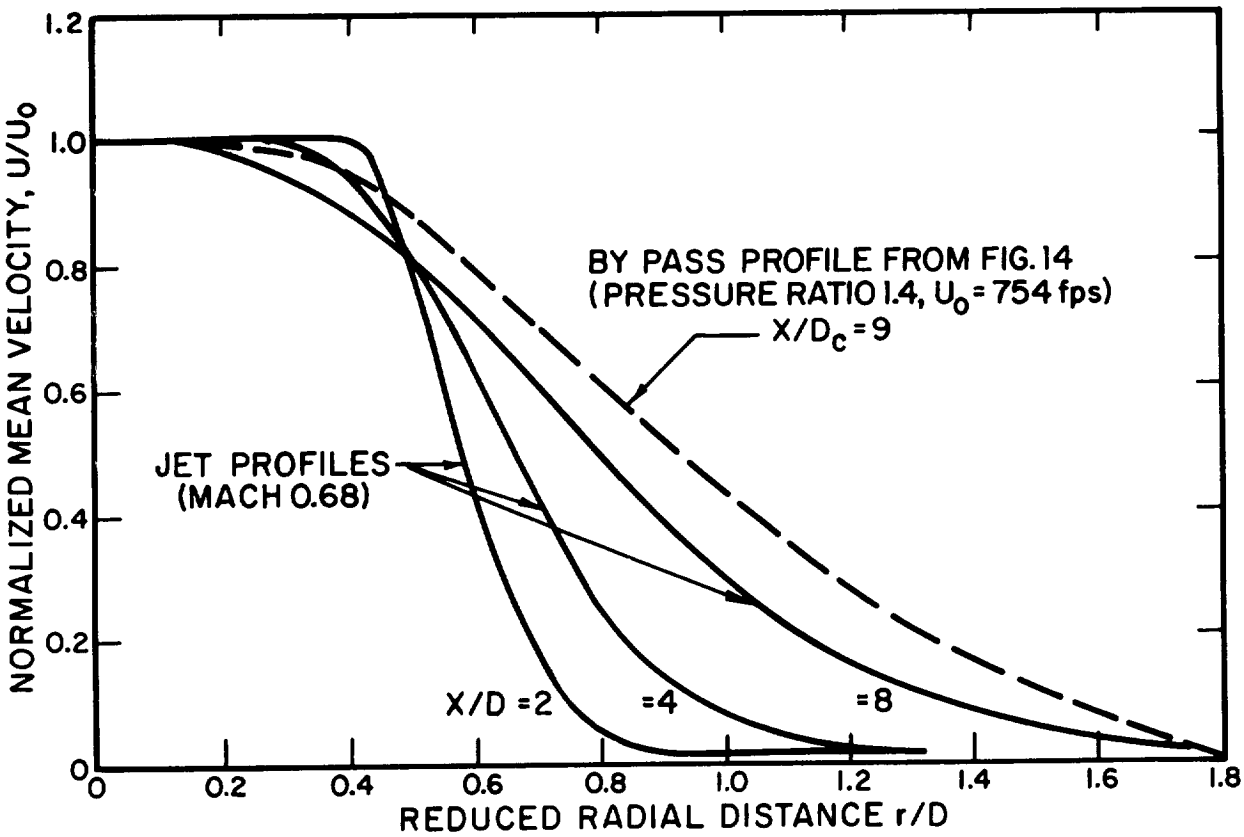

FIG. 15 JET VELOCITY PROFILES (FROM REF. 27), COMPARED WITH BYPASS NOZZLE EXHAUST PROFILE.

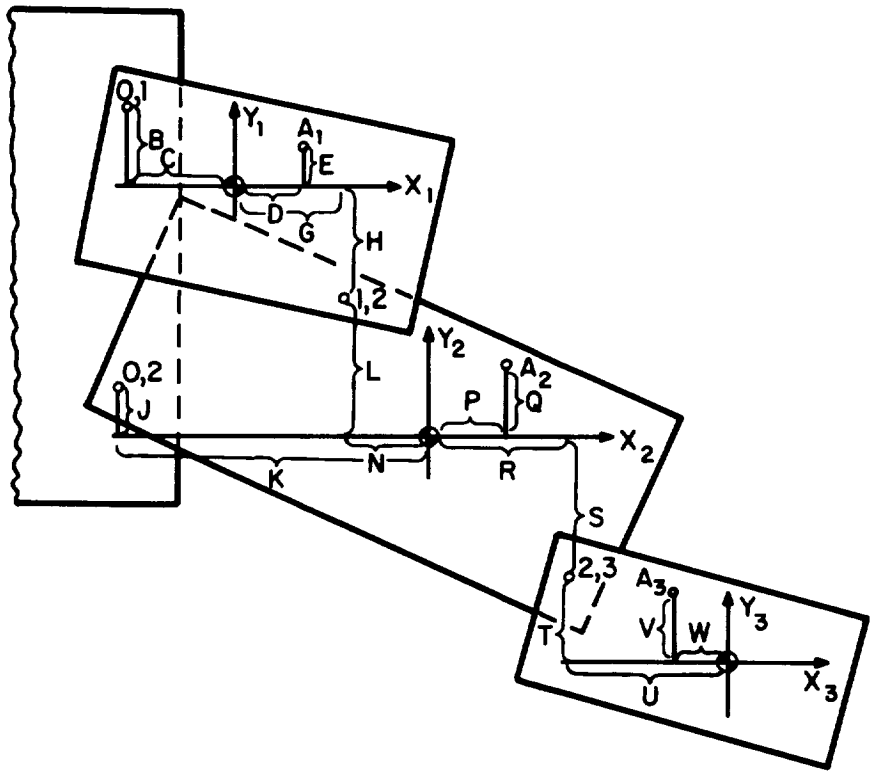

FIG. 13 ILLUSTRATIVE IDEALIZED FLAP SYSTEM.

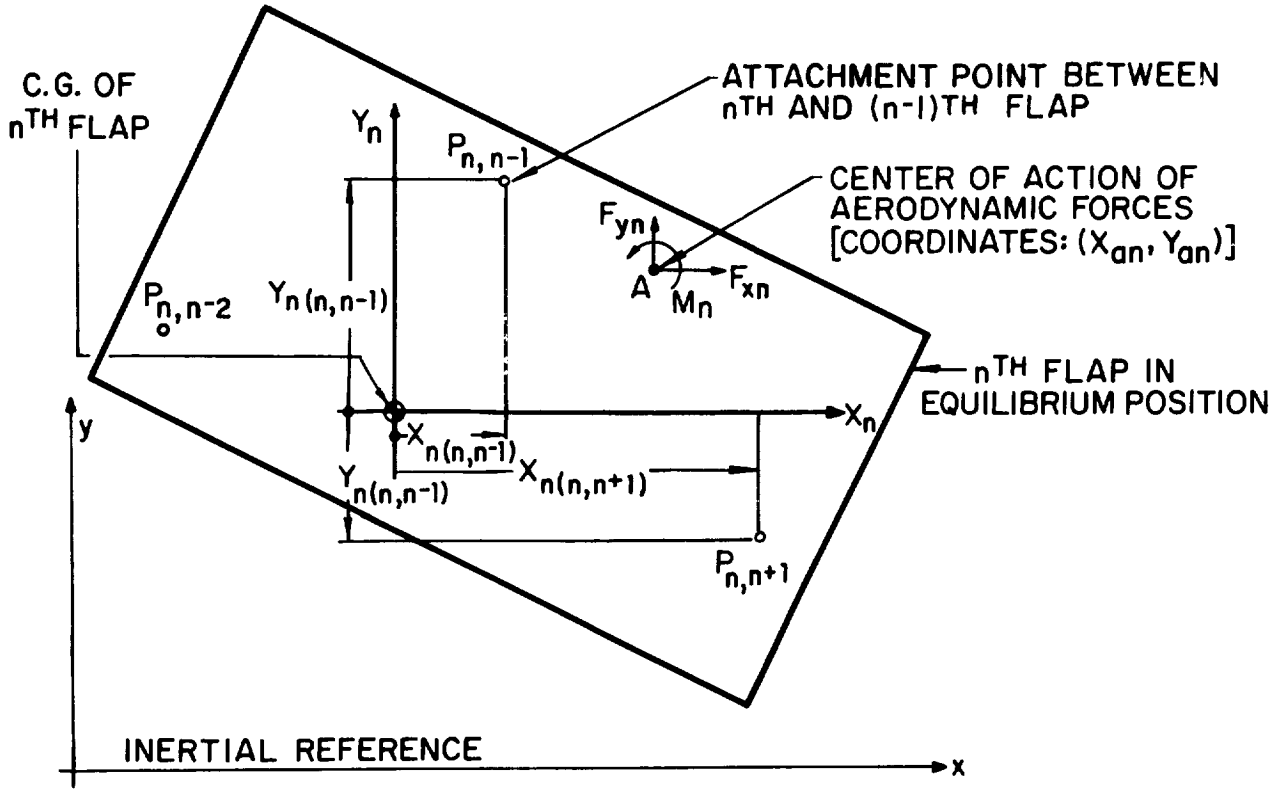

FIG. 11 COORDINATED SYSTEM ATTACHED TO TYPICAL FLAP ELEMENT, INDICATING LOCATIONS OF INTERCONNECTION AND AERODYNAMIC FORCE APPLICATION POINTS.

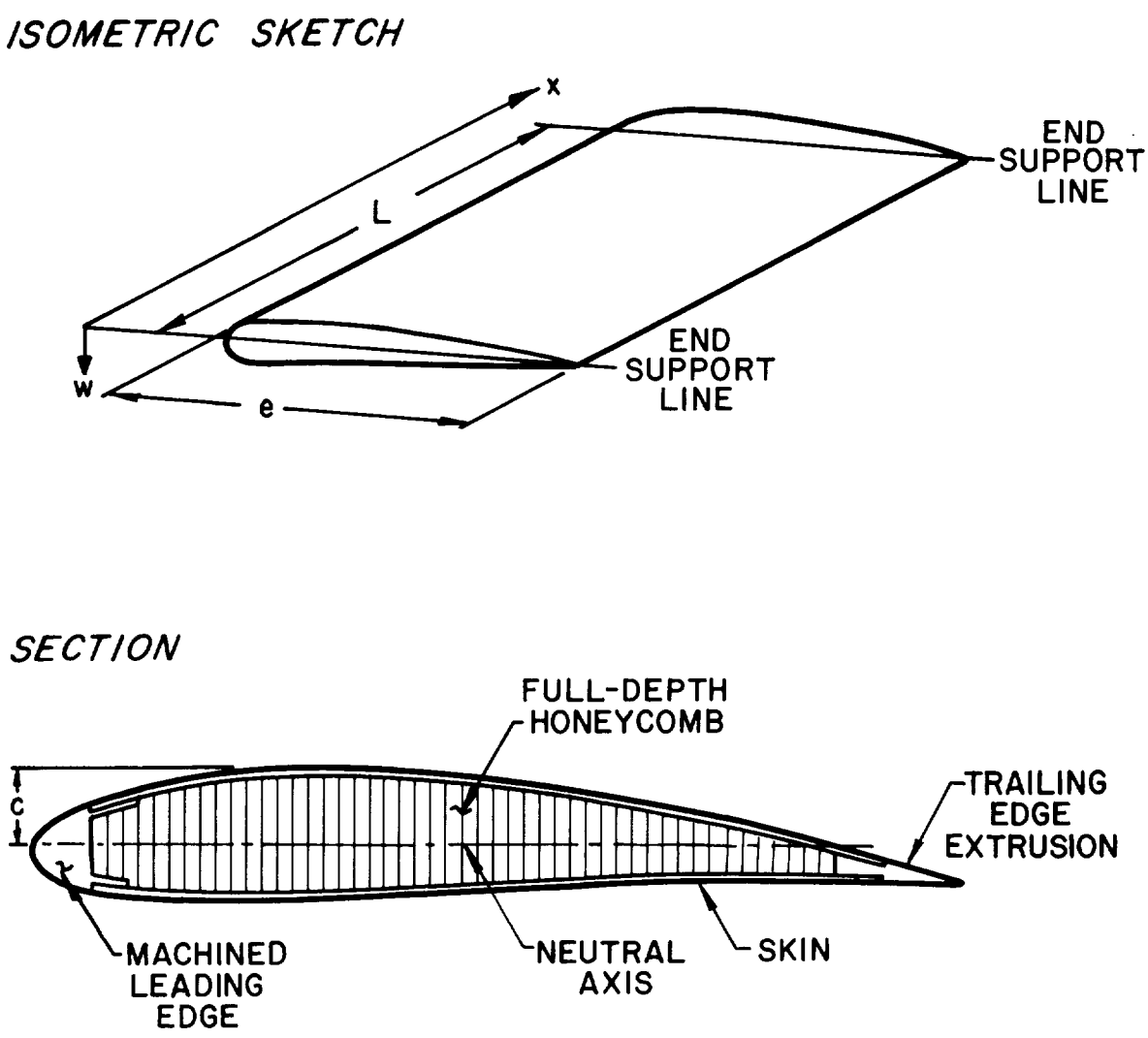

FIG. 9 TYPICAL HONEYCOMB-CORE SANDWICH FLAP ELEMENT.

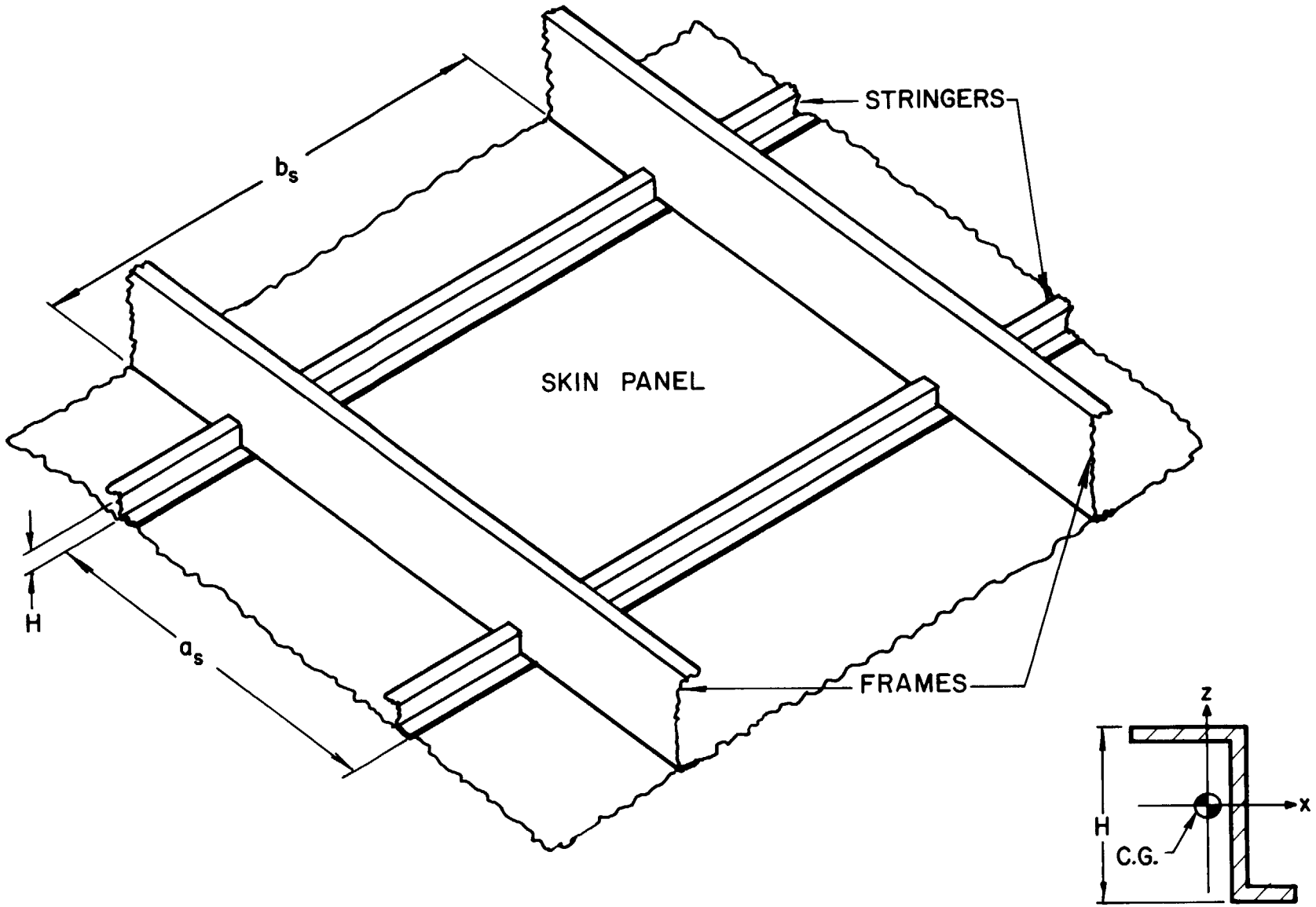

FIG. 7 TYPICAL BAY OF SKIN-STRINGER STRUCTURE, AND TYPICAL STRINGER CROSS-SECTION.

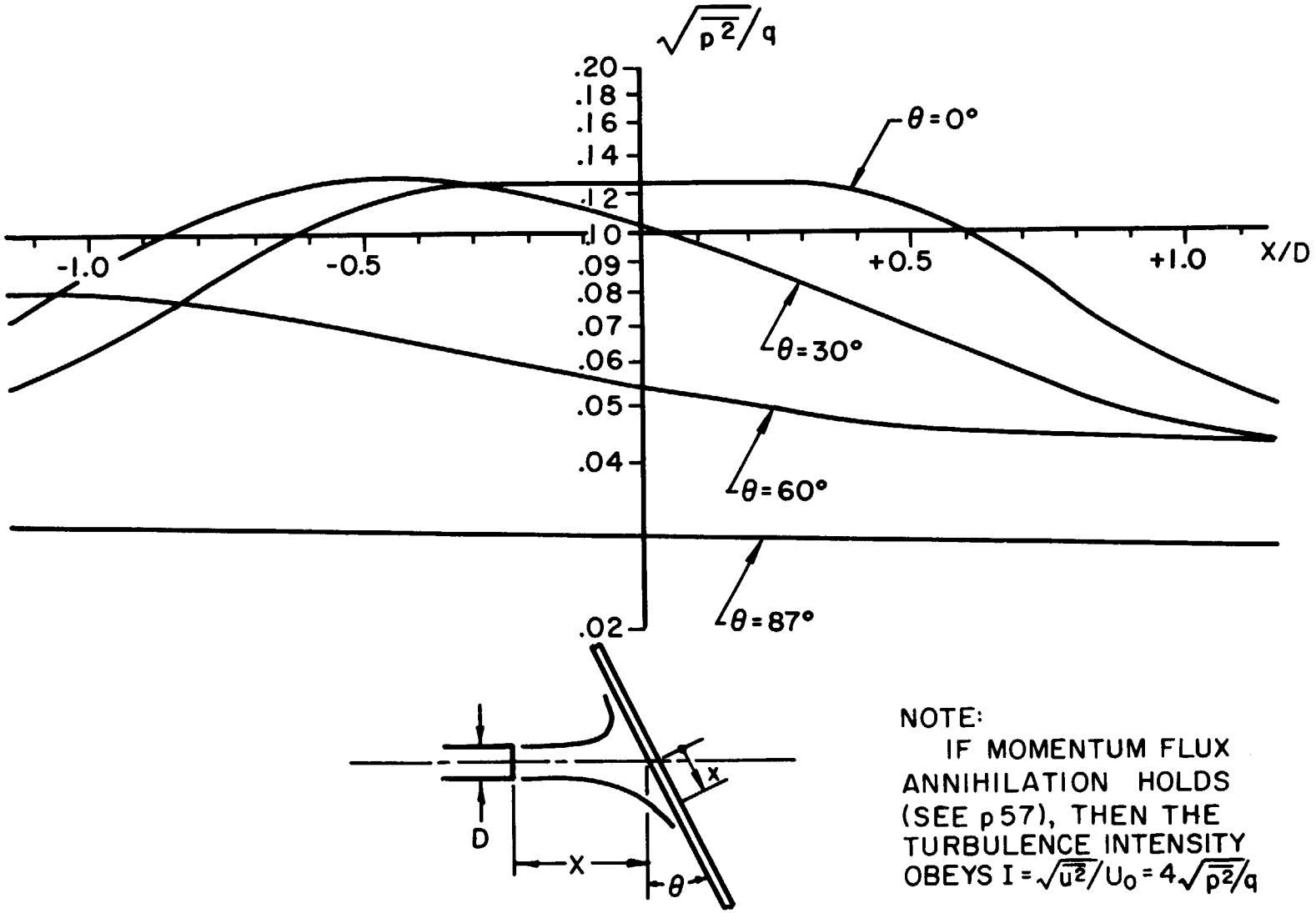

FIG. 5. VARIATION OF SURFACE PRESSURE FLUCTUATION ON A FLAT PLATE DUE TO JET IMPINGEMENT WITH LOCATION, AT X/D = 7 AND SEVERAL ANGLES OF INCLINATION (FROM REF. 5).

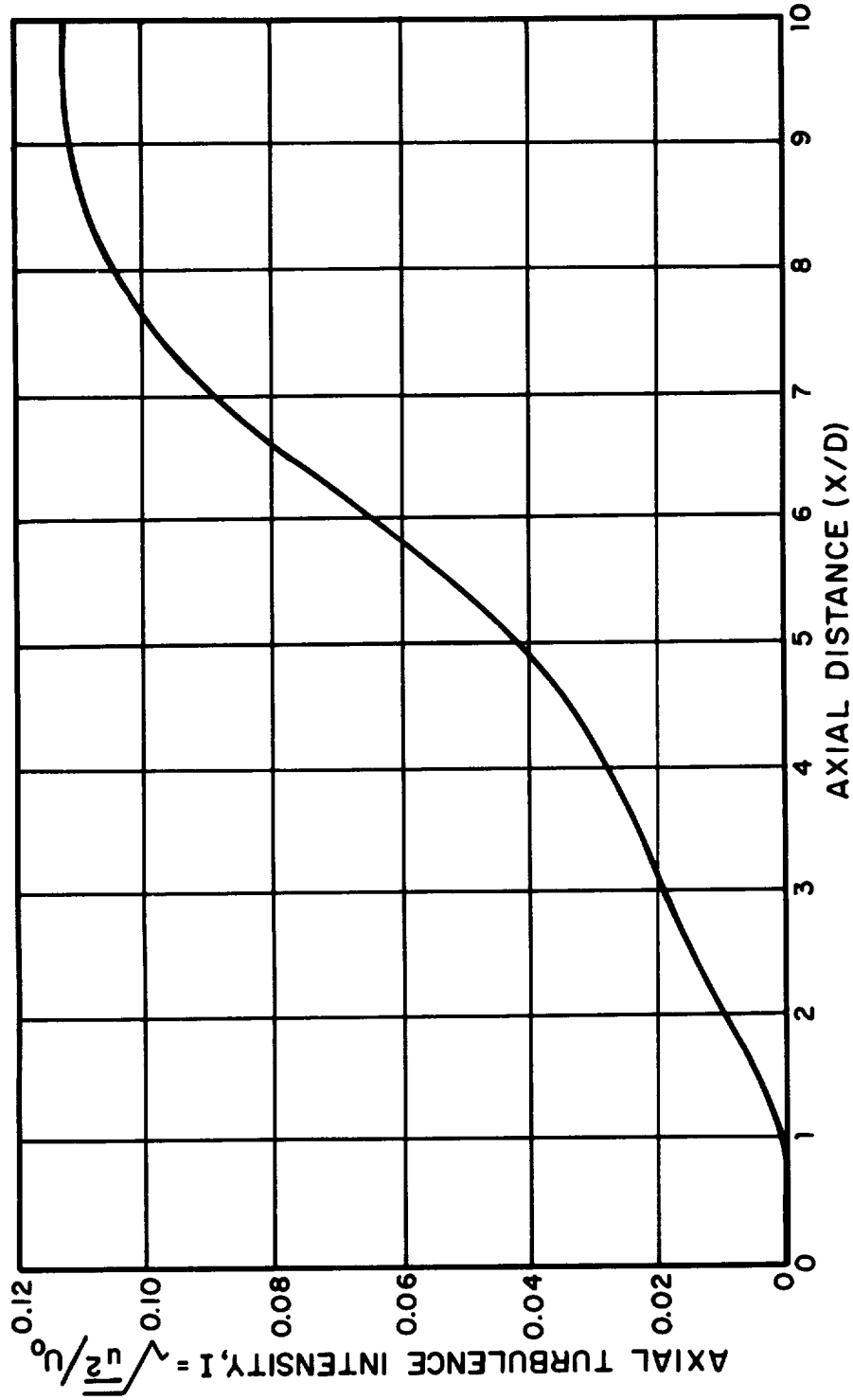

FIG. 3. VARIATION OF AXIAL TURBULENCE INTENSITY ALONG JET AXIS (FROM REF. 4).

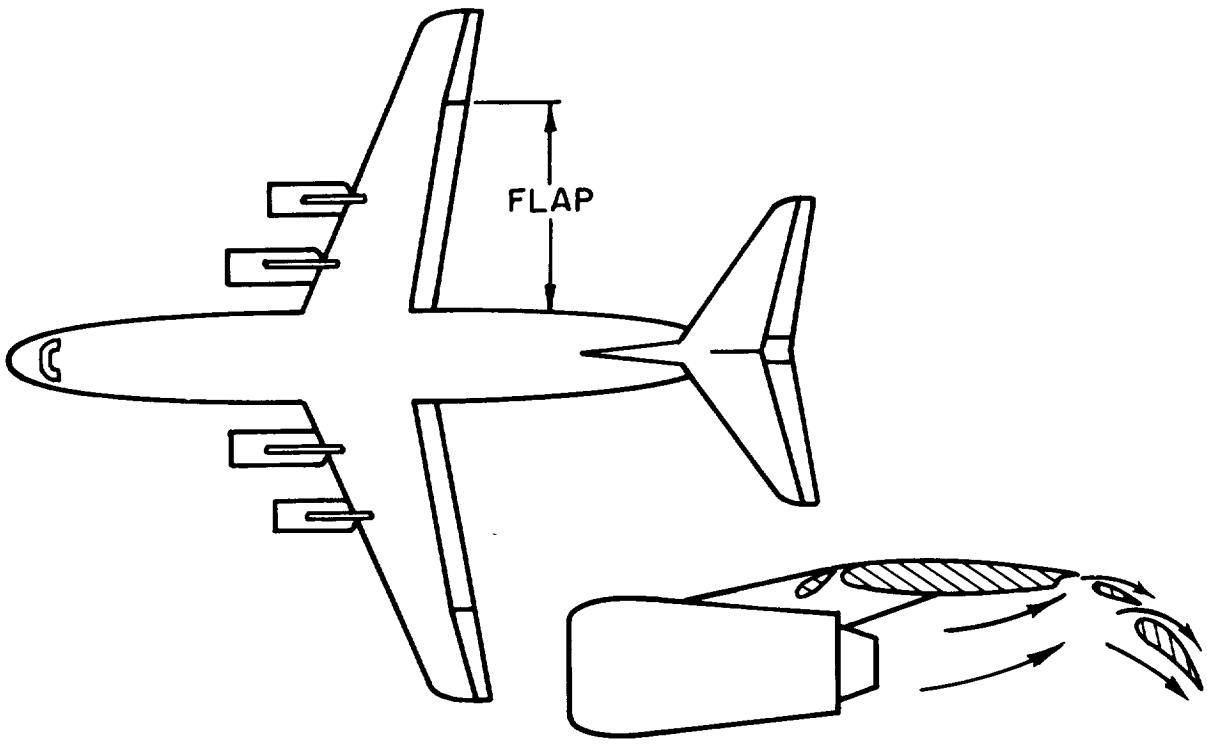

FIG. 1. EXTERNALLY-BLOWN-FLAP STOL AIRPLANE (FROM REF. 1).

TABLE I. — FACTORS BY WHICH PANEL FATIGUE LIFE CHANGES FOR GIVEN CHANGES IN PARAMETERS

Factor Change in Parameter	0.50	0.80	0.90	1.10	1.20	1.50	2.00
h	5.3×10^{-3}	.096	0.33	2.7	6.8	71.	1.45×10^{3}
a	3.6×10^{3}	14.	3.4	0.32	0.12	8.3×10^{-3}	2.8×10^{-4}
c_L	0.40	0.75	0.87	1.13	1.27	1.69	2.5
n, X	0.20	0.60	0.78	1.25	1.52	2.5	4.9
ρ_o	24.	2.8	1.6	0.65	0.43	0.155	0.041
U_o	2.9×10^{3}	13.	3.4	0.33	0.125	9.4×10^{-3}	3.3×10^{-4}

TABLE II. — FACTORS BY WHICH STRINGER FATIGUE LIFE CHANGES FOR GIVEN CHANGES IN PARAMETERS

Factor Change in Parameter	0.50	0.80	0.90	1.10	1.20	1.50	2.00
a	0.53	0.82	0.91	1.09	1.18	1.44	1.87
b	2.14	1.28	1.12	0.90	0.82	0.64	0.47
I/H	0.68	0.88	0.94	1.05	1.10	1.25	1.46
h, c_L	1.65	1.18	1.08	0.93	0.88	0.75	0.61
n, X	0.83	0.94	0.97	1.03	1.05	1.12	1.20
ρ_o	1.46	1.13	1.06	0.95	0.91	0.80	0.69
U_o	2.58	1.36	1.15	0.88	0.78	0.57	0.39

13. B.L. Clarkson and R.D. Ford, "The Response of Typical Aircraft Structure to Jet Noise," *J. Royal Aeronautical Soc.*, 66, pp. 31-40, Jan. 1962.

14. B.L. Clarkson and R.D. Ford, "An Experimental Investigation of the Random Excitation of a Tailplane Section by Jet Noise," ASD-TDR-62-680, July 1962.

15. D.R.B. Webb, A.R. Keeler, G.R. Allen, "Surface Pressures and Structural Strains Resulting from Fluctuations in the Turbulent Boundary Layer of a Fairey Delta 2 Aircraft," R.A.E. Tech. Note Structures 313, May 1962.

16. J.F. Wilby, W.V. Baht, F.L. Gloyna, "Airplane Fuselage Response to Turbulent Boundary Layers," ASME Paper 70-WA/DE-10, Nov. 1970.

17. G. Bayerdörfer, "Experimental Investigations to Establish Acoustic Fatigue Design Charts," *J. Sound Vib.*, 17, pp. 55-62 1971 .

18. E.E. Ungar, "Damping of Panels," Chapter 14 of *Noise and Vibration Control*, L.L. Beranek, Ed., McGraw-Hill Book Co., Inc., New York 1971 .

19. E.E. Ungar and J.R. Carbonell, "On Panel Vibration Damping Due to Structural Joints," AIAA Journal 4, pp. 1385-1390, August 1966.

20. L. Cremer and M. Heckl, Körperschall, Chapter III, Springer Verlag, Berlin 1967

21. S.H. Crandall, "Measurement of Stationary Random Processes," Chapter 2 of *Random Vibration*, 2, S.H. Crandall, Ed., The M.I.T. Press, Cambridge, Mass. 1963 .

22. J.P. Den Hartog, *Mechanical Vibration*, McGraw-Hill Book Co., Inc., New York, Fourth Edition 1956 , p. 432.

23. E.E. Ungar, "Mechanical Vibrations", Sec. 6 of *Mechanical Design and Systems Handbook*, H. Rothbart, Ed., McGraw-Hill Book Co., Inc., New York, 1964.

24. S.H. Crandall, "Statistical Properties of Response to Random Vibration", Chap. 4 of *Random Vibration*, 1, S.H. Crandall, Ed., The M.I.T. Press, Cambridge, Mass., 1958.

corresponds to an intersection of the $k_b(\omega)$ curve, which is a plot of Eq. (6), with the $\omega = \omega_1$ line. Obviously, one may expect the product (integrand) to exhibit a very strong peak if the peaks of the factor functions coincide. The two frequencies at which this condition can occur are readily identifiable in the diagram: (1) at ω_o, for which $k_b = k_o$, the admittance peak occurs at the same location as the jet noise peak. (2) At ω_H, for which $k_b = k_H$, the admittance peak occurs at the same wavenumber as the turbulent flow peak.

Stresses. – Since the root-mean-square strain in a uniform beam or plate is very nearly equal to the ratio of the root-mean-square velocity to the longitudinal wave velocity in the material, calculation of the rms strain is a simple matter once one knows the mean-square velocity. Of course, one then merely needs to apply Hooke's law to obtain the rms stress.

Methods are also available that permit one to account for the stress increases at boundaries, supports, or reinforcements. Determination of the motions of supporting structures (e.g., of plate ribs or frames) and of the associated stresses involves additional calculations, which often can be formulated in relatively simple terms.

The (space and time) Fourier transform of Eq. (4), when written in terms of the velocity v instead of the displacement y, may be shown to be

$$(k^4 - k_b^4)v = \tilde{p}(k,\omega) \ , \qquad (5)$$

where k and ω represent the wavenumber and radian frequency (which replace x and t as a result of the Fourier transform process) and $\tilde{p}(k,\omega)$ represents the Fourier transform of $p(x,t)$ — i.e., the spectral pressure amplitude. The wavenumber k_b obeys

$$k_b^4 = \omega^2 m/B \qquad (6)$$

and is that wavenumber at which free bending waves travel without dimunition (in the absence of damping).

The admittance Y is defined as the ratio of the spectral velocity to the spectral pressure; for the beam under consideration here one finds

$$Y(k,\omega) = \frac{v}{\tilde{p}} = \left[\omega m \left(1 - \frac{k^4}{k_b^4}\right)\right]^{-1} \ . \qquad (7)$$

As evident from this equation or from the sketch of this function appearing in Fig. 21, the admittance has a sharp peak at $k = k_b$. In fact, this peak rises to infinity for undamped systems, but remains finite for realistic structures that always have some damping.

Admittances of Other Structures. — Equation (7) probably represents the simplest admittance function of practical interest. However, expressions are also available for the admittances of beams with uniformly spaced masses attached, or of one-dimensional plates with uniformly spaced ribs. These expressions are more complicated than that for a uniform beam, but are no different in concept.

For two-dimensional structures, the admittance functions involve two wavenumbers, corresponding to Fourier transformations on the two spatial coordinates, but otherwise again do not differ in concept from the simple beam admittance.

$$\Phi(k,\omega) = |\tilde{p}(k,\omega)|^2 \; L^{-1}T^{-1} \qquad (3)$$

where L and T, respectively, denote the spatial interval (here, in one dimension for this introductory one-dimensional discussion) and the time interval over which the pressures are sampled.

Surface Pressures in Turbulent Flow. – Figure 19 indicates schematically the typical behavior of the pressure spectral density $\Phi(k,\omega)$ associated with turbulent flow along a surface. If one considers the curves of constant spectral density as "contour lines" in the k,ω plane, one notes that the Φ hill has a ridge along a line whose slope is $\omega/k = U_\infty$, where U_∞ represents the speed of the flow along the surface. For blown flap surfaces, U_∞ generally is considerably less than the speed of sound c_o, as also indicated in the figure.

All points on the $\omega = kU_\infty$ line represent energy travelling at the speed of the flow. If all of the energy would travel at the flow speed, – i.e., if the turbulence were "frozen" into the flow and would convect at the flow speed – the contour lines would collapse into the U_∞ line. The spread of the contour lines about this line reflects the "unfrozen" nature of boundary flow, – i.e., the presence of a distribution of components travelling with different speeds.

At any particular frequency ω_1, the component that travels with the speed of the flow has a certain wavenumber k_H. This is called the hydrodynamic wavenumber at that frequency, and it is the wavenumber at which there exists the greatest fluctuating-pressure energy at that frequency. Similarly, the component at ω_1 that travels with the speed of sound has a wavenumber k_o, the acoustic wavenumber. Sound waves travelling (at grazing incidence) along the surface correspond to the c_o line of the figure.

The lower part of Fig. 19 shows a "slice" taken through the upper plot at the constant frequency ω_1. The peak in the spectral density at the hydrodynamic wavenumber k_H again displays the fact that most of the energy travels at the speed of the flow. It is important to observe, however, that significant amounts of energy also travel at other speeds, particularly at speeds near U_∞. Indeed, the fact that $\Phi(\omega_1,k)$ is finite for a range of values of k below k_o indicates that some energy travels at speeds greater than the sound speed.

first of these functions is known to acousticians (and to radar and sonar engineers) as the directivity pattern of the source of excitation; it represents the spectral density of the surface pressures. The function representing the structural stiffness is known to structural dynamicists as the surface (spectral) admittance of the structure, and to acousticians as its array receiving pattern. The available physical understanding of these functions should facilitate direction and evaluation of research and design programs. Since only integrals of products of functions are required, only minimal computational difficulty is involved.

Experimental Savings and Accuracy Gain. — With the STSD approach, the (spatial) spectral density of fluctuating pressures acting on a structural surface may be measured by means of an array of pressure sensors flush-mounted on the surface; the outputs of all of the (spatially distributed) sensors are sampled simultaneously and recorded. The records are later digitized and entered into a digital computer for calculation of the spectral densities. Only one experimental run is needed for each set of independent variables.

Alternate approaches to representing surface loads in essence require the repositioning of pairs of transducers and many repetitive runs for each set of independent variables. The recorded sensor outputs from all such runs typically are cross-correlated for a range of time delays, leading to space-time cross-correlation functions. Because data from different runs are obtained and analyzed separately in these approaches, loss of accuracy results due to random experimental errors. The STSD approach, on the other hand, is based on a single run — not only reducing this source of errors drastically, but also leading to a considerable saving in run time.

Extensions. — The STSD approach is ideally suited for dealing with the responses of surface (e.g., skin) structures to spatially homogeneous excitation. Where the responses of interior or supporting structures (e.g., ribs, stringers) are of interest, these may be expected to be determined relatively simply from the surface structural responses.

As the spatial inhomogeneities of the exciting pressure field and of the structure increase, the STSD descriptions required to provide sufficient accuracy become more complex. In

TABLE C-I. – FATIGUE LIFE CORRECTION FACTORS FOR ALUMINUM ALLOYS

Alloy	Temper	Tensile Yield Stress* (ksi) = Y	Fatigue Stress† (ksi) = S	$S/S_{7075\text{-}T6}$	$Y/Y_{7075\text{-}T6}$	$Y/Y_{5052\text{-}H38}$	Correction Factor, k_m			
							Skin Panels, $\beta = 4.60$	Stringers, $\beta = 2.74$	Facing Sheets, $\beta = 4.06$	Honeycomb Core, $\beta = 7.05$
2014	T6	66			1.00	2.00	1.00	1.00	1.00	130.
Clad 2014	T6	57	15	0.75	0.87	1.75	0.27	0.46	0.31	52.
2024	T42	39			0.59	1.17	0.088	0.24	0.12	3.0
"	T3	45	18	0.90	0.68	1.37	0.62	0.75	0.65	9.3
"	T4	43			0.65	1.30	0.14	0.31	0.17	6.3
"	T36	56	19	0.95	0.85	1.70	0.75	0.87	0.81	42.
Clad 2024	T3	42	13	0.65	0.64	1.27	0.14	0.31	0.17	5.4
"	T36	52	13	0.65	0.79	1.57	0.14	0.31	0.17	24.
"	T4	40			0.61	1.21	0.10	0.26	0.13	3.9
"	T42	35			0.53	1.06	0.050	0.17	0.052	1.51
"	T6	47			0.71	1.42	0.21	0.39	0.25	11.8
"	T81	55	13	0.65	0.83	1.67	0.14	0.31	0.17	37.
"	T86	63	13	0.65	0.95	1.91	0.14	0.31	0.17	95.
5052	H32	20			0.30	0.61	0.0040	0.037	0.0075	0.031
"	H34	23			0.35	0.70	0.0080	0.056	0.0020	0.081
"	H36	29			0.44	0.88	0.023	0.106	0.036	0.41
"	H38	33			0.50	1.00	0.041	0.15	0.060	1.00
6061	T4	16			0.24	0.48	0.0014	0.021	0.0030	0.0057
"	T6	35	13	0.65	0.53	1.06	0.14	0.31	0.17	1.51
7075	T6	66	20	1.00	1.00	2.00	1.00	1.00	1.00	130.
Clad 7075	T6	62	13	0.65	0.94	1.88	0.14	0.31	0.17	85.
7079	T6	66			1.00	2.00	1.00	1.00	1.00	130.
7178	T6	73			1.11	2.21	1.62	1.33	1.53	270.
Clad 7178	T6	68			1.03	2.06	1.15	1.08	1.13	163.
5083	O	18			0.27	0.55	0.0024	0.028	0.0050	0.015
"	H113	29			0.44	0.88	0.023	0.106	0.036	0.41
5086	H32	27			0.41	0.82	0.016	0.089	0.027	0.25
"	H34	33			0.50	1.00	0.041	0.15	0.060	1.00
"	H36	37			0.56	1.12	0.070	0.205	0.095	2.2
5454	H32	26			0.39	0.79	0.013	0.074	0.022	0.18
"	H34	29			0.44	0.88	0.023	0.106	0.036	0.41
5456	O	19			0.29	0.58	0.0034	0.034	0.0066	0.022
"	H24	38			0.58	1.15	0.082	0.225	0.110	2.7

*Average value for thin sheet specimens, Ref. 34.

†Completely reversed flexural stress that flat specimens can endure for 10^8 cycles. From Table 3.3.1(c), Ref. 34.

take the endurance limit as the fatigue stress. Aluminum alloys do not have endurance limits, in general (Refs. 34 and 35); for such alloys one needs to define S as corresponding to any fixed number of cycles, say $N = 10^8$.

Correction for Fatigue Stress. — If one summarizes Eqs. (45), (52), (71) and (75), as

$$N = B(\sigma_1/\sigma_{ref})^{-\beta} , \tag{2}$$

then one may write

$$\frac{\sigma_1}{\sigma_{ref}} = \left(\frac{N}{B}\right)^{-1/\beta} \tag{3}$$

and, introducing Eq. (1),

$$\frac{\sigma_2}{\sigma_{ref}} = \frac{S_2}{S_1}\frac{\sigma_1}{\sigma_{ref}} = \frac{S_2}{S_1}\left(\frac{N}{B}\right)^{-1/\beta} . \tag{4}$$

Then, the number N of cycles that material 2 can withstand is found to obey

$$N = B\left(\frac{\sigma}{\sigma_{ref}}\right)^{-\beta}\left(\frac{S_2}{S_1}\right)^{\beta} = N_1 \cdot k_m , \tag{5}$$

where N_1 denotes the number of cycles one calculates for the basic material — i.e., by use of Eq. (2) — and

$$k_m = (S_2/S_1)^{\beta} \tag{6}$$

is a correction factor that accounts for differences in the material's fatigue properties.

Since the fatigue life is proportional to the number of cycles to failure, one may obtain the fatigue life of a structural component of any aluminum alloy by multiplying the life one calculates for that component on the basis of Eqs. (45), (52), (71), (75), by the appropriate correction factor k_m, as

where E represents the modulus of elasticity of the skin material. The shear stress in the core obeys

$$\tau = Gw_s' = -\frac{B}{A} w_b''' = \frac{B}{A}\left(\frac{\pi}{L}\right)^3 w_0 \cos\left(\frac{\pi x}{L}\right) . \tag{11}$$

Thus, the maximum shear stress τ_{max}, which may be seen to occur at the ends of the beam, is related to the maximum skin stress σ_{max} due to flexure (which occurs at the beam center) as

$$\frac{\tau_{max}}{\sigma_{max}} = \frac{\pi B}{LAcE} . \tag{12}$$

Rectangular Section Beam. — For a full-depth honeycomb beam with a rectangular cross-section of width e and thickness H, and with facing sheets (skin) of thickness t_s,

$$B \approx EH^2 e t_s/2 , \qquad A \approx eH . \tag{13}$$

Then the correction factor term appearing in Eq. (8) becomes

$$\frac{\pi^2 B}{L^2 AG} = \frac{\pi^2 E}{G}\frac{Ht_s}{L^2} . \tag{14}$$

Since Ht_s/L^2 generally is very small, the expression of Eq. (14) may be expected to be small compared to unity, except for very soft cores, for which $\pi^2 E/G$ is very large. Thus, except for such soft cores, the bending natural frequency expression of Eq. (9) may be expected to suffice, since the factor by which ω_b is multiplied in Eq. (8) then is very nearly equal to unity.

By substitution of Eqs. (13) into (12) and noting that $c = H/2$ one finds that for a rectangular section beam

$$\frac{\tau_{max}}{\sigma_{max}} \approx \pi \frac{t_s}{L} . \tag{15}$$

APPENDIX B

SHEAR EFFECTS IN HONEYCOMB-CORE SANDWICH BEAMS

Since the honeycomb core, when considered as a continuum, has a relatively low shear modulus, shear deflection may play an important role in the dynamics and stresses of honeycomb core sandwich beams. This appendix presents an approximate analysis of the effects of the honeycomb beam shear stiffness.

In Ref. 26 there is summarized an analysis of the stress response of simply supported honeycomb-core sandwich panels. The analysis presented below proceeds in the same manner as that of Ref. 26, but applies for beams instead of panels.

Relation Between Flexural and Shear Deflections. – The total deflection w of a beam may be considered as composed of a component w_b due to bending and of a component w_s due to shear, that is,

$$w = w_b + w_s \ . \tag{1}*$$

For a beam vibrating at its fundamental resonance frequency ω, one finds from simple beam theory that the deflections must satisfy the differential equation

$$w_b'''' = \frac{\mu}{B} \omega^2 w \tag{2}$$

where the primes indicate differentiation with respect to the longitudinal coordinate x, B denotes the flexural stiffness of the beam, and μ its mass per unit length.

From elementary beam bending theory one finds that the shear force Q is given by

$$Q = -Bw_b''' \ . \tag{3}$$

Since the shear strain is equal to w_s', the shear force must also obey

$$Q = GAw_s' \ , \tag{4}$$

*For the sake of simplicity, new equation numbering sequences are begun in each appendix. All equation numbers mentioned in this appendix refer to equations presented in this appendix.

density $\overline{p^2}\Phi_n(\omega)$ of the fluctuating pressure due to turbulence on an EBF is given by Eqs. (5) and (10), but with the latter reduced by a factor of 4.4 (or 10 log 4.4 ≈ 6.5 dB).

Correlations. – If one approximates the pressure field as spatially homogeneous, as was done for the momentum annihilation case, one may write the wavenumber-frequency spectrum of the boundary-layer-like fluctuating pressure field as

$$\Phi_p(\underline{k},\omega) = \overline{p^2}\Phi_n(\omega)\Phi_x(k_x)\Phi_y(k_y) \tag{17}$$

where $\underline{k}$, k_x, k_y have the same meanings as previously. The forms of the component spectra Φ_x and Φ_y and the magnitudes of the parameters that enter them may be determined on the basis of data given in Ref. 8 relating to the spatial correlations of the fluctuating pressures. One finds that

$$\Phi_x(k_x) = \frac{L_x/\pi}{1 + (k_x - k_h)^2 L^2} \tag{18}$$

$$\Phi_y(k_y) = \frac{L_y/\pi}{1 + k_y^2 L_y^2} \tag{19}$$

Here k_h denotes the hydrodynamic (or "convective") wavenumber, i.e., the wavenumber corresponding to pressure fluctuations that pass an observation point at the flow convection velocity V_c;

$$k_h = \omega/V_c. \tag{20}$$

This convection velocity is related to the jet exit velocity U_o as

$$V_c \approx 0.45\ U_o \tag{21}$$

$$\Phi_p(\underline{k},\omega) = \frac{1}{(2\pi)^3}\iiint \phi_p(\underline{x},\tau)\, e^{-i(\underline{k}\cdot\underline{x} - \omega\tau)}\, dxdyd\tau \qquad (11)$$

$$\phi_p(\underline{x},\tau) = \iiint \Phi_p(\underline{k},\omega)\, e^{i(\underline{k}\cdot\underline{x} - \omega\tau)} dk_x dk_y d\omega \qquad (12)$$

The pressure correlation $\phi_p(s,\tau)$ given by Eqs. (6) and (3) is isotropic; — i.e., it is a function of only the separation $s = [(x_1 - x_2)^2 + (y_1 - y_2)^2]^{1/2}$ rather than of the coordinates (x_1,y_1) and (x_2,y_2) of the two observation points. This isotropy implies that the wavenumber-frequency spectrum is a function of only the magnitude $k = [k_1^2 + k_2^2]^{1/2}$ of the wavenumber, rather than of the vector $\underline{k}$; that is,

$$\Phi_p(\underline{k},\omega) = \Phi_p(k,\omega) \qquad (13)$$

Since the pressure correlation $\phi_p(s,\tau)$ consists of a product of a spatial and a time function, the wavenumber-frequency spectrum consists of the product of a frequency and a wavenumber function;

$$\Phi_p(k,\omega) = \overline{p^2}\Phi_n(\omega)\Phi(k) \qquad (14)$$

where here

$$\Phi(k) = \frac{1}{(2\pi)^2}\iint e^{-s/L}\, e^{-i\underline{k}\cdot\underline{x}}\, dxdy. \qquad (15)$$

With the above relation for the separation s,

$$\Phi(k) = \frac{1}{2\pi}\int_o^\infty e^{-s/L} J_o(ks)ds = \frac{L^2}{2\pi}[1 + k^2L^2]^{-3/2} \qquad (16)$$

where J_o is the zero-order Bessel function of the first kind.

suggest that this correlation depends only on the separation distance s between the two observation locations, and not on the direction from one point to the other. Furthermore, these data indicate that the correlation length (i.e., the distance within which the correlation decays to a small fraction of its maximum value) is considerably smaller than the distances over which there occur significant variations in the mean velocity U or in the mean-square fluctuating velocity $\overline{u^2}$. Thus, one is justified in considering u to be a nearly spatially homogeneous field. Taking account of the exponentially decaying character of the correlation indicated by the data, one therefore may write

$$\phi_{u_1 u_2}(\tau) = \phi_u(s,\tau) = \overline{u^2}\, e^{-s/L}\, e^{-|\tau|/T_f} \tag{3}$$

where L and T_f denote the correlation length and the correlation time, respectively, of the fluctuating velocity.

The data also suggest that one may estimate the two above-mentioned correlation parameters from

$$L \approx 2.5 \times 10^{-2} X \tag{4}$$

$$T_f \approx 0.1 X/U_o \tag{5}$$

where U_o represents the jet exit velocity.

In terms of the previously indicated approximations, one may express the pressure correlation (Eq. 2) on the EBF as

$$\phi_{p_1 p_2}(\tau) = \phi_p(s,\tau) = 4\rho^2 U^2 \phi_u(s,\tau) \tag{6}$$

For distances X of interest for realistic flaps (i.e., X/D ≈ 9), the local velocity U is very nearly equal to the exit velocity U_o or U_c (see Figs. 14b and 15).

Mean-square pressure. — From Eq. (6) one finds that the mean-square fluctuating pressure $\overline{p^2}$ is given by

$$\overline{p^2} = \phi_p(0,0) = 4\rho^2 U^2 \overline{u^2} \approx (4qI)^2 \tag{7}$$

APPENDIX A

MODELS AND ESTIMATES OF AEROACOUSTIC LOADS ON EXTERNALLY BLOWN FLAPS

Jet Efflux Configuration

A typical idealized jet efflux configuration is sketched in Fig. 2, showing a converging conical "potential core" surrounded by a spreading conical expansion region. It is expected that externally blown flap (EBF) structures will be inserted in this spreading region, in order to deflect the flow downward, so as to provide lift. The problem to be considered here consists of characterizing the fluctuating pressures that will act on the flap surfaces, so that one may estimate the corresponding vibratory stresses for design purposes.

At first glance it may seem inappropriate to consider the flow produced by a fan-jet engine like that from a simple jet. However, one may conclude from Fig. 14 that the simple jet gives a reasonable approximation to the flow profile in those regions which EBF surfaces are likely to be. Whereas Fig. 14a indicates that a pronounced low-velocity fan-flow annulus may be discerned near the exit plane, Fig. 14b shows that the fan flow plays only a relatively minor role at locations several diameters from the nozzle plane. Indeed, if one plots the fan-jet data of Fig. 14b in non-dimensionalized form and compares it with similar data for an ideal circular jet (Fig. 15), one finds that the fan-jet profiles are quite consistent with profiles* corresponding to an ideal jet issuing from the core nozzle (with diameter D_c) with the core exhaust velocity U_c.

If one assumes that the aeroacoustic noise field in the engine exhaust stream is, like the flow profile, similar to that for an ideal circular jet, then one may use the rather extensive data available for ideal jets to estimate the fluctuating pressures acting on an EBF inserted in the exhaust stream.

---

*Such dimensionless mean velocity profiles are known to vary only little with the jet Mach number M.

CONCLUDING REMARKS; RECOMMENDATIONS

The approach suggested here for estimation of fluctuating pressures associated with engine exhausts is based on extrapolation of nondimensionalized fluctuating pressure data obtained from simple jets and on interpretation of similar velocity distribution data from measurements in the exhausts of a very limited number of fan-jet engines. Clearly, the availability of data on the fluctuating pressure distribution in the exhaust of the engine to be used in any particular application may be expected to improve the characterization of these pressures and to increase the confidence one has in fatigue life estimates based on these pressures. Comparison of predictions based on the approach suggested in this report with corresponding full-scale fan-jet engine fluctuating-pressure data would also serve as a useful check on the validity of the suggested approach.

The response, stress, and fatigue life estimation approaches presented in this report follow the earlier literature in assuming only the fundamental mode of the structure to be of importance. Although this assumption may lead to conservative designs and life estimates in many cases, one can easily visualize practical situations where higher modes predominate. Such cases are particularly likely to occur with engine exhaust excitation, where the excitation pressures are correlated over small areas, have spectral peaks at frequencies considerably higher than the fundamental structural resonance, and convect along the structural surface. Indeed, there also exists some experimental evidence that shows that higher structural modes play important roles in responses to flow excitation. Of course, the importance of higher modes in determining fatigue life is also enhanced by the higher fatigue damage accumulation rates associated with their higher resonance frequencies. Thus, it appears advisable to use the response, stress, and fatigue estimation approaches suggested here with some caution. Reexamination of these approaches, and their extension to include appropriate higher mode responses, is recommended.

Any but the most grossly empirical fatigue life prediction method must be based on information concerning how the number of loading cycles that a structure can withstand varies with the fluctuating stress. The method suggested in this report is based on sonic fatigue data derived from tests on panel specimens of only one material for each panel type. In particular, the data pertaining to the fatigue of honeycomb-core sandwich structures is extremely limited. Thus, although one may expect the suggested prediction technique to yield good results for structures

Approximations for Small Angular Displacements. — For small angular displacements, for which $\cos\theta_n \approx 1$, $\sin\theta_n = \theta_n$, the above relations reduce to

$$F_{x1} = m_1\ddot{x}_1 + k_{x(1,0)}[x_1 - C - B\theta_1] + k_{x(1,2)}[x_1 - x_2 + G + N + H\theta_1 + L\theta_2]$$

$$F_{y1} = m_1\ddot{y}_1 + k_{y(1,0)}[y_1 + B - C\theta_1] + k_{y(1,2)}[y_1 - y_2 - H - L + G\theta_1 + N\theta_2]$$

$$M_1 + F_{y1}D - F_{x1}E = I_1\ddot{\theta}_1 + k_{\theta(1,0)}[\theta_1 - \theta_0] + k_{\theta(1,2)}[\theta_1 - \theta_2]$$

$$-k_{x(1,0)}[x_1-C-B\theta_1](B-C\theta_1)-k_{y(1,0)}[y_1+B-C\theta_1](C+B\theta_1)$$

$$+k_{x(1,2)}[x_1 - x_2 + G + N + H\theta_1 + L\theta_2][H - G\theta_1]$$

$$-k_{y(1,2)}[y_1 - y_2 - H - L + G\theta_1 + N\theta_2][G + H\theta_1]$$

$$F_{x2} = m_2\ddot{x}_2 + k_{x(2,0)}[x_2 - K - J\theta_2] + k_{x(2,1)}[x_2 - x_1 - G - N - H\theta_1 - L_2]$$

$$+ k_{x(2,3)}[x_2 - x_3 + R + U + S\theta_2 + T\theta_3]$$

$$F_{y2} = m_2\ddot{y}_2 + k_{y(2,0)}[y_2 + J - K\theta_2] + k_{y(2,1)}[y_2 - y_1 + H + L - G\theta_1 - N\theta_2]$$

$$+ k_{y(2,3)}[y_2 - y_3 - 5 - T + R\theta_2 + U\theta_3]$$

$$F_{x2} = m_2\ddot{x}_2 + k_{x(2,0)}[\xi_2 - \xi_0]_{(2,0)} + k_{x(2,1)}[\xi_2 - \xi_1]_{(1,2)}$$

$$+ k_{y(2,3)}[\xi_2 - \xi_3]_{(2,3)}$$

$$F_{y2} = m_2\ddot{y}_2 + k_{x(2,0)}[\eta_2 - \eta_0]_{(2,0)} + k_{y(2,1)}[\eta_2 - \eta_1]_{(1,2)}$$

$$+ k_{y(2,3)}[\eta_2 - \eta_3]_{(2,3)}$$

$$M_2 + F_{y2}P - F_{x2}Q = I_2\ddot{\theta}_2 + k_{\theta(2,0)}(\theta_2 - \theta_0) + k_{\theta(2,1)}(\theta_2 - \theta_1)$$

$$+ k_{\theta(2,3)}(\theta_2 - \theta_3)$$

$$-k_{x(2,0)}[\xi_2 - \xi_0]_{(2,0)}\ [J\cos\theta_2 - K\sin\theta_2]$$

$$+k_{y(2,0)}[\eta_2 - \eta_0]_{(2,0)}\ [-K\cos\theta_2 - J\sin\theta_2]$$

$$-k_{x(2,1)}[\xi_2 - \xi_1]_{(2,1)}\ [L\cos\theta_2 - N\sin\theta_2]$$

$$+k_{y(2,1)}[\eta_2 - \eta_1]_{(2,1)}\ [-N\cos\theta_2 - L\sin\theta_2]$$

$$-k_{x(2,3)}[\xi_2 - \xi_3]_{(2,3)}\ [-S\cos\theta_2 + R\sin\theta_2]$$

$$+k_{y(2,3)}[\eta_2 - \eta_3]_{(2,3)}\ [R\cos\theta_2 + S\sin\theta_2]$$

whence

$$\xi_{(n)(n,s)} - \xi_{(s)(n,s)} \equiv \left[\xi_{(n)} - \xi_{(s)}\right]_{(n,s)}$$

$$= x_n - x_s + X_{n(n,s)}\cos\theta_n - X_{s(n,s)}\cos\theta_s$$

$$- Y_{n(n,s)}\sin\theta_n + Y_{s(n,s)}\sin\theta_s \qquad (100)$$

$$\eta_{(n)(n,s)} - \eta_{(s)(n,s)} \equiv \left[\eta_{(n)} - \eta_{(s)}\right]_{(n,s)}$$

$$= y_n - y_s + Y_{n(n,s)}\cos\theta_n - Y_{s(n,s)}\cos\theta_s$$

$$+ X_{n(n,s)}\sin\theta_n - X_{s(n,s)}\sin\theta_s$$

One may note that all k's, X's, Y's, as well as F_x, F_y, M, m, and I represent known or given quantities. On the other hand, the x's, y's and θ's are the unknowns. Thus, one has three unknowns per flap element, as well as three equations of motion per element, so that one has as many equations of motion as there are elements.

Equations for Illustrative Flap System

Dimensions. — The rather formidable appearance of the foregoing equations is due to the somewhat intricate notation, which was introduced for the sake of generality. In order to obtain a clearer view of the nature of these equations (and of the meaning of the notation), it may be instructive to refer to the particular configuration sketched in Fig. 13. If the various capital letters indicated in that figure denote (positive) dimension values, then in terms of the previously introduced notation,

displaced by the amounts ξ,η in the x and y directions, respectively, if the flap center of gravity is displaced by the amounts x_n and y_n in the coordinate directions, and if the flap is rotated through an angle θ_n, where

$$\xi = x_n + X\cos\theta_n - Y\sin\theta_n$$

$$\eta = y_n + Y\cos\theta_n + X\sin\theta_n \tag{97}$$

Spring Forces. – The difference between the displacements of the force-interconnection points on two flap elements, which points coincide when the flap system is in equilibrium, may thus be found from the difference between the ξ's and η's for the two points. This difference corresponds to the extension (or compression) of the interconnection springs, and therefore determines the spring forces.

Dynamic Equilibrium of Flap Element. – Using the attachment-point coordinate designations* indicated in Fig. 11, one may find the following equations of motion for the nth flap element:

$$F_{xn} = m_n\ddot{x}_n + k_{x(n,n-1)}\left|\xi_{(n)} - \xi_{(n-1)}\right|_{(n,n-1)} + k_{x(n,n+1)}\left|\xi_{(n)} - \xi_{(n+1)}\right|_{(n,n+1)} + \cdots$$

$$F_{yn} = m_n\ddot{y}_n + k_{y(n,n-1)}\left|\eta_{(n)} - \eta_{(n-1)}\right|_{(n,n-1)} + k_{y(n,n+1)}\left|\eta_{(n)} - \eta_{(n+1)}\right|_{(n,n+1)} + \cdots \tag{98a}$$

*E.g., $Y_{n(n,n-1)}$ denotes the Y coordinate, as measured in the system attached to the nth flap element, of the point at which the nth and (n-1)th elements are interconnected.

Changes in the flap element's flexural rigidity and mass per unit length may be seen to have somewhat lesser effects on these two fatigue lives. On the other hand, the core density affects the core's fatigue life very significantly, with a 10% increase extending the fatigue life by a factor of about 2.7. Again, the jet exit velocity is the most important jet parameter, with a 10% decrease in U_o leading to increases in the skin and core fatigue lives by factors of 2.9 and 6.4, respectively.

If one again substitutes for Φ_p from Eq. (81), one obtains

$$\frac{T_h}{10^{18}\,\tau_{ref}^{7.05}\,d_{ref}^{-10.6}} = \begin{cases} 640\left(L^2\left[\frac{\mu}{B}\right]^{2.26}\left[\frac{A}{e}\right]^{7.05} d^{10.6}\eta^{3.525}\right)\left(\frac{1}{X^{3.525}\rho_o^{7.05}U_o^{10.575}}\right) & \text{for } f \ll f_T \\ 3.1\left(\frac{d^{10.6}(A/e)^{7.05}\eta^{3.525}}{L^{12.1}(\mu/B)^{1.265}}\right)\left(\frac{X^{3.525}}{\rho_o^{7.05}U_o^{17.625}}\right) & \text{for } f \gg f_T \end{cases} \quad (94)$$

Design Considerations. – Equations (90) and (93) show that the fatigue lives of facing sheets and honeycomb cores increase with decreasing exciting pressure spectral density (evaluated at the flap element's fundamental natural frequency). This trend is as one would expect intuitively. Since the spectral density decreases with increasing frequency, as indicated by Eq. (9), one may obtain greater fatigue life by designing the flap element to have a higher fundamental resonance. In view of Eq. (55), a high fundamental resonance results from use of short unsupported spans L and of large stiffness/mass ratios B/μ.

As evident from Eqs. (92) and (94), reductions in L can result in quite dramatic increases in fatigue life, provided that the flap element's fundamental frequency f_1 is above the transition frequency f_T. If $f_1 < f_T$, then the facing sheet fatigue life increase produced by a given amount of length reduction is somewhat less dramatic – and this length reduction may indeed be expected even to reduce the core's fatigue life.

From Eqs. (91) and (93) one may determine that

$$\frac{T_h}{T_f} \approx \frac{2.6\times10^{11}}{B_1}\left(\frac{A}{cr}\right)^{2.99}\left(\frac{cL}{r^2}\right)^{4.06}\left(\frac{d}{d_{ref}}\right)^{10.6}\left(\frac{\tau_{ref}}{\sigma_{ref}}\right)^{7.05}\left[\frac{\eta_1 r\,\sigma_{ref}^2}{c_f\Phi_p(f_1)}\right]^{1.495} \quad (95)$$

$$\frac{T}{T_s} \approx 81 \left(\frac{5.6 \times 10^9}{3.7 \times 10^7}\right) \left(\frac{1}{100}\right)^{10.7} \left(\frac{20}{1}\right)^{1.1} \left[\left(\frac{10^3}{2}\right)^2 \left(\frac{20}{1}\right) \left(\frac{25}{1}\right) (0.01)\right]^2 \approx 2.1 \times 10^{-4},$$

which indicates that stringers typically have much longer fatigue lives than skin panels – in agreement with experimental observations.

Thus, one generally should first design the panels so that they have adequate fatigue lives, and then verify that the stringer design selected (usually on the basis of other than fatigue considerations) has a fatigue life that is no less than that of the panels.

Honeycomb-Core Sandwich Flaps

Facing Sheets (Skin). – If one substitutes into the fatigue life expression of Eq. (47) the number of cycles to failure as given by Eq. (71) and the natural frequency expression of Eq. (55) – with $\alpha_1 = 2.36$, to account for boundaries that are neither simply supported nor fully clamped, – and if one also uses the second stress expression of Eq. (68), which applies for the same boundary conditions, one finds that

$$T_f \approx 360\ B_1\ L^2 \sqrt{\frac{\mu}{B}} \left[\frac{(\mu B^3)^{1/4} \sigma_{ref}}{ecLE} \sqrt{\frac{\eta_1}{\Phi_p(f_1)}}\right]^{4.06}$$

$$\approx 360\ B_1\ \frac{\mu^{1.515} B^{2.545}}{L^{2.06}} \left(\frac{\sigma_{ref}}{ecLE}\right)^{4.06} \left(\frac{\eta_1}{\Phi_p(f_1)}\right)^{2.03} . \qquad (90)$$

In order to display the dimensional correctness of this expression clearly, one may define an effective flap density $\rho_f = \mu/A$, an effective radius of gyration $r = \sqrt{B/EA}$, and an effective longitudinal wavespeed $c_f = \sqrt{E/\rho_f}$. With these substitutions, one may rewrite Eq. (90) as

$$T_f \approx 360\ B_1 \left(\frac{L^2}{c_f r}\right) \left(\frac{Ar}{ecL}\right)^{4.06} \left(\frac{\eta_1 r \sigma_{ref}^2}{c_f \Phi_p(f_1)}\right)^{2.03} . \qquad (91)$$

$$\frac{T_s}{\sigma_{ref}^{0.548} B_s} = \begin{cases} 1.6 \left(\dfrac{a^2}{b^{1.096}} \dfrac{(I^*/H)^{0.548} \eta^{0.274}}{(hc_L)^{1.274}} \right) \left(\dfrac{1}{X^{0.274} \rho_o^{0.548} U_o^{0.822}} \right) & \text{for } f << f_T \\ 0.55 \left(\dfrac{a^{0.904}}{b^{1.096}} \dfrac{(I^*/H)^{0.548} \eta^{0.274}}{(hc_L)^{0.726}} \right) \left(\dfrac{X^{0.274}}{\rho_o^{0.548} U_o^{1.370}} \right) & \text{for } f >> f_T \end{cases} \qquad (87)$$

Design Considerations. – As is evident from Eqs. (80) and (86), the fatigue lives of skin panels and of stringers increase as the excitation – represented by the pressure spectral density $\Phi_p(f)$ – decreases. This behavior is as one would expect intuitively, of course. Since this spectral density decreases with increasing frequency, as indicated in Eq. (7), one should design the skin panel to have as high a fundamental resonance frequency f as possible. In view of Eq. (79), this implies that one should choose the largest admissible panel thickness h and the smallest panel edge length a. One might also consider choosing materials with large longitudinal wavespeeds c_L, but most acceptable structural materials have wavespeeds that differ by no more than about 10% from each other, so that one stands to gain little by choosing alternate materials on this basis.

Table I, which has been developed on the basis of the high-frequency part of Eq. (83), shows by what factors the fatigue life of a blown flap *panel* may be expected to change as the result of changing the various parameters. Thus, for example, one finds that a change in the skin thickness h by a factor of 1.50 (i.e., a 50% increase) would increase the fatigue life by a factor of 71; similarly, decreasing the panel edge length a by 20% would lengthen the fatigue life by a factor of 14, whereas doubling the damping η would increase that life by a factor of 4.9.

As evident from both Eq. (83) and Table I, relatively small changes in h and a can lead to quite considerable changes in panel fatigue life; the effects of changes in the other structural parameters are much less significant. Small changes in the distance X of the flap from the engine exit have relatively little effect on the fatigue life, and changes in the gas density (associated with exhaust temperature changes) that can occur with a

If the panel resonance frequency f is in a range where $\Phi_p(f)$ varies little with changes in f, then Eq. (80) exhibits all of the dependences of the fatigue life on the panel parameters. On the other hand, if $\Phi_p(f)$ varies significantly with f, then the dependence of f on the panel parameters gives rise to additional effects. From Eqs. (8), (15) and (16) one finds that

$$\Phi_p(f) \approx \begin{cases} 0.0115\ \rho_o^2 U_o^3 X & \text{for } f << f_T \\ 0.29\ \rho_o^2 U_o^5 / X f^2 & \text{for } f >> f_T \end{cases} \tag{81}$$

where the transition frequency f_T obeys*

$$f_T \approx 1.5\ U_o / X. \tag{82}$$

Substitution of Eq. (81) into (80) and use of Eq. (79) results in

$$\frac{T}{10^3 \sigma_{ref}^{4.60} B} \approx \begin{cases} 3.2 \times 10^3 \left(\dfrac{h^{5.90}\ \eta^{2.30}}{a^{2.60}\ c_L^{3.30}} \right) \left(\dfrac{1}{X^{2.30}\ \rho_o^{4.60}\ U_o^{6.90}} \right) & \text{for } f << f_T \\ 1.9 \left(\dfrac{h^{10.50}\ \eta^{2.30}\ c_L^{1.30}}{a^{11.80}} \right) \left(\dfrac{X^{2.30}}{\rho^{4.60}\ U_o^{11.50}} \right) & \text{for } f >> f_T \end{cases} \tag{83}$$

where the first parentheses enclose all relevant panel parameters, whereas the second enclose the jet parameter terms.

Stringers. – Again for the purpose of exhibiting the salient parametric effects most simply, it is useful to consider the common case where the stringer length is the same as the greater of the two panel edge lengths, and where the spacing between stringers is equal to the shorter panel edge length. With $b_s = b$ and $a_s = a$, assuming $b/a > 3$, and using Eq. (79), one may approximate Eq. (48) by

---

*For the typical values of U_o = 750 ft/sec and X = 10 ft, one finds $f_T \approx 110$ Hz.

Estimation Procedure. — In order to estimate the fatigue life of a honeycomb core sandwich flap element, the following procedure is recommended:

1. Calculate the fundamental beam resonance frequency f_1 from Eq. (55). If the beam end conditions are not well defined, take $\alpha_1 = 2.36$.

2. Determine the spectral density $\Phi_p(f_1)$ of the pressure acting on the flap at frequency f_1 from corresponding data, or estimate it from Eqs. (15) or (16).

3. Find the maximum root-mean-square stress in the skin from Eq. (65), if the end conditions (and the associated fundamental mode shapes) are well defined. Otherwise, find that stress by use of Eq. (68). Take $\eta = 0.04$, unless better data are available.

4. Estimate the maximum root-mean-square shear stress in the core as the basis of Eq. (69).

5. Calculate N_f from Eq. (72) or (73) and find the skin fatigue life T_f from Eq. (74) for the confidence limit of interest. For materials other than 5052-H39 aluminum, multiply T_h by k_m from Appendix C.

6. Calculate N_h from Eq. (75) or (76) and find the honeycomb core fatigue life T_h from Eq. (77). For materials other than 7075-T6 aluminum, multiply T_f by k_m from Appendix C.

7. Take the effective fatigue life of the entire structure as the lesser of the values of T_f and T_h.

Fatigue Life

Facing Sheets. – From Fig. 51 of Ref. 9, which summarizes the results of a regression analysis of data obtained on panels with 7075-T6 aluminum alloy facing sheets, one may deduce the following relation between the maximum skin stress σ_1 and the number of cycles N_f that the skin can withstand without failing:

$$\log N_f = -4.06 \log\left(\frac{\sigma_1}{\sigma_{ref}}\right) + \log B_1 \tag{70}$$

or

$$N_f = B_1 \, (\sigma_1/\sigma_{ref})^{-4.06} \ . \tag{71}$$

Here, as before, $\sigma_{ref} = 10^3$ psi; for the present case

$$\log B_1 = \left\{\begin{matrix} 9.22 \\ 9.53 \\ 9.75 \end{matrix}\right\} \quad \text{for the} \quad \left\{\begin{matrix} -95\% \\ -50\% \\ 0\% \end{matrix}\right\} \quad \text{confidence limit,} \tag{72}$$

corresponding to

$$B_1 = \left\{\begin{matrix} 1.6 \times 10^9 \\ 3.4 \times 10^9 \\ 5.6 \times 10^9 \end{matrix}\right\} \quad \text{for the} \quad \left\{\begin{matrix} -95\% \\ -50\% \\ 0\% \end{matrix}\right\} \quad \text{confidence limit .} \tag{73}$$

The discussion that follows Eq. (46) applies here again; the fatigue life T_{fC} of the facing sheet corresponding to the -C% confidence limit may be found from

$$T_{fC} = N_{fC}/f_1 \tag{74}$$

where, of course, f_1 represents the fundamental natural frequency of the sandwich beam and N_{fC} is found from Eq. (70) or (71).

rms stress associated with beam vibrations in the fundamental mode as

$$\sigma_1 = Ec(u''_{rms})_{max} = EcU_{rms}\,\phi''_{max} , \tag{64}$$

where the primes indicate differentiation with respect to the lengthwise coordinate x, E denotes the modulus of elasticity of the skin material, and ϕ''_{max} represents the maximum absolute value of $\phi''(x)$.

If one combines Eqs. (60), (61), (62), and (64), one finds that the maximum root-mean-square skin stress obeys

$$\sigma_1 = \frac{ecEJ_1\phi''_{max}}{\pi^{3/2}2^{5/2}\mu L f_1^2}\sqrt{\frac{f_1\Phi_p(f_1)}{\eta_1}} . \tag{65}$$

The similarity of the term under the square-root sign to the square-root terms appearing in Eqs. (29) and (47) is obvious.

The term $J_1\phi''_{max}$ depends only on the mode shape, and thus only on the boundary conditions. Since the mode shape, normalized in accordance with Eq. (57), is given (Refs. 23, 25) by

$$\phi(x) = \begin{cases} \sqrt{2}\,\sin(\pi x/L) & \text{for simply supported ends} \\ \cosh(\beta x/L) - \cos(\beta x/L) - \gamma[\sinh(\beta x/L) - \sin(\beta x/L)] & \text{for clamped ends} \end{cases} \tag{66}$$

where $\beta \approx 4.730$, $\gamma \approx 0.9825$, one may determine that

$$J_1\phi''_{max} = \begin{cases} 4\pi/L \approx 12.6/L & \text{for simply supported ends} \\ 37.4/L & \text{for clamped ends} . \end{cases} \tag{67}$$

where L denotes the beam's length, B its bending stiffness*, and μ its mass per unit length. The parameter α_1 represents a constant that depends on the boundary conditions; for a beam that is simply supported on both ends, $\alpha_1 = \pi/2 \approx 1.57$, and for a clamped-clamped (or free-free) beam, $\alpha_2 \approx 3.56$. Since in a realistic flap element the boundary conditions are likely to be somewhere between simply supported and fully clamped, one may reasonably take $\alpha_1 \approx \sqrt{(1.57)(3.56)} \approx 2.36$ as a first estimate, in absence of better information.

Resonant Response of Fundamental Mode. – In order to analyze the response of a uniform beam in its fundamental mode in general terms, it is convenient to introduce the mode shape $\phi(x)$ associated with that mode. One may then express any time-dependent beam deflection $u(x,t)$ in the first mode (Ref. 33) as

$$u(x,t) = U(t)\phi(x) \quad . \tag{56}$$

The mode shape $\phi(x)$ is defined physically only within a multiplicative constant; of the various normalizations possible, the one chosen here (to facilitate use of available tables and references) is

$$\int_0^L \phi^2(x)dx = L \quad . \tag{57}$$

It is well known that the dynamic response $U(t)$ of any structural mode is like that of a simple spring-mass-dashpot system with a mass equal to the modal mass

$$M_1 = \int_0^L \mu\phi^2(x)dx = \mu L \quad , \tag{58}$$

exposed to a force that is equal to the modal force

*For a homogeneous beam of a material with Young's modulus E and with a section having a moment of inertia I, the bending stiffness is B = EI.

The following procedure is recommended for estimation of stringer fatigue life:

1. Calculate the panel fundamental resonance frequency f and the pressure spectral density $\Phi_p(f)$ as in the panel fatigue life estimation procedure.

2. Evaluate the approximate maximum rms stress σ_b in the stringer from Eq. (48), using $\eta = 10^{-2}$, unless better damping data are available.

3. Find the corrected rms stress estimate from Eq. (49).

4. Calculate N_{sC} from Eq. (50) or (52), and find T_{sC} from Eq. (54).

5. For materials other than 7075-T6 aluminum, multiply T_{sC} by k_m from Appendix C.

between the rivet lines of adjacent stringers, H the stringer depth (see Fig. 7), and I an effective moment of inertia of the stringer cross-section, given by

$$I = I_{xx} - \frac{I_{xz}^2}{I_{zz}} \quad . \tag{48a}$$

Here I_{xx} denotes the centroidal moment of inertia of the stringer cross section about an axis parallel to the panel surface (see Fig. 8), I_{zz} represents a similar moment of inertia about an axis normal to the panel surface, and I_{xz} denotes a similar mixed moment of inertia.* As previously, f denotes the fundamental resonance frequency of a skin panel, η represents its loss factor, and $\Phi_p(f)$ denotes the spectral density of the fluctuating excitation pressure (at the frequency f).

Correction of rms stress estimate on basis of test data. – Since the various assumptions involved in the derivation of Eq. (48) may represent rather poor approximations of conditions occurring in practical structures, one would expect predictions made on the basis of Eq. (48) to deviate from corresponding experimental results. Comparison of such predictions with experimental data (Ref. 7) indicates that the experimentally observed root-mean-square stress σ_e on the average is related to the corresponding σ_b calculated from Eq. (48) as

$$\frac{\sigma_e}{1 \text{ psi}} = 900 \left(\frac{\sigma_b}{1 \text{ psi}} \right)^{1/5} \quad . \tag{49}$$

The above relation was derived on the basis of calculated σ_b values ranging from about 150 to 3000 psi; its applicability to values outside this range remains to be established.

Cycles to failure; survival probability; fatigue life. – Data presented in Fig. 44 of Ref. 7 indicates that the number N_s

---

*That is, $I_{xx} = \int_A z^2 dA$, $I_{zz} = \int_A x^2 dA$, $I_{xz} = \int_A xz dA$, where A represents the area of the stringer cross-section. Appendix I of Ref. 7 gives expressions for these moments of inertia for zee, channel, and hat sections.

Although the time-variation of a randomly varing parameter like the panel stress is not a simple sinusoid, and one can not speak of cycles in the strictest terms, one may expect the panel vibrations to be approximately sinusoidal in time as long as they are dominated by a single mode – as was previously assumed in the response analysis. One may then consider the stress signal between successive zero crossings as a half cycle, with the signal varying approximately like a sinusoid at the natural frequency of the system. Knowing this frequency and the number of cycles N that produce failure, one may calculate the fatigue life.

For failure probability distributions that are symmetric about the mean, (50-C/2)% of the samples fail under fewer stress cycles than the number corresponding to the -C% confidence limit (Ref. 21). Thus, for example, if $N = 10^7$ cycles corresponds to a confidence limit of -50% for a given panel design exposed to a given excitation, one may expect 25% of all panels to fail at less than 10^7 cycles (i.e., one may expect 75% of all panels to survive after 10^7 cycles).

Fatigue life. – The fatigue life of a structure obviously must be defined in terms of a failure probability or similar statistical measure. Here it is convenient to use the fatigue life corresponding to the -C% confidence limit, which one may find from

$$T_C = N_C/f \ , \tag{47}$$

where N_C is obtained from Eqs. (45) and (46) for the confidence limit in question and f denotes the natural frequency of the panel under consideration.

In order to estimate the fatigue life of a given panel, the following procedure is recommended:

1. Calculate the panel fundamental resonance frequency from Eq. (35), using the correction of Eq. (37) for curved panels.

2. Determine the spectral density $\Phi_p(f)$ of the pressure acting on the panel at the resonance frequency f from corresponding data or from Eq. (15) or (16).

3. Find the maximum root-mean-square stress from Eq. (41), modifying the result according to Eq. (42) for curved panels. Take $\eta = 10^{-2}$, unless better data are available.

Fig. 5.2 of Ref. 8); the estimates tend to be too high – by as much as a factor of 5 at low stress values, and generally by less at higher stresses. Means for improving the estimates are not available at present.

Below are tabulated values f_R/f and σ_R/σ calculated from Eqs. (37) and (42), taking for b^2/hR the greatest reasonable value. This value is $b^2/hR = A^2(a/h)_{max}(a/R)_{max} \approx 175\ A^2$, where $(a/h)_{max} = 500$ is the greatest likely practical value for this ratio, and where $(a/R)_{max} = 0.35$ is the greatest value of which Eqs. (37) and (42) hold. For smaller values of a/h and a/R – that is, for smaller b^2/hR – both f_R/f and σ_R/σ are nearer to unity.

b/a	0.3	1.0	3.0
f_R/f	1.55	8.45	13.1
σ_R/σ	0.76	0.33	0.83

Panel loss factors. – Because the responses of panels to random excitation are dominated by the responses of resonant modes, the damping of a skin panel – as characterized by the loss factor η – is important in establishing the magnitude of its response and the associated oscillatory stresses. As evident from Eq. (29) and from the relations derived from that equation, the root-mean-square stress varies inversely as $\sqrt{\eta}$.

References 18 and 19 suggest a method for estimating the loss factors of panels with riveted edges, taking account of such parameters as rivet spacing, width of contact area, and panel wavelength (as a function of frequency). However, this method may be somewhat too cumbersome for preliminary design purposes. Abundant experimental evidence* indicates that for conventional aircraft structures (i.e., for structures not provided with special damping treatments), η differs little from 10^{-2}. This value may therefore be taken as a reasonable estimate, unless measured data for the particular structure under consideration are available.

---

*E.g., see Ref. 20. Reference 8 suggests $\eta = 0.0085$ for typical aircraft structures, based on values between 0.008 and 0.009 reported for fuselage panels in Ref. 13, and on 0.0085 reported for tailplane panels in Ref. 14. The loss factors of the test panels investigated in Ref. 9 ranged between 0.005 and 0.009.

On the other hand, if one uses the expression (35) corresponding to more realistic boundary conditions, one finds

$$\sigma = 1.10 \sqrt{\frac{c_L \Phi_p(f)}{a\eta}} \left(\frac{b}{h}\right)^{3/2} \left(\frac{a}{b} + \frac{b}{a}\right)^{1/4} F^{-7/4} \qquad (40)$$

In Ref. 9 there is derived yet another expression for σ, on the basis of a regression analysis of experimental data for $1 \leq b/a \leq 3$ and $120 \leq b/h \leq 500$, arranged in nondimensional groups of variables deduced from ideal clamped-edge panel analysis. This expression (when rewritten in consistent units) corresponds to

$$\sigma = 0.24 \sqrt{\frac{c_L \Phi_p(f)}{a\eta}} \left(\frac{b}{h}\right)^{7/4} \eta^{-0.06} F^{-1.68} \quad . \qquad (41)$$

It is instructive to compare the stress estimates one obtains from the three foregoing equations. Clearly, Eqs. (39) and (40) differ only in the functions of the aspect ratio b/a they involve and (slightly) in their numerical coefficients. If one evaluates the aforementioned functions (Fig. 8), one finds that for practical values of the aspect ratio the two functions differ by about ten percent in magnitude and exhibit very nearly the same trend. Because of the differences in the magnitudes of these functions and in the coefficients of Eqs. (39) and (40), the stress one calculates by use of Eq. (39) is higher by a factor of about 1.2 than the stress estimate one finds from Eq. (40).

The function $F^{1.68}$, which appears on the right-hand side of Eq. (41) obviously depends more strongly on b/a than the function $F^{3/2}$ associated with Eq. (39); this stronger dependence is evidenced by the slightly steeper slope of the $F^{1.68}$ curve in Fig. 8. The function $F^{1.68}$ also is found to exceed $F^{3/2}$ by about 21% for b/a = 1, and by about 67% for b/a = 10. However, Eq. (41) differs from Eqs. (39) and (40) also in the exponent on (b/h) and in the added $\eta^{-0.06}$ term. For the typical value of $\eta = 10^{-2}$, the latter term amounts to 1.32. For values of (b/h) between 100 and 500, corresponding to the panels used in tests which served as the basis of development of Eq. (41), the value of $(b/h)^{1/4}$ lies between 3.17 and 4.72. Thus, on the average, $(b/h)^{7/4} \eta^{-0.06} F^{-1.68} / (b/h)^{3/2} F^{-3/2} \approx (4.0)(1.3)(1.4)^{-1} \approx 3.7$. If one multiplies the numerical coefficient 0.24 by this value, one obtains 0.90; comparison of this result with the coefficient

$$f_s = \frac{\pi}{2}\sqrt{\frac{D}{m}}\left(\frac{1}{a^2} + \frac{1}{b^2}\right) \tag{30}$$

and that of a clamped panel obeys (Ref. 9)

$$f_c \approx \frac{2\pi}{3}\sqrt{\frac{D}{m}}\ \frac{F(b/a)}{ab}\ , \tag{31}$$

where m denotes the mass per unit area of the panel and D its flexural rigidity, and

$$F(b/a) = [2 + 3b^2/a^2 + 3a^2/b^2]^{1/2}\ . \tag{32}$$

For homogeneous panels

$$D = \frac{Eh^3}{12(1-\nu^2)}\ , \tag{33}$$

$$m = \rho_s h\ , \tag{34}$$

where E represents Young's modulus, ν Poisson's ratio, and ρ_s the density of the structural material. One may thus estimate the fundamental natural frequency of a skin-stringer panel from

$$f = \sqrt{f_s f_c} = \frac{hc_L}{a^2}\,G(b/a) \tag{35}$$

where $c_L = \sqrt{E/\rho_s}$ represents the longitudinal wave velocity* in the panel material and

$$G(b/a) = \frac{\pi}{6}\left[\frac{a}{b}\left(1 + \frac{a^2}{b^2}\right)F(b/a)\right]^{1/2} \approx \begin{cases} 1.25 \text{ for } b/a = 1 \\ 0.69 \text{ for } b/a >> 1\ . \end{cases} \tag{36}$$

---

*For most structural metals, one may take $c_L = 2 \times 10^5$ in/sec with adequate accuracy. Since $\nu^2 << 1$ typically, Poisson's Ratio does not appear in these approximate expressions.

be well justified in many practical cases. Once the panel motions have been determined, the sonic fatigue analysis method proceeds to determine the stresses induced in the stringers as the result of the loads imposed on them by the vibrating panels, and it then compares these calculated stresses with experimental stress and fatigue data.

Skin

Relation between dynamic and static stress. – In Ref. 6 analysis of the response of elastic structures to random pressure fields is discussed in general terms, and simplified results are presented for the case where:

(1) One mode predominates in the frequency range of interest.
(2) The excitation pressure is in phase over the entire structure of interest.
(3) The spectrum of the excitation does not change rapidly in the vicinity of the resonance frequency of the dominant mode.

It is shown in Ref. 6 that if the foregoing conditions hold, then the root-mean-square stress σ induced at a given location in a structure (or panel) by a random pressure field may be expressed in terms of the stress σ_o induced at that same location by a uniformly distributed static pressure of unit magnitude as

$$\sigma = \sqrt{\frac{\pi}{2\eta} f_n \Phi_p(f_n)}\ \sigma_o \ . \tag{29}$$

Here η represents the structural loss factor (of the dominant mode at its resonance), f_n denotes the (cyclic) resonance frequency of the dominant mode, and $\Phi_p(f_n)$ represents the spectral density of the exciting pressure at the frequency f_n.

Resonance frequencies of flat rectangular panels. – A method for determining the natural frequencies of multi-bay systems, taking into account the flexural and torsional stiffnesses of the various stringers, is presented in Ref. 7. An alternate method, applicable to structures with many equi-spaced identical stringers between flexurally stiff frames, is summarized in Ref. 8. These methods, however, are relatively complex; – perhaps too complex for preliminary design purposes. It is likely also

corresponds to the previously chosen reference values and to the reference frequency f_{ref} = 100 Hz. Substitution of Eq. (20) then yields

$$L_{s,hi\ freq} = 153.5 + 50 \log\left(\frac{U_o}{U_{ref}}\right) - 10 \log\left(\frac{X}{X_{ref}}\right) - 20 \log\left(\frac{f}{f_{ref}}\right) - 20 \log \frac{T_o + 460}{520} \quad (28)$$

Overall fluctuating pressure level. – The overall fluctuating pressure level L_{OA} is a logarithmic measure (expressed in decibels) of the mean-square fluctuating pressure $\overline{p^2}$, defined as*

$$L_{OA} = 10 \log (\overline{p^2}/p^2_{ref}), \text{ dB} \tag{17}$$

where p_{ref} is a reference pressure. Substitution of Eq. (13) into the above then permits one to write

$$L_{OA} = C + 20 \log (\rho_o/\rho_{ref}) + 40 \log (U_o/U_{ref}) \tag{18}$$

where ρ_{ref} and U_{ref} are reference values of the density and velocity, and

$$C = 20 \log (0.24\rho_{ref}U^2_{ref}/p_{ref}), \text{ dB} . \tag{19}$$

If one chooses $\rho_{ref} = 0.0735$ lb/ft^3 (corresponding to air at at room temperature and one atmosphere), $U_{ref} = 750$ ft/sec (a typical core engine exhaust velocity), and $p_{ref} = 2.9 \times 10^{-9}$ psi (= 0.0002 microbar, the international standard reference value for acoustic pressures), one obtains $C \approx 177.5$ dB.

Since the density of a gas is inversely proportional to its absolute temperature, one may replace the density ratio of Eq. (18) by a corresponding temperature ratio and write

$$L_{OA} \approx 177.5 + 40 \log \left(\frac{U_o}{U_{ref}}\right) - 20 \log \frac{T_o + 460}{520} , \tag{20}$$

where T_o represents the temperature of the exhaust stream in °F.

Pressure spectrum level. – The spectrum level of the fluctuating pressure is a logarithmic measure (expressed in decibels) of the spectral density $\Phi_p(f)$, defined as

$$L_s = 10 \log \left[\frac{\Phi_p(f)}{\Phi_{p,ref}(f)}\right] \tag{21}$$

where $\Phi_{p,ref}(f)$ is an appropriate reference value, usually taken as p^2_{ref}/Hz.

---

*All logarithms in this report are base 10.

which show how $\sqrt{\overline{p^2}}/q$ varies in the stream-wise and cross-wise directions along a plate inclined at various angles to an impinging jet, one finds that $\sqrt{\overline{p^2}}/q$ does not exceed 0.1 for $X/D \geq 9$ and for angles between the plate surface and flow-normal greater than 30°. This value of 0.1 is considerably smaller than the value of $\sqrt{\overline{p^2}}/q = 4I \approx 4(0.12) = 0.48$ one obtains from Eq. (5) for a normally impinging jet with the near-maximum turbulence intensity I = 0.12.

The frequency-spectral density $\Phi_p(\omega)$ of the fluctuating pressures associated with nearly tangential flows may again be approximated by Eqs. (7) and (8). The pressure cross-correlation function here is more complex, however, being characterized (see Appendix A) by different correlation lengths (or "eddy decay scales") L_x and L_y in the stream-wise and transverse directions, with

$$L_x \approx 13.5\ V_c/\omega$$
$$L_y \approx 2.0\ V_c/\omega \quad , \tag{11}$$

where

$$V_c \approx 0.45\ U_o \tag{12}$$

represents the convection velocity of the flow.

Design Pressures and Pressure Levels

Maximum mean-square pressure. — Although one may use the data shown in Figs. 3-6, together with the previously given equations, to estimate the fluctuating pressures that occur at any specific location, one usually need not consider all this detail for design purposes. By inspection of Figs. 3 and 4 one finds that for $8 \leq X/D \leq 20$, corresponding to typical locations where EBF surfaces may be expected to be placed normal to the flow, the turbulence intensity does not exceed 0.12. Since one also may note that in the high-turbulence region (i.e. for $r/D \leq 1$) the turbulence intensity decreases slowly with X/D, approximately according to Eq. (3), one may choose I = 0.12 for general conservative design purposes.

varies along the axis of a jet, and Fig. 4 shows how this intensity varies along the radial coordinate. Here U_o represents the jet exit velocity (which, for a fan-jet engine is taken to be the core engine exit velocity) and $\overline{u^2}$ denotes the mean-square axial fluctuating velocity.

As is evident from Fig. 3, the intensity I on the jet axis is at approximately its maximum value of 0.11 at X/D ≈ 10. Figure 4 shows that for X/D ≥ 8, I does not exceed approximately 0.12. From examination of the peak values of Fig. 4 one may determine, in fact, that for X/D > 9, the maximum value of I obeys

$$I_{max} \approx 0.165 - 0.0044\ X/D \qquad (3)$$

and occurs at a radial coordinate r_{peak}, given by

$$\frac{r_{peak}}{D} \approx 0.15\ \frac{X}{D} - 1.0 \qquad (4)$$

The velocity and pressure fluctuations within the potential core typically are much smaller than those in the flow outside the core. Thus, for the regions of interest with respect to blown flaps, I ≈ 0.12 may be expected to represent an upper bound suitable for conservative design purposes.

Pressure Fluctuations on Flap Surfaces

Normally Impinging Jets. — For flap surfaces on which the jet flow impinges essentially normally, one may take the momentum flux in the flow to be annihilated at the structural surface. With this assumption, the mean-square fluctuating pressure $\overline{p^2}$ is found to be related to the mean-square fluctuating velocity $\overline{u^2}$ (see Appendix A) as

$$\overline{p^2} = 4\rho^2 U^2 \overline{u^2} \approx (4qI)^2 \ , \qquad (5)$$

where ρ denotes the local fluid density and U the local mean velocity. For most locations of interest for EBF's, the local velocity U is nearly equal to the exit velocity U_o and the local gas density ρ differs little from the density ρ_o at the exit. With these assumptions one obtains the above indicated approximate equality, where

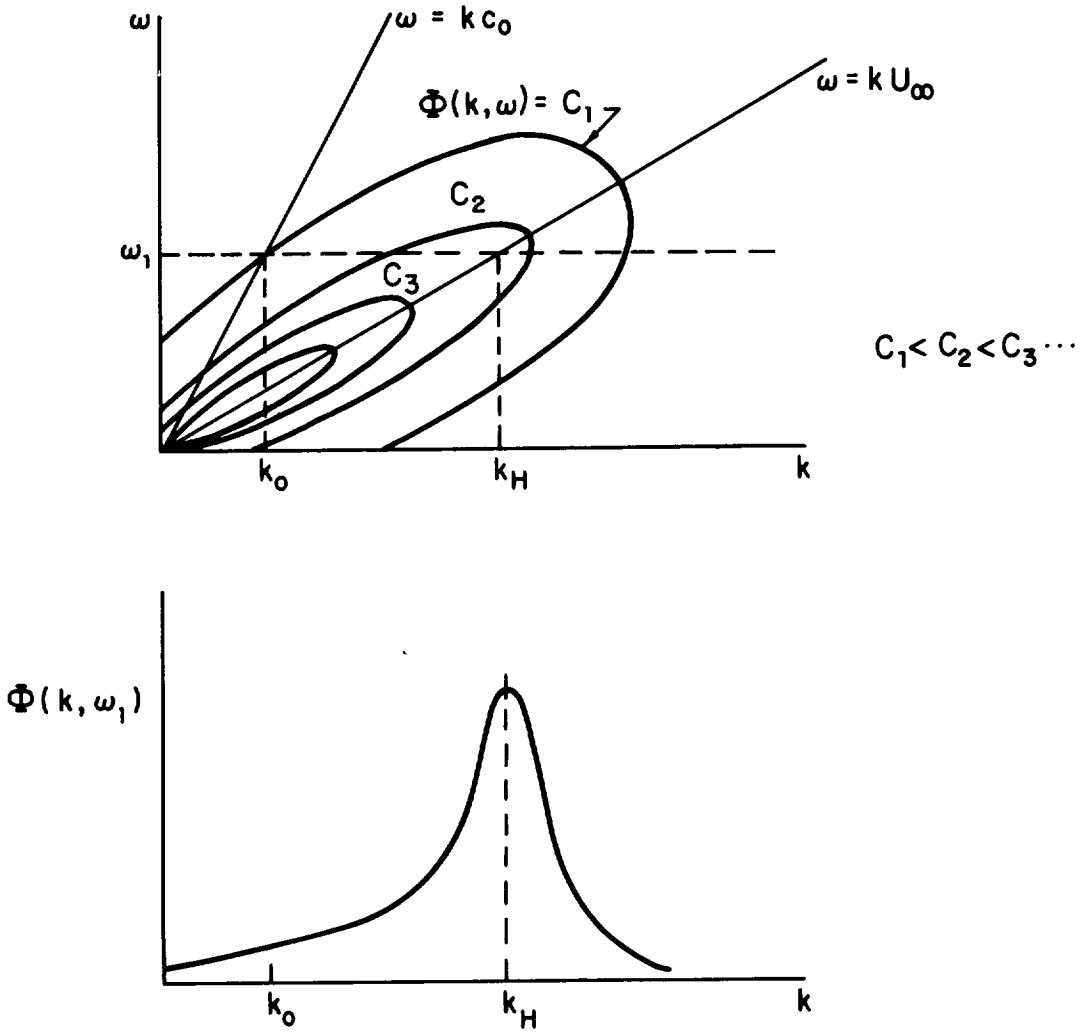

FIG. 19 TYPICAL BEHAVIOR OF SURFACE PRESSURE SPECTRAL DENSITY $\Phi(k,\omega)$ ASSOCIATED WITH TURBULENT FLOW.

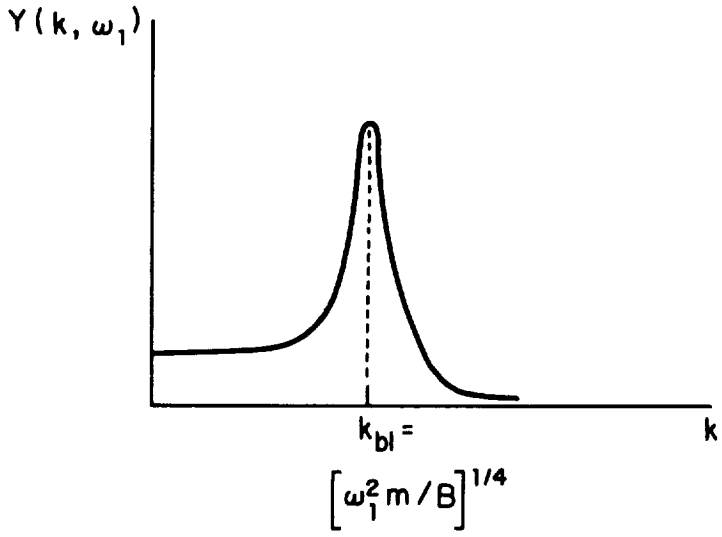

FIG. 21 ADMITTANCE Y OF UNIFORM BEAM AT FREQUENCY ω_1.

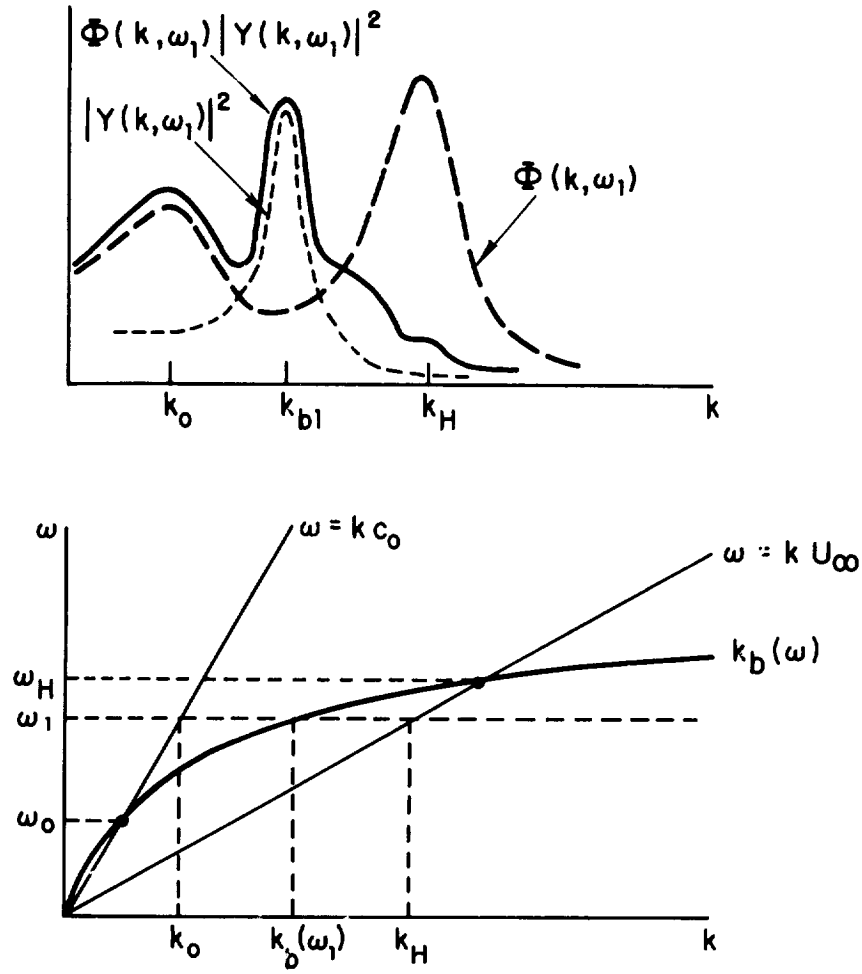

FIG. 22 CHARACTERISTICS OF BEAM RESPONSE TO JET NOISE AND FLOW EXCITATION.

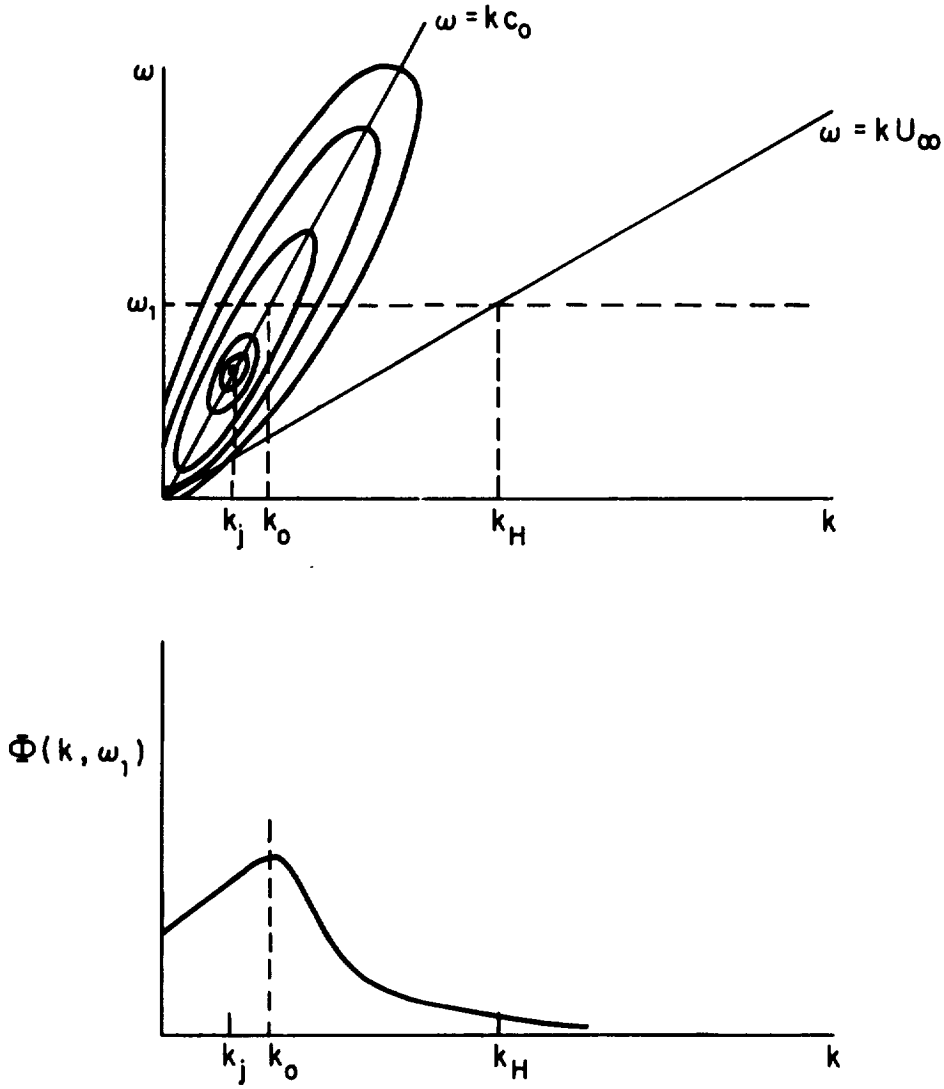

FIG. 20 TYPICAL BEHAVIOR OF SURFACE PRESSURE SPECTRAL DENSITY $\Phi(k,\omega)$ ASSOCIATED WITH JET NOISE.

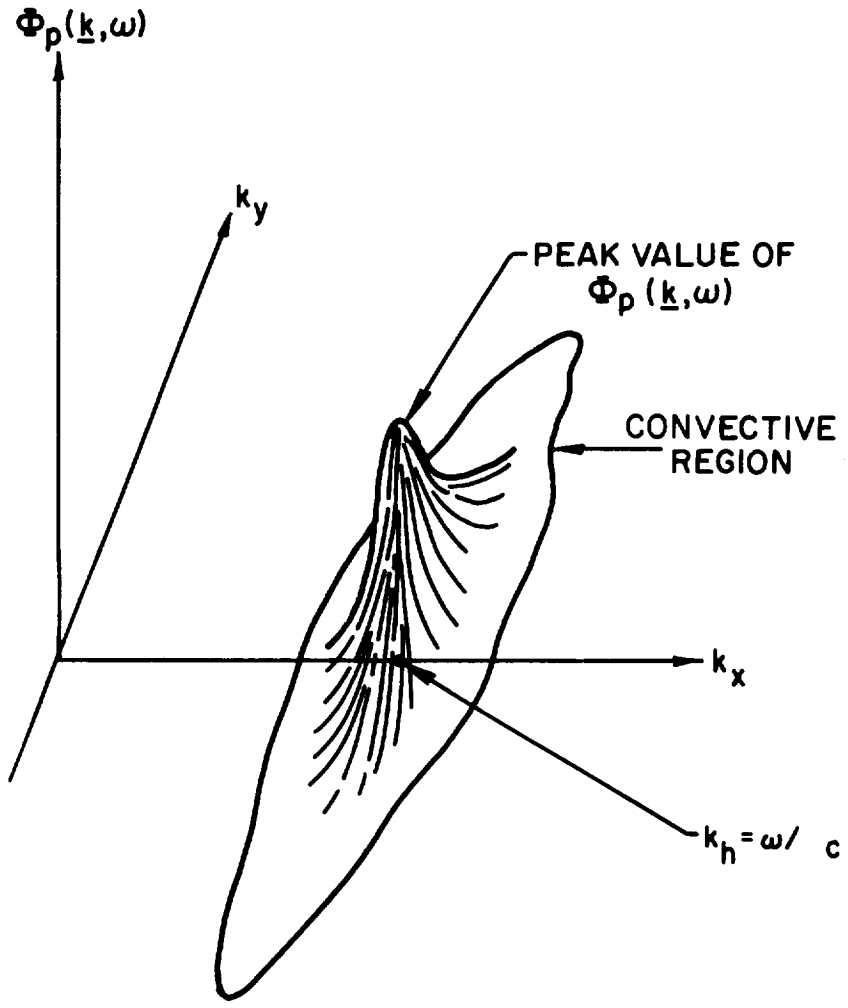

FIG. 18 VARIATION OF PRESSURE SPECTRUM $\phi_p(k,\omega)$ AT CONSTANT FREQUENCY ω.

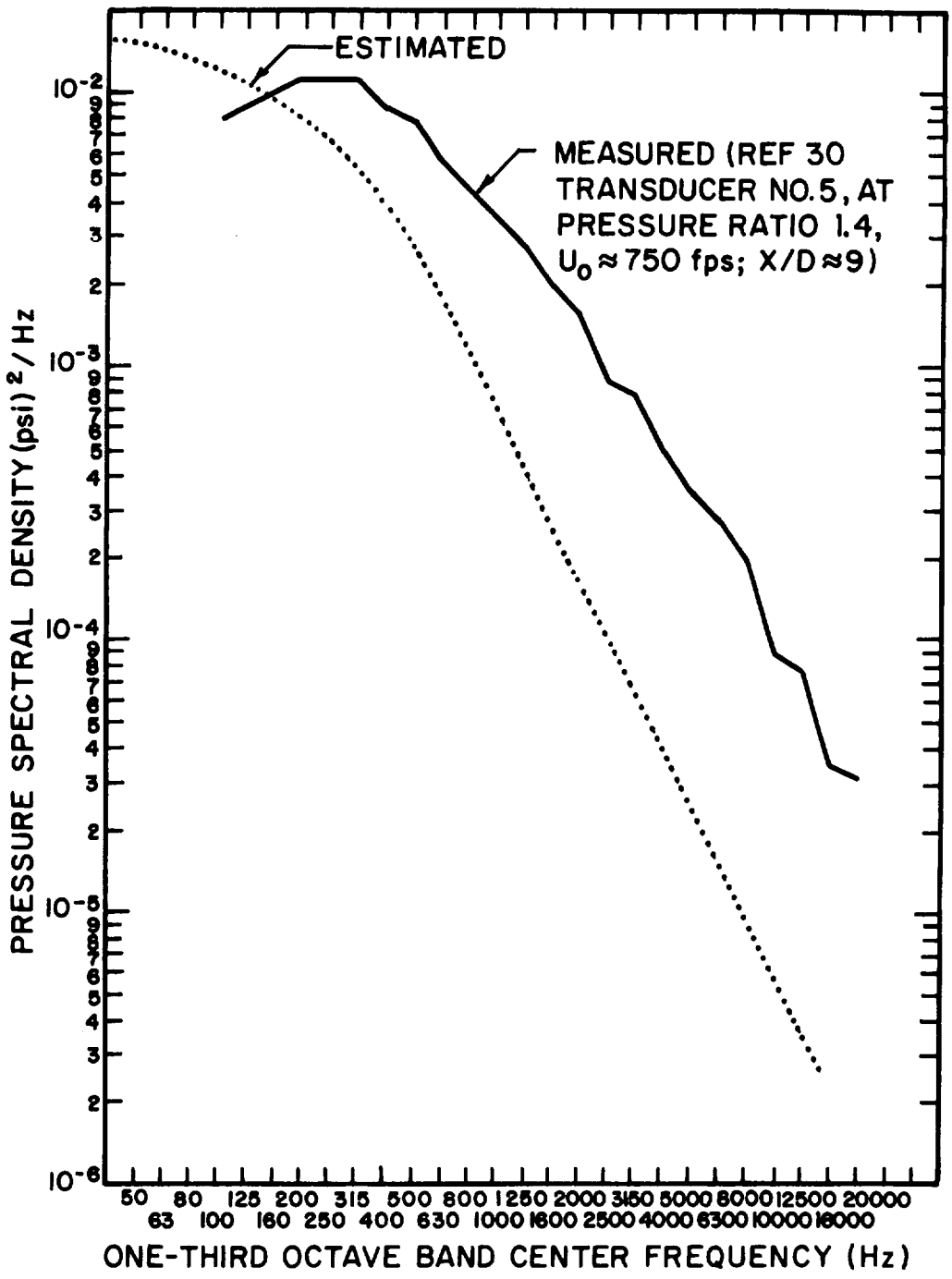

FIG. 13 COMPARISON OF ESTIMATED AND MEASURED PRESSURE SPECTRAL DENSITY.

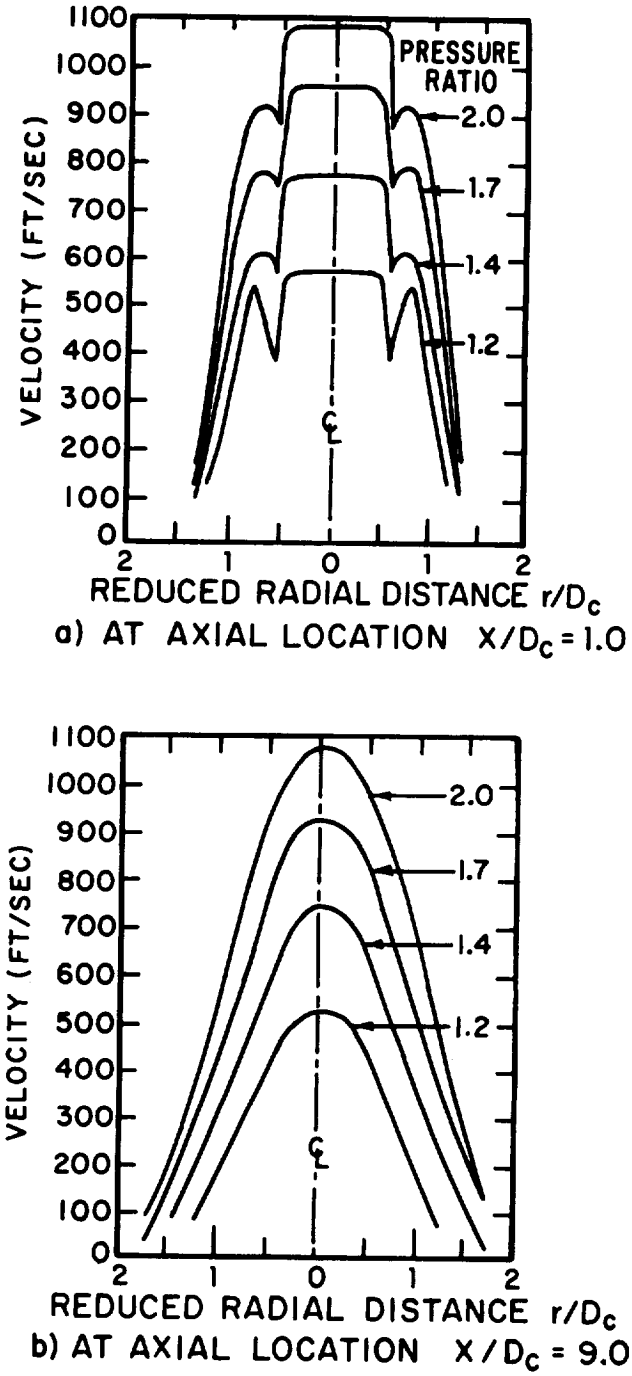

FIG.14 BYPASS NOZZLE EXHAUST VELOCITY PROFILES FOR VARIOUS PRESSURE RATIOS; CORE NOZZLE DIAMETER D_C= 8 in., BYPASS RATIO ≈ 6, (AFTER REF.1)

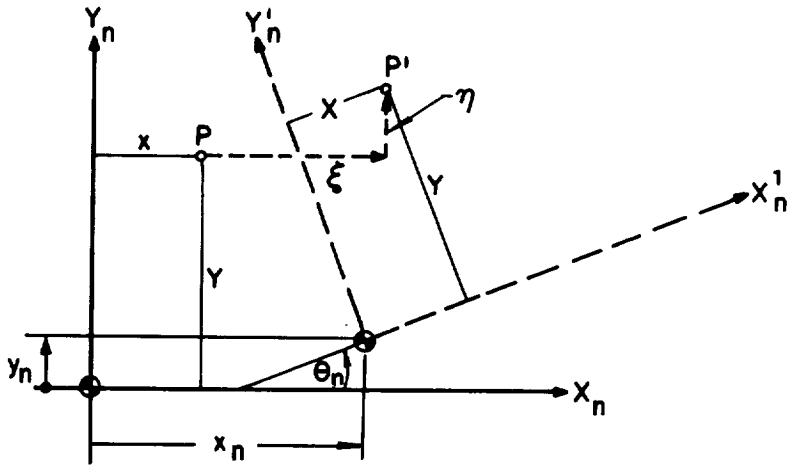

FIG. 12 DISPLACEMENTS (ξ,η) OF TYPICAL POINT ON FLAP ELEMENT DUE TO DISPLACEMENTS (x_n, y_n, θ_n) OF FLAP ELEMENT.

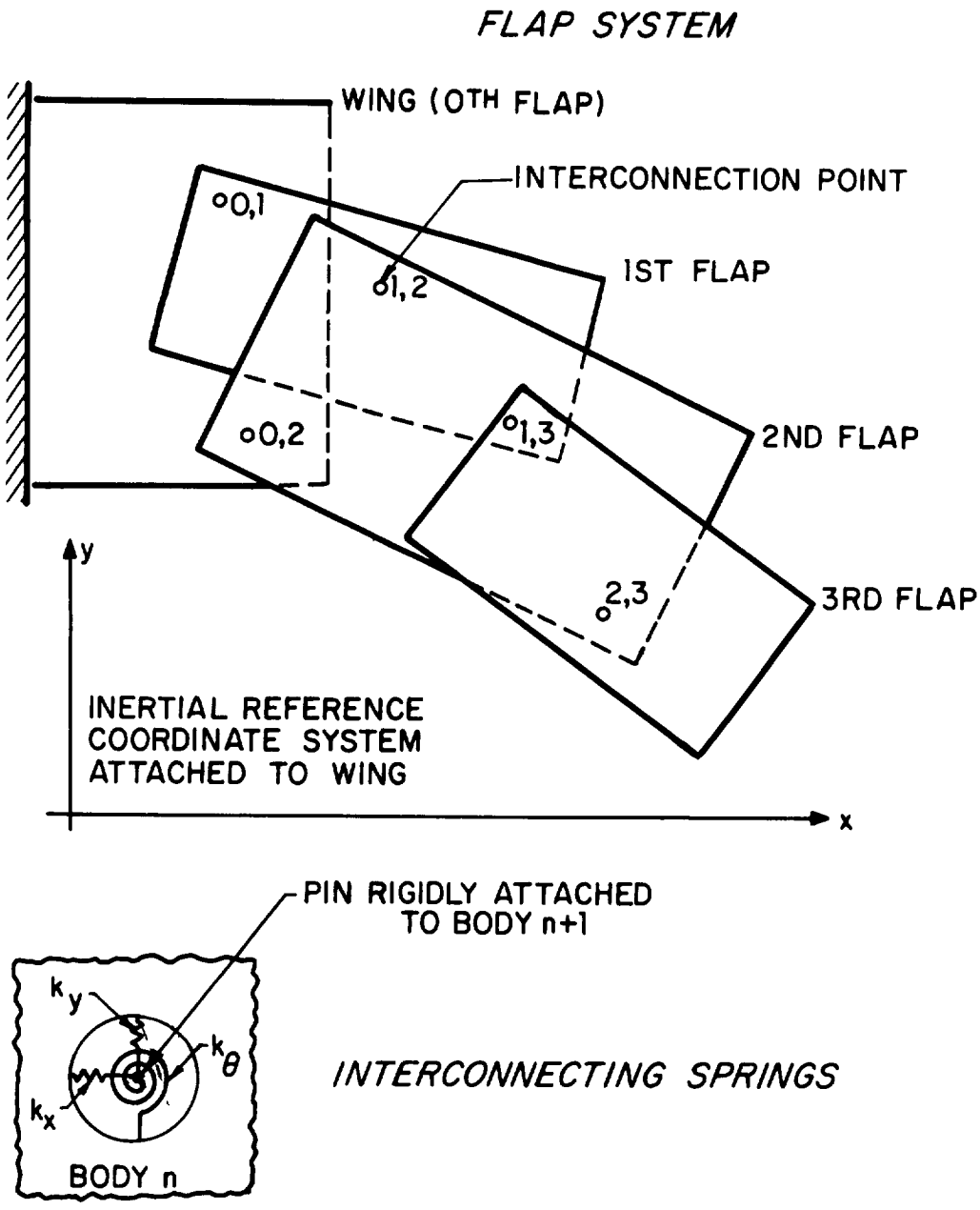

FIG. 10 TYPICAL TWO-DIMENSIONAL IDEALIZATION OF FLAP SYSTEM, AS INTERCONNECTED RIGID BODIES.

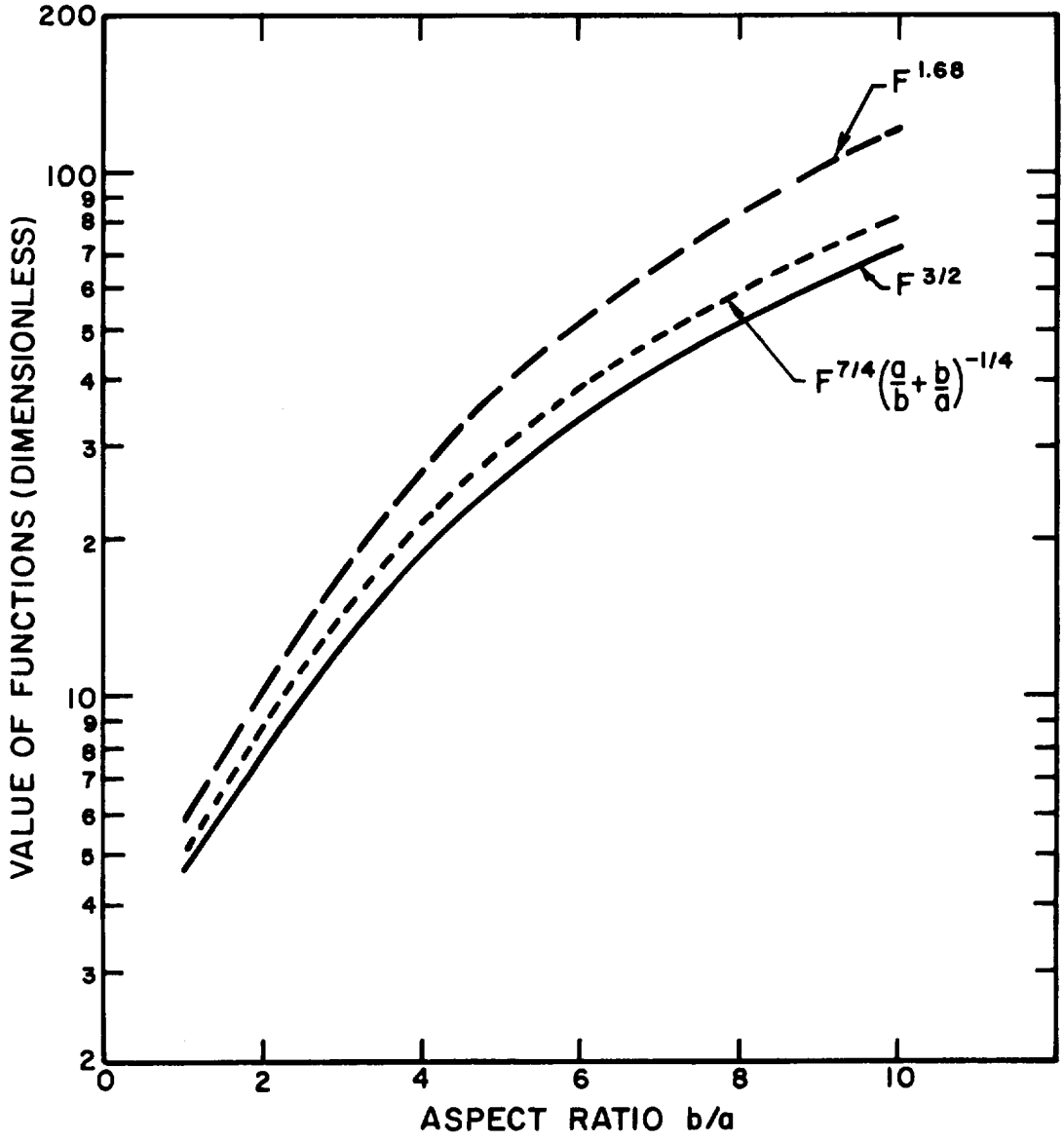

FIG. 8. COMPARISON OF PANEL STRESS ESTIMATES.

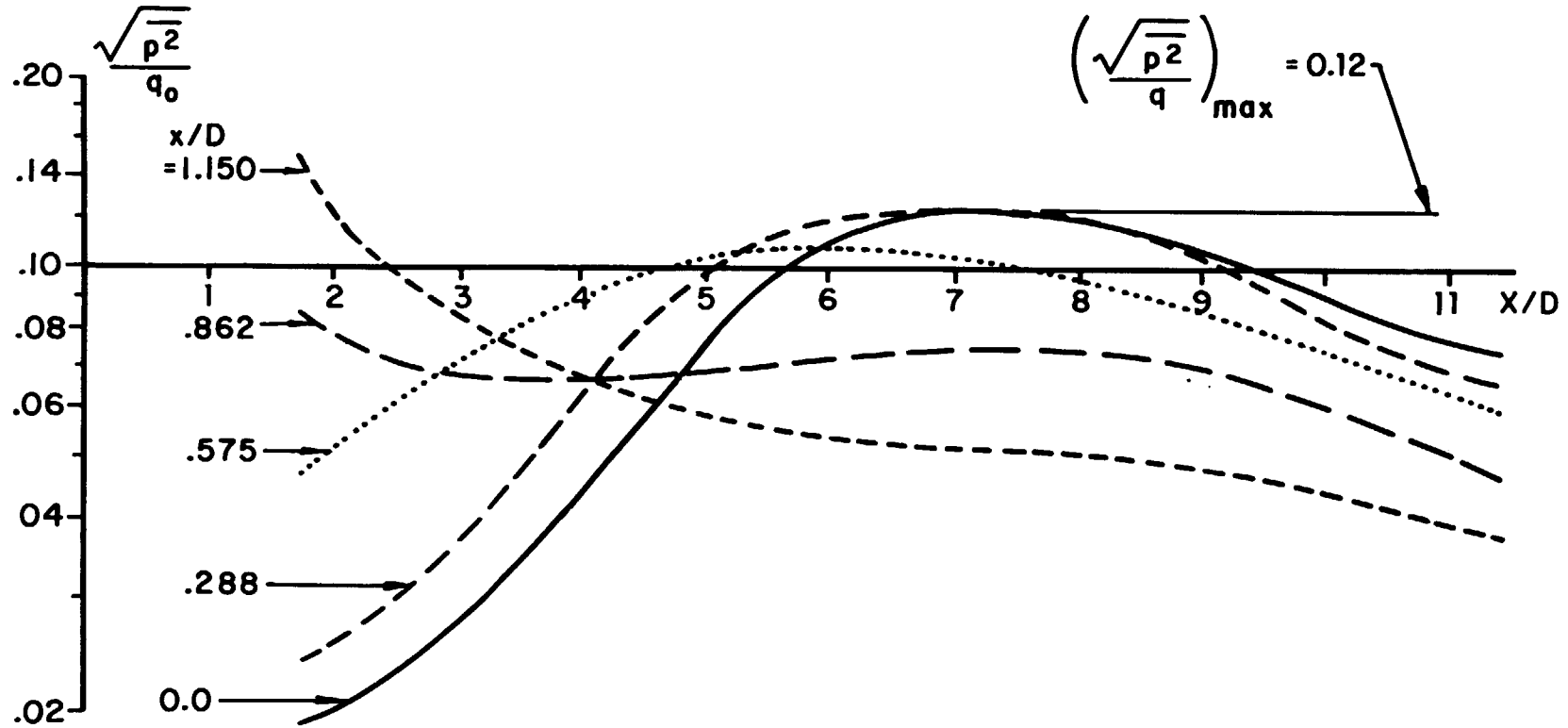

NOTE:
IF MOMENTUM FLUX ANNIHILATION HOLDS (SEE p57), THEN THE TURBULENCE INTENSITY OBEYS $I = \sqrt{\overline{u^2}}/U_o = 4\sqrt{\overline{p^2}}/q$

FIG. 6. VARIATION OF SURFACE PRESSURE FLUCTUATION ON A FLAT PLATE DUE TO NORMAL JET IMPINGEMENT (θ = 0°) WITH X/D, AT SEVERAL LOCATIONS ALONG PLATE (FROM REF. 5).

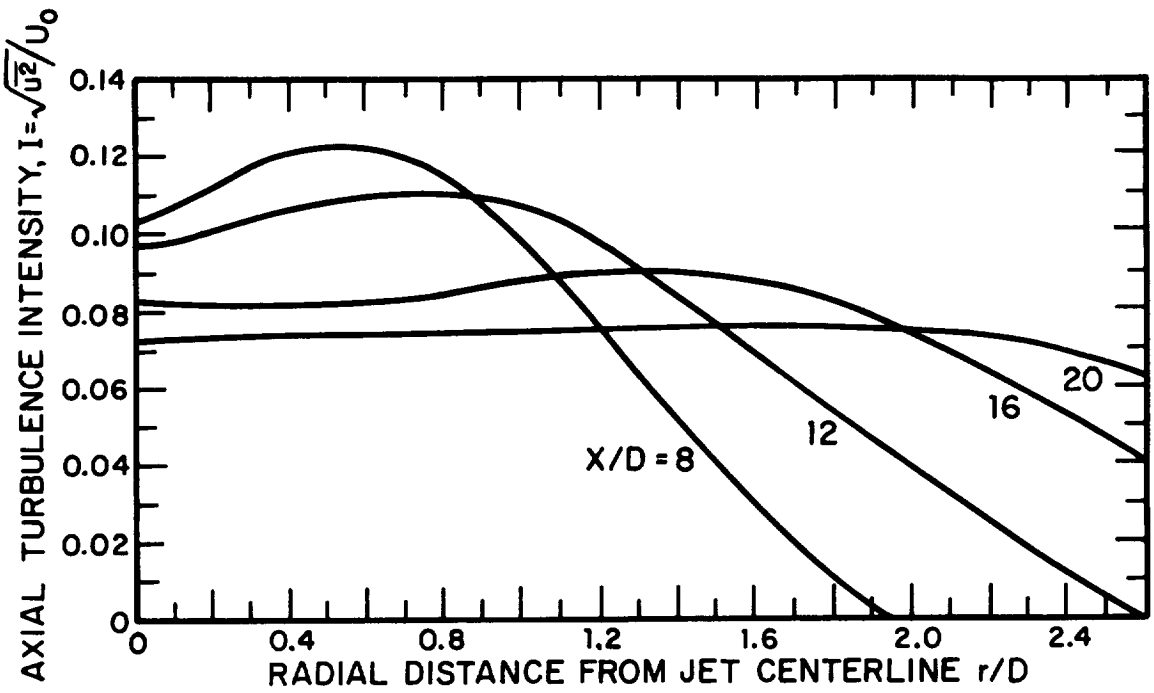

FIG. 4. VARIATION OF AXIAL TURBULENCE INTENSITY WITH DISTANCE FROM JET CENTERLINE (FROM REF. 4).

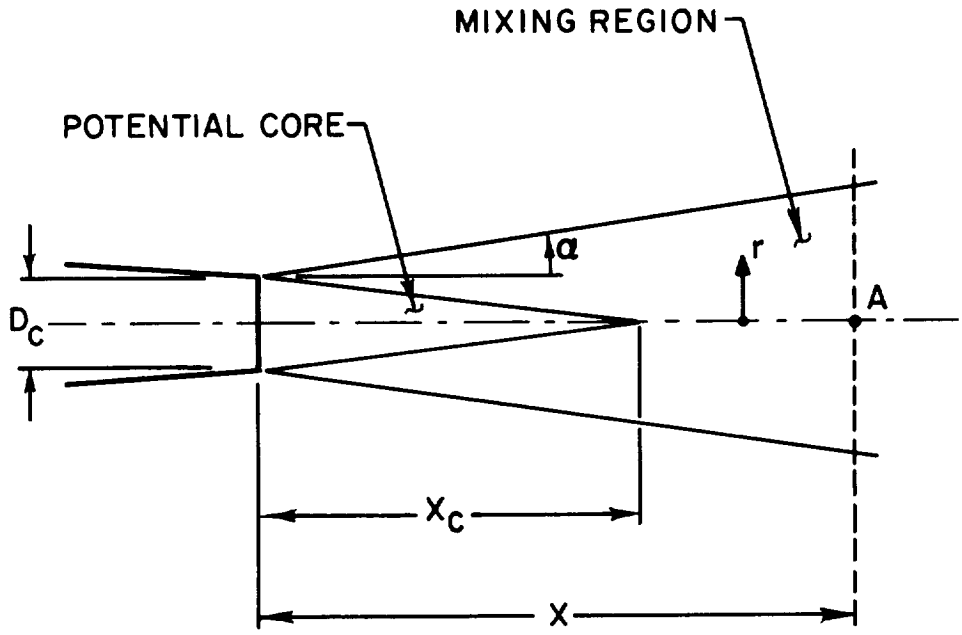

FIG. 2. CONFIGURATION OF IDEAL JET.

TABLE III. – FACTORS BY WHICH FACING SHEET FATIGUE LIFE CHANGES FOR GIVEN CHANGES IN PARAMETERS

Factor Change In Parameter	0.50	0.80	0.90	1.10	1.20	1.50	2.00
B	0.042	0.36	0.62	1.55	2.3	6.4	24.
η, X	0.24	0.64	0.81	1.21	1.45	2.3	4.1
μ	1.4	1.12	1.05	0.95	0.91	0.81	0.70
L	1.9×10^{4}	24	4.5	0.26	0.052	3.0×10^{-3}	5.0×10^{-5}
e, c, E, ρ_o	17.	2.5	1.53	0.68	0.48	0.19	0.060
U_o	1.2×10^{3}	9.7	2.9	0.38	0.16	0.016	9.0×10^{-4}

TABLE IV. – FACTORS BY WHICH CORE FATIGUE LIFE CHANGES

Frequency Change In Parameter	0.50	0.80	0.90	1.10	1.20	1.50	2.00
d	6.5×10^{-4}	0.094	0.33	2.7	6.9	74	3100
(A/e)	7.6×10^{-3}	0.21	0.43	1.94	3.6	17.5	130
η, X	0.088	0.46	0.69	1.39	6.4	4.2	11.4
L	4.5×10^{3}	15	3.6	0.32	0.11	7.4×10^{-3}	7.6×10^{-4}
(μ/B)	2.4	1.32	1.14	0.88	0.79	0.60	0.42
ρ_o	130	4.8	2.1	0.51	0.28	0.058	7.6×10^{-3}
U_o	2.0×10^{5}	52	6.4	0.19	0.040	7.7×10^{-4}	5.0×10^{-6}

25. R.E.D. Bishop and D.C. Johnson, *Vibration Analysis Tables*, Cambridge University Press, Cambridge, 1956.

26. C.E. Wallace, "Stress Response and Fatigue Life of Acoustically Excited Sandwidh Panels". *Acoustical Fatigue in Aerospace Structures*, W.J. Trapp and D.M. Forney, Jr., Eds., Syracuse University Press 1965 , pp. 228-244.

27. P. Bradshaw, D.H. Ferris, and R.F. Johnson, "Turbulence in the Noise-Producing Region of a Circular Jet," AGARD Rept. No. 450, April 1963.

28. D.C. Wodten, C.E. Wooldridge, A.J. Amaro, and G.R. Plapp, "A Study of the Structure of Jet Turbulence Producing Jet Noise," NASA-CR-1836, July 1971.

29. K.L. Chandiramani, "Fundamentals Regarding Spectral Representation of Random Fields - Application to Wall Pressure Field Beneath a Turbulent Boundary Layer," BBN Rept. No. 1728, Sept. 1968.

30. J.C. Hardin, W. Kreim, and R. Dorsch, "Dynamic Pressure Measurements on a Half-Scale Externally Blown Flap Model," Langley Working Paper 989, Part E, Sept. 1971.

31. W.A. Olsen, R.G. Dorsch, and J.H. Miles, "Noise Produced by a Small Scale, Externally Blown Flap", NASA TN-D-6636, March 1972.

32. G.M. Corcos, "The Structure of the Turbulent Pressure Field in Boundary-Layer Flows," *J. Fluid Mech.*18, 353-378 March 1964 .

33. P.R. McGowan, et al "Structural Design for Acoustic Fatigue", ASD-TDR-63-820, October 1963. Fig. 48, p. 92.

34. Anon., *Strength of Metal Aircraft Elements*, MIL-HDBK-5, March 1961. Armed Forces Supply Support Center, Washington, D.C.

35. V.M. Faires, *Design of Machine Elements*, 3rd ed., The Macmillan Co., New York, 1955. Chap. IV.

REFERENCES

1. R.G. Dursch, W.J. Kreim, and W.A. Olsen, "Externally Blown Flap Noise," AIAA Paper No. 72-129, Jan. 1972.

2. L.C. Sutherland *et al*, "Sonic and Vibration Environments for Ground Facilities – A Design Manual," Wyle Laboratories, Research Staff Report No. WR 68-2 (Contract NAS8-11217), pp. 6-13, March 1968.

3. L.D. Landau and E.M. Lifshitz, *Fluid Mechanics*, Perganon Press, p. 133, London, 1959.

4. J.C. Laurence, "Intensity Scale and Spectra of Turbulence in Mixing Region of Free Subsonic Jet," Lewis Flight Propulsion Laboratory, Cleveland, Ohio, Report No. 1292.

5. D.R. Strong, T.E. Siddon, and W.T. Chu, "Pressure Fluctuations on a Flat Plate With Oblique Jet Impingement," UTIAS Note No. 107, Feb. 1967.

6. B.L. Clarkson, "Stresses in Skin Panels Subjected to Random Acoustic Loading," AFML-TR-67-199, June 1967.

7. F.F. Rudder, Jr., "Acoustic Fatigue of Aircraft Structural Component Assemblies," AFFDL-TR-71-107, Feb. 1972.

8. A.G.R. Thomson, "Acoustic Fatigue Design Data, Part I," AGARDograph 162, May 1972.

9. J.R. Ballentine, F.F. Rudder, Jr., J.T. Mathis, and H.E. Plumblee, Jr., "Refinement of Sonic Fatigue Structural Design Criteria," AFFDL-TR-67-156, Jan. 1968.

10. L.W. Lassiter and R.W. Hess, "Calculated and Measured Stresses in Simple Panels Subject to Intense Random Acoustic Loading Including the Near Noise Field of a Turbojet Engine," NACA Report No. 1367 1958 .

11. J.F. Wilby, "Random Excitation of a Simple Panel, Some Experimental Results," University of Southampton, AASU Report No. 231, Jan. 1963.

12. J.R. Ballentine, H.E. Plumblee, Jr., and C.W. Schneider, "Sonic Fatigue in Combined Environment," AFFDL-TR-66-7, May 1966.

Response Calculation

Beam. – For the purpose of illustrating the general technique, it is again convenient to discuss the response of a uniform beam. Treatment of more complex structures involves no different concepts, only more intricate calculations.

From the definitions of the admittance and of the pressure spectral density, one finds that the mean-square velocity of the beam at any given frequency ω_1 obeys

$$\overline{v^2(\omega_1)} = \frac{1}{2\pi} \int_{-\infty}^{\infty} \Phi(k,\omega_1) |Y(k,\omega_1)|^2 \, dk \qquad (8)$$

Thus, if one knows both $\Phi(k,\omega)$ and $Y(k,\omega)$, one may calculate the mean-square velocity at any frequency.

Because the two functions appearing in the integrand typically have pronounced peaks, these peak values usually dominate the response, permitting one readily to obtain simple approximations for the integral. Figure 22 illustrates this behavior for a one-dimensional structure subject to simultaneous jet noise and turbulent flow excitation.

The upper part of this figure shows a sketch of the pressure spectral density function, which for this simultaneous excitation consists of the sum of the functions due to the separate excitations (see Figs. 19 and 20). Thus, the density function here exhibits one peak at the acoustic wavenumber k_o (at the frequency ω_1 under consideration), and a second peak at the hydrodynamic wavenumber k_H. Also shown is the square of the admittance function (see Fig. 21) and the product of these two functions, which is the integrand of Eq. (8). The relative magnitudes and locations of these peaks, of course, depend on the relative strengths of the two excitation sources, on the structural damping, on the structural mass and stiffness, on the flow speed relative to the speed of sound, and also on the frequency.

A k,ω plot like that shown in the lower portion of Fig. 22 permits one to obtain considerable insight into the variation of the positions of these peaks. As previously discussed in connection with Figs. 19 and 20, the pressure spectral peaks occur at the acoustic and hydrodynamic wavenumbers, which correspond to intersections of the acoustic and flow velocity lines, respectively, with the fixed frequency line $\omega = \omega_1$. Similarly, the admittance peak occurs at the wavenumber $k_{b1} = k_b(\omega_1)$; this wavenumber

Surface Pressures due to Jet Noise. — The typical behavior of the spectral density associated with surface pressures produced by jet noise is indicated in Fig. 20. One may note that the contour plot here is much like that of Fig. 19, except that the contour lines here cluster about the $\omega = kc_o$ line, indicating that most of the energy associated with jet-noise-induced surface pressures travels at the speed of sound.

If all of the sound from the jet would impinge on the surface at grazing incidence, all of the contour lines would collapse upon the c_o line. In practice, however, a flap surface is subject to sound arriving with a distribution of angles of incidence, as well as to acoustic nearfield components, so that there occurs a distribution of energy about the sound speed line. Nevertheless, the peak in the spectral density at a given frequency ω_1 occurs at the acoustic wavenumber $k_o = \omega_1/c_o$.

The peak of the $\Phi(k,\omega)$ hill is a noteworthy feature. It represents a concentration of fluctuating-pressure energy that generally is important for structural fatigue and noise considerations, and it occurs at the jet wavenumber $k_j \approx 2\pi/D_j$, where D_j represents the jet diameter.

Spectral Characterization of Structural Response

Admittance of Beam. — It is instructive to illustrate application of the spectral response characterization for a one-dimensional system, such as a beam or one-dimensional plate deforming in flexure; generalization to two-dimensional systems then can be accomplished relatively simply. The well-known equation of flexural motion of a uniform beam is

$$B \frac{\partial^4 y}{\partial x^4} + m \frac{\partial^2 y}{\partial t^2} = p(x,t) \ , \qquad (4)$$

where y represents the beam's lateral displacement, B denotes its flexural rigidity, and m its mass per unit area. On the right-hand side there appears the exciting load per unit length p(x,t),which is a function of the axial coordinate x and time t.

the most extreme case, the structural response calculation then involves the same mathematical process as for more conventional space-time descriptions – namely, convolution of a spatial structural kernel with a load cross-correlation function. At worst, the STSD approach leads to no more complexity than other approaches.

Spectral Description of Random Pressures

Spectral Densities. – From classical Fourier analysis it follows that a pressure wave that is harmonic over all space and time can be represented (in terms of the usual complex variable notation) by an amplitude and an exponential phase factor. It is also well known that a general pressure function can be represented as an infinite sum of such harmonic waves; this representation is called the Fourier transform.

A pressure wave that is periodic in space and time, that travels with velocity U in the positive x-direction, and that passes any fixed point at the (radian) frequency ω, thus may be described by

$$p(k,\omega)e^{i(kx-\omega t)} ,$$

where $p(k,\omega)$ denotes the amplitude of the wave and

$$k = \omega/U \tag{1}$$

is known as the wavenumber. Generalized harmonic analysis permits any arbitrary random pressure $p(x,t)$ to be represented by

$$p(x,t) = \frac{1}{(2\pi)^2}\int_{-\infty}^{\infty}\int_{-\infty}^{\infty} \tilde{p}(k,\omega)e^{i(kx-\omega t)}dkd\omega, \tag{2}$$

where $\tilde{p}(k,\omega)$, the density of the amplitude distribution in k and ω space, is the Fourier transform of $p(x,t)$.

From the square of the magnitude of this density one may determine the so-called pressure spectral density

APPENDIX D

AN INTRODUCTION TO THE SPACE-TIME SPECTRAL DENSITY APPROACH TO EXCITATION AND RESPONSE CHARACTERIZATION

Introduction

As has been pointed out in the main body of this report, the responses of flap structures to fluctuating pressures depend not only on the temporal (frequency) characteristics of these pressures, but also on their spatial characteristics. The presently available sonic fatigue analysis and design approaches, including those summarized in the main body of this report, avoid the complexities associated with accounting for the spatial characteristics by making the assumption that the exciting pressures are uniformly distributed over the structure under consideration and that the structure's most significant response occurs in its fundamental mode. Although this assumption often leads to conservative designs, one may readily show that it need not in all cases — and, indeed, there exists some flight data (e.g., Refs. 15 and 16) that indicate that the structural responses are not described adequately by the sonic fatigue analysis approaches in current use.

This appendix serves as a brief introduction to an approach which should be able to provide a logical framework for the guidance of data acquisition programs for load and response characterization, and which also may be expected to lead to more realistic predictions. This approach, which makes use of space-time spectral density (STSD) concepts, has been developed quite extensively for dealing with the vibrations of ship structures induced by sound and flow (and with the underwater sound radiated by these vibrations), and has been applied to such problems with considerable success. As discussed below, it has the additional advantages of being relatively simple in concept, of leading to little computational difficulty, of permitting great experimental simplification and savings, and of leading to increased accuracy.

Conceptual and Computational Simplicity. - For spatially homogeneous excitation, the STSD approach permits one to calculate the structural response as an integral over the product of two functions, of which one characterizes the fluctuating pressure, the other,the dynamic stiffness of the structure. The

given by Eq. (6). The exponent β, of course, depends on the component – i.e., on which of the aforementioned equations apply. The table at the end of this appendix gives the correction factors corresponding to these equations and to a wide variety of aluminum alloys.

Estimation of Fatigue Stress Ratio. – Unfortunately, S-N curves are available for only a few alloys. For alloys for which no fatigue data are available, one may use the rough approximation that

$$\frac{S_2}{S_1} \approx \frac{Y_2}{Y_1} \tag{7}$$

where Y represents the yield stress of the material (Ref. 35). As evident from the table at the end of this appendix, this approximation is very close for some materials, but may be about 20% too high or too low for others. Nevertheless, in absence of better information, one can do no better than to use the above relation. The correction factors given in the table below are based on fatigue stress ratios where these are available, and on yield stress ratios otherwise.

Materials Other Than Aluminum. – It should be noted that the procedure suggested here for aluminum alloys cannot readily be extended to other materials, unless their S-N curves have the same slopes (on a log-log plot) as those for aluminum. Unfortunately, most other materials have different slopes and many – notably steels – have segments of greatly differing slopes. For such materials, further analysis and/or experimental investigation is required.

APPENDIX C

FATIGUE LIFE CORRECTIONS FOR ALUMINUM ALLOYS

The various fatigue life estimates presented in the main text were obtained on the basis of experimental data on structures made of only one kind of material — namely, 7075-T6 aluminum for skin/stringer structures and for the facing sheets of honeycomb sandwich structures, and 5052-H39 aluminum for honeycomb cores. This appendix suggests how one may correct the estimates pertaining to the aforementioned materials so as to obtain corresponding estimates for other aluminum alloys.

Similarity of S-N Curves. — The fatigue behavior of materials generally is described by so-called "S-N" curves, which are plots of the fully reversed stress amplitude S versus the number of stress cycles N at which a specimen fails when subjected to cyclic stress of that amplitude. When plotted on log-log scales, the S-N curves for most aluminum alloys appear very nearly like parallel straight lines, at least in the low stress and large N region [E.g., see Ref. 33 and Table 3.3.1(c) of Ref. 34]. Although the classical S-N curves are obtained from experiments where the stress amplitude is held constant (for each data point), whereas the S-N curves represented by Eqs. (45), (52), (71) and (75) correspond to random stress variations with a given mean-square value, one may expect the latter log-log curves for various alloys to be parallel, if the former are parallel.

If one assumes that the root-mean-square stress σ that different alloys can withstand for a given number of cycles is proportional to the "fatigue stress" S of the material, then for two different materials (indicated by subscripts 1 and 2),

$$\frac{\sigma_2}{\sigma_1} = \frac{S_2}{S_1} \quad . \tag{1}*$$

For materials that exhibit a definite endurance limit (i.e., a stress amplitude that the material can withstand essentially for an unlimited number of cycles), one would be inclined to

---

*For the sake of simplicity, new equation numbering sequences are begun in each appendix. All equation numbers mentioned in this appendix refer to equations presented in this appendix.

where G denotes the effective shear modulus of the core (considered as a continuum) and A represents the beam's cross-sectional area. By equating Eqs. (3) and (4) and integrating the result one may determine that

$$w_s = \frac{-B}{AG} w_b'' \quad . \tag{5}$$

Fundamental Natural Frequency. – Substitution of Eq. (5) into Eq. (2) yields

$$w_b'''' = \frac{\mu}{B} \omega^2 \left(w_b - \frac{B}{AG} w_b'' \right) \quad . \tag{6}$$

For a deflection given by

$$w_b = w_0 \sin \frac{\pi x}{L} \quad , \tag{7}$$

which corresponds to the fundamental mode of a simply supported beam, Eq. (6) yields

$$\omega = \omega_b \left(1 + \frac{\pi^2 B}{L^2 AG} \right)^{-1/2} \tag{8}$$

where

$$\omega_b = \frac{\pi^2}{L^2} \sqrt{\frac{B}{\mu}} \tag{9}$$

may be recognized as the classical expression for the natural frequency, corresponding to the case where shear effects are neglected (i.e., where AG, the shear stiffness per unit length, is assumed infinite).

Flexural and Shear Stresses. – The flexural stress in the outer-most skin fiber, taken to be a distance c from the neutral axis, may be found from elementary beam theory to be given by

$$\sigma = -Ecw_b'' = Ec(\pi/L)^2 w_0 \sin(\pi x/L) \quad , \tag{10}$$

The parameters L_x and L_y represent the eddy decay scales in the flow and transverse directions, respectively, and obey

$$L_x \approx 13.5\ V_c/|\omega| \tag{22}$$

$$L_y \approx 2\ V_c/|\omega| \tag{23}$$

The pressure field described by Eqs. (17) to (23) is the same as that associated with a turbulent boundary layer, except for the numerical constants that appear in Eqs. (21) to (23). Detailed interpretations of such fields are given in Ref. 29; some salient features are summarized below.

Because the hydrodynamic wavenumber k_h appears in the denominator of Eq. (18), the wavenumber spectrum $\Phi_x(k_x)$ is asymmetric in k_x. This asymmetry represents a mean convection of the fluctuating pressure field in the positive x-direction with a velocity V_c. The fact that L_x and L_y have finite values accounts for the decay of the correlations with increasing separation. Inverse variation of L_x and L_y with frequency (in keeping with the "similarity hypothesis" of Ref. 32) accounts for the decrease in the correlation lengths with increasing frequency.

Figure 18 indicates qualitatively how $\Phi_p(\underline{k},\omega)$ varies with k_x and k_y at a fixed value of ω. The peak value of $\Phi_p(\underline{k},\omega)$ occurs at $k_x = k_h$, $k_y = 0$. Because $L_x > L_y$, the shape of the $\Phi_p(\underline{k},\omega)$ function is much more elongated in the k_y than in the k_x direction. Since the peak occurs at the nonzero wavenumber k_h, there is a region centered around the wavenumber vector $\underline{k} = (k_h,0)$ over which $\Phi_p(\underline{k},\omega)$ has relatively high values. This region, which is important in relation to vibration response, is known as the "convective region" of the wavenumber plane; its location and extent clearly are frequency-dependent.

Comparison of estimated and measured spectral density. – The frequency spectral density $\overline{p^2}\Phi_n(\omega)$ of the fluctuating pressure measured (by means of a small flush-mounted microphone) on a half-scale EBF model, at a point near the axis of a cold jet (at X/D = 9, with $U_L \approx 750$ fps, pressure ratio 1.4) is shown in Fig.16, together with an estimate based on Eqs. (5), (7), (10) and on Fig. 3. Considering the courseness of the various approximations that underlie this estimate, the agreement between it and the data is quite reasonable.

Estimation on Basis of Boundary Layer Flow

Turbulent boundary layer pressures. – The foregoing estimation approach was based on the assumption of momentum annihilation, and thus in essence assumed flow impingement essentially normal to the flap surface. However, since at least at some locations on the flap the flow is essentially parallel to the surface (see Fig. 17), it is useful to consider a model of the fluctuating pressure on an EBF that resembles that for a turbulent boundary layer.

Extensive data on pressure fluctuations produced at the surface of a flat plate by a jet impinging at various angles are reported in Ref. 5. Figures 5 and 6 reproduce some of this non-dimensionalized data, showing how the root-mean-square pressure $\sqrt{\overline{p^2}}$ varies along the plate surface. One may observe that for fixed X/D and θ the mean-square pressure $\overline{p^2}$ varies slowly with the distance x along the plate, indicating that the fluctuating pressure field is spatially inhomogeneous to a slight extent. As evident from Fig. 6, this inhomogeneity decreases at increasing distances X from the jet exit plane.

From Figs. 5 and 6 one may find that $\sqrt{\overline{p^2}}/q \approx 0.1$ provides an upper bound for boundary layer pressures on typical EBF configurations ($\theta \approx 30°$, X/D = 9). From Eq. (8), on the other hand, one finds that for normally impinging flow (with I = 0.11), $\sqrt{\overline{p^2}}/q \approx 0.44$.

Examination of data of Ref. 5 pertaining to the frequency spectra of fluctuating pressures on the surface of the test plate (see Fig. 5 for test geometry) indicates that the normalized frequency spectrum $\Phi_n(\omega)$ of the fluctuating pressures for the turbulent boundary layer case has the same shape as that for the normal impingement case. Thus, one may estimate that the spectral

where

$$q = \frac{1}{2} \rho U_o^2 \tag{8a}$$

denotes the dynamic pressure at the jet exit and

$$I = \sqrt{u^2}/U_o \tag{8b}$$

represents the axial component of the turbulence intensity on the axis at the axial distance X of interest. Figure 3 shows how I varies with X; note that for the typical location X/D = 9 for an EBF, one finds I ≈ 0.11.

Normalized correlations and frequency spectrum. – From Eqs. (1) and (6) one finds that the *normalized* time-correlations of pressure and velocity obey

$$\frac{\phi_p(0,\tau)}{\phi_p(0,0)} = \frac{\phi_u(0,\tau)}{\phi_u(0,0)} = e^{-|\tau|/T_f} \tag{9}$$

The normalized frequency spectrum $\Phi_n(\omega)$ is the Fourier transform of the normalized correlation, so that the normalized frequency spectrum of pressure (or velocity) obeys*

$$\Phi_n(\omega) = \frac{1}{2\pi} \int e^{-|\tau|/T_f} e^{i\omega\tau} d\tau = \frac{T_f/\pi}{1 + \omega^2 T_f^2} \tag{10}$$

Wavenumber-frequency spectrum. – The general space-time correlation $\phi_p(\underline{x},t)$ is closely related to the corresponding wavenumber-frequency spectrum $\phi_p(\underline{k},\omega)$, where $\underline{x} = (x,y)$ is a two-dimensional position vector (representing the Cartesian coordinates x and y of the observation point in the plane of the flap and $\underline{k} = (k_x,k_y)$ is the corresponding wavenumber vector. For spatially homogeneous and temporally stationary fields (Ref. 29),

---

*Unless otherwise indicated, all integrations are to be taken from negative to positive infinity.

Estimation on Basis of Momentum Flux

Pressure-momentum relation. — At any given location in the jet, the axial momentum flux may be written as $\rho(U + u)^2$ in terms of the fluid density ρ, the mean axial velocity U and the fluctuating axial velocity u at the location of interest. If this momentum flux is entirely annihilated as the jet impinges on the EBF surface, then the fluctuating component p of the pressure acting on the surface is of the order of the fluctuating component of the momentum flux. Thus, for the usual case where the fluctuating velocity component is much smaller than the steady component ($u << U$), one obtains

$$p \approx 2\rho u U \ . \qquad (1)^*$$

Cross-correlations. — The cross-correlation $\phi_{p_1 p_2}(\tau)$ of the pressures p_1 and p_2 at two different locations on the flap, defined as

$$\phi_{p_1 p_2}(\tau) = < p_1(t) p_2(t + \tau) >$$

thus is related to the corresponding velocity cross-correlation

$$\phi_{u_1 u_2}(\tau) = < u_1(t) u_2(t + \tau) >$$

as

$$\phi_{p_1 p_2}(\tau) = 4\rho^2 U_1 U_2 \phi_{u_1 u_2}(\tau) \ . \qquad (2)$$

In the above expressions, the brackets <...> denote averaging with respect to time t; τ represents a time interval, and U_1 and U_2 denote the mean velocities at the two locations of interest.

In order to obtain some simple estimates readily, it is convenient to consider locations near the jet axis (i.e., near point A of Fig. 2) in a plane normal to that axis. Data for the velocity correlation $\phi_{u_1 u_2}(0)$ for this special case (Refs. 27,28)

---

*For the sake of simplicity, new equation numbering sequences are begun in each appendix. All equation numbers mentioned in this appendix refer to equations presented in this appendix.

that are closely related to those whose fatigue data were used in development of the technique, its reliability is much reduced for other structures. Accumulation of a more extensive data base is recommended, particularly for the types of configurations and materials likely to be used for future externally blown flaps.

Because of the great potential utility of the space-time spectral density approach, it is recommended that application of this approach to EBF and related problems be pursued vigorously, both in relation to characterization of the fluctuating pressures produced by the impingement of engine exhaust on flap surfaces and in relation to the estimation of structural response spectra.

$$M_2 + F_{y2}P - F_{x2}Q = I_2\ddot{\theta}_2 + k_{\theta(2,0)}(\theta_2-\theta_0) + k_{\theta(2,1)}(\theta_2-\theta_1) + k_{\theta(2,3)}(\theta_2-\theta_3)$$

$$-k_{x(2,0)}[x_2-K-J\theta_2][J-K\theta_2] - k_{y(2,0)}[y_2+J-K\theta_2][K+J\theta_2]$$

$$-k_{x(2,1)}[x_2 - x_1 - G - N - H\theta_1 - L\theta_2][L - N\theta_2]$$

$$+k_{y(2,1)}[y_2 - y_1 + H + L - G\theta_1 - N\theta_2][N + L\theta_2]$$

$$+k_{x(2,3)}[x_2 - x_3 + R + U + S\theta_2 + T\theta_3][S - R\theta_2]$$

$$+k_{y(2,3)}[y_2 - y_3 - S - T + R\theta_2 + U\theta_3][R + S\theta_2]$$

$$F_{x3} = m_3\ddot{x}_3 + k_{x(2,3)}[x_2 - x_3 + R + U + S\theta_2 + T\theta_3]$$

$$F_{y3} = m_3\ddot{y}_3 + k_{y(2,3)}[y_3 - y_2 + S + T - R\theta_2 - U\theta_3]$$

$$M_3 - F_{y3}W - F_{x3}V = I_3\ddot{\theta}_3 + k_{\theta(3,2)}(\theta_3 - \theta_2)$$

$$-k_{x(3,2)}[x_3 - x_2 - R - U - S\theta_2 - T\theta_3][T - U\theta_3]$$

$$-k_{y(3,2)}[y_3 - y_2 + S + T - k\theta_2 - U\theta_3][U + T\theta_3]$$

$$F_{x3} = m_3\ddot{x}_3 + k_{x(3,2)}[\xi_3 - \xi_2]_{(3,2)}$$

$$F_{y3} = m_3\ddot{y}_3 + k_{y(3,2)}[\eta_3 - \eta_2]_{(3,2)}$$

$$M_3 + F_{y3}(-W) - F_{x3}V = I_3\ddot{\theta}_3 + k_{\theta(3,2)}(\theta_3 - \theta_2)$$

$$-k_{x(3,2)}[\xi_3 - \xi_2]_{(2,0)}\ [T\cos\theta_3 - U\sin\theta_3]$$

$$+k_{y(3,2)}[\eta_3 - \eta_2]_{(2,0)}\ [-U\cos\theta_3 - T\sin\theta_3]$$

where

$$[\xi_1 - \xi_0]_{(1,0)} = x_1 + (-C)\cos\theta_1 - B\sin\theta_1$$

$$[\eta_1 - \eta_0]_{(1,0)} = y_1 + 3\cos\theta_1 + (-C)\sin\theta_1$$

$$[\xi_1 - \xi_2]_{(1,2)} = x_1 - x_2 + G\cos\theta_1 + N\cos\theta_2 + H\sin\theta_1 + L\sin\theta_2$$

$$[\eta_1 - \eta_2]_{(1,2)} = y_1 - y_2 - H\cos\theta_1 - L\cos\theta_2 + G\sin\theta_1 + N\sin\theta_2$$

$$[\xi_2 - \xi_0]_{(2,0)} = x_2 + K\cos\theta_2 - U\sin\theta_2$$

$$[\eta_2 - \eta_0]_{(2,0)} = y_2 + J\cos\theta_2 - K\sin\theta_2$$

$$[\xi_2 - \xi_1]_{(2,1)} = -[\xi_1 - \xi_2]_{(1,2)}$$

$$[\eta_2 - \eta_1]_{(2,1)} = -[\eta_1 - \eta_2]_{(1,2)}$$

$$[\xi_2 - \xi_3]_{(2,3)} = x_2 - x_3 + R\cos\theta_2 + U\cos\theta_3 + S\sin\theta_2 + T\sin\theta_3$$

$$[\eta_2 - \eta_3]_{(2,3)} = y_2 - y_3 - S\cos\theta_2 - T\cos\theta_3 + R\sin\theta_2 + U\sin\theta_3$$

$$[\xi_3 - \xi_2]_{(3,2)} = -[\xi_2 - \xi_3]_{(2,3)}$$

$$[\eta_3 - \eta_2]_{(3,2)} = -[\eta_2 - \eta_3]_{(2,3)}$$

$X_{1(0,1)} = -C$ $\quad$ $X_{2(0,2)} = -K$ $\quad$ $X_{3(2,3)} = -U$

$Y_{1(0,1)} = B$ $\quad$ $Y_{2(0,2)} = J$ $\quad$ $Y_{3(2,3)} = T$

$X_{1(1,2)} = G$ $\quad$ $X_{2(1,2)} = -N$ $\quad$ $X_{a3} = -W$

$Y_{1(1,2)} = D$ $\quad$ $Y_{2(1,2)} = L$ $\quad$ $Y_{a3} = V$

$X_{a1} = D$ $\quad$ $X_{2(2,3)} = R$

$Y_{a1} = E$ $\quad$ $Y_{2(2,3)} = -S$

$X_{a2} = P$

$Y_{a2} = Q$

Equations of Motion. — The equations of motion for this configuration then may be written as

$$F_{x1} = m_1\ddot{x}_1 + k_{x(1,0)}[\xi_1 - \xi_0]_{(1,0)} + k_{x(1,2)}[\xi_1 - \xi_2]_{(1,2)}$$

$$F_{y1} = m_1\ddot{y}_1 + k_{y(1,0)}[\eta_1 - \eta_0]_{(1,0)} + k_{y(1,2)}[\eta_1 - \eta_2]_{(1,2)}$$

$$\begin{aligned} M_1 + F_{y1}D - F_{x1}E = {} & I_1\ddot{\theta}_1 + k_{\theta(1,0)}[\theta_1 - \theta_0] + k_{\theta(1,2)}[\theta_1 - \theta_2] \\ & - k_{x(1,0)}[\xi_1 - \xi_0]_{(1,0)}[B\cos\theta_1 - C\sin\theta_1] \\ & - k_{x(1,2)}[\xi_1 - \xi_2]_{(1,2)}[-H\cos\theta_1 + G\sin\theta_1] \\ & + k_{y(1,0)}[\eta_1 - \eta_0]_{(1,0)}[-C\cos\theta_1 - B\sin\theta_1] \\ & + k_{y(1,2)}[\eta_1 - \eta_2]_{(1,2)}[G\cos\theta_1 + H\sin\theta_1] \end{aligned}$$

$$M_n + F_{yn}X_{an} - F_{xn}Y_{an} = I_n\ddot{\theta}_n + k_{\theta(n,n-1)}\left(\theta_n - \theta_{n-1}\right)$$

$$+ k_{\theta(n,n+1)}\left(\theta_n - \theta_{n+1}\right) + \cdots$$

$$- k_{x(n,n-1)}\left|\xi_{(n)} - \xi_{(n-1)}\right|_{(n,n-1)}\left|Y_{n(n,n-1)}\cos\theta_n + X_{n(n,n-1)}\sin\theta_n\right|$$

$$- k_{x(n,n+1)}\left|\xi_{(n)} - \xi_{(n+1)}\right|_{(n,n+1)}\left|Y_{n(n,n+1)}\cos\theta_n + X_{n(n,n+1)}\sin\theta_n\right| + \cdots$$

$$+ k_{y(n,n-1)}\left|\eta_{(n)} - \eta_{(n-1)}\right|_{(n,n-1)}\left|X_{n(n,n-1)}\cos\theta_n - Y_{n(n,n-1)}\sin\theta_n\right|$$

$$+ k_{y(n,n+1)}\left|\eta_{(n)} - \eta_{(n+1)}\right|_{(n,n+1)}\left|X_{n(n,n+1)}\cos\theta_n - Y_{n(n,n+1)}\sin\theta_n\right| + \cdots$$

(98b)

Here m_n represents the mass of the nth flap element, and I_n denotes the moment of inertia of that element about its center of gravity. F_{xn} and F_{yn} denote the unsteady components of the aerodynamic force acting on the nth element in the x and y coordinate directions, respectively, and M represents the aerodynamic moment. Furthermore $k_{x(n,s)}$ represents the stiffness of the spring, in the x direction, connecting the nth and sth elements; $k_{y(n,s)}$ represents the stiffness of the corresponding spring acting in the y direction; $k_{\theta(n,s)}$ denotes the (rotational) stiffness of the rotational spring connecting these two elements. Also, if one lets $\xi_{(n)(n,s)}$ and $\eta_{(n)(n,s)}$ represent the x and y displacement components of that attachment point between the nth and sth elements which is located in the nth element, one finds from Eqs.(97) that one may write

$$\xi_{(n)(n,s)} = x_n + X_{n(n,s)}\cos\theta_n - Y_{n(n,s)}\sin\theta_n$$

$$\eta_{(n)(n,s)} = y_n + Y_{n(n,s)}\cos\theta_n + X_{n(n,s)}\sin\theta_n \qquad (99)$$

GENERAL TWO-DIMENSIONAL EQUATIONS OF MOTION OF MULTI-ELEMENT FLAP SYSTEM

Idealization

Masses and Springs. – In order to idealize a multi-element flap system as a two-dimensional (planar) dynamic system, it is convenient to consider each flap element (consisting of airfoil, guide-rails, and supporting structures) as a rigid body, and to take each such rigid body as connected to each other body at a single point by one set of springs – each set consisting of a single spring acting in the x-direction, one acting in the y-direction, and one acting rotationally. Thus, the flap system, as modeled in two dimensions, reduces to an array of planar rigid bodies interconnected by springs, as shown in Fig. 10. A schematic representation of the interconnecting springs is shown in the lower part of that figure.

One may obtain the spring constants (analytically or experimentally) and the effective attachment point locations by disconnecting all attachments except the one of interest, holding all bodies fixed except the one of interest, applying a force or moment, and observing the resulting displacements.

Coordinates Attached to Flap Elements; Notation. – It is convenient to select a Cartesian coordinate system attached to each flap element, with the origin of this system located at the element's center of gravity, and with the system's X-axis aligned parallel to the x-axis of an inertial reference system (attached to the wing) when the flap is in its static equilibrium configuration. This coordinate system serves to locate the various force-application points (i.e., the aerodynamic force locations and the interaction spring attachment points) on the element with respect to the element's center of gravity. Figure 11 shows the coordinate system on a typical flap element and indicates the notation used in the present analysis.

Equations of Motion

Displacement of General Point on Flap Element. – One may readily find (see Fig. 12) that a typical point P, whose coordinates are (X,Y) in the system attached to the nth flap, is

and from Eqs. (55) and (81) one may determine that for $f >> f_T$,

$$\frac{\eta_1 r\, \sigma_{ref}^2}{c_f \phi_p(f_1)} \approx 4.8\, \eta_1 \left(\frac{\sigma_{ref}}{q_o}\right)^2 \left(\frac{r}{L}\right)^3 \left(\frac{X}{L}\right)\left(\frac{c_f}{U_o}\right) \quad . \tag{96}$$

For typical orders of magnitude for the various parameters, one finds that

$$\left(\frac{\sigma_{ref}}{q_o}\right)^2\left(\frac{r}{L}\right)^3\left(\frac{X}{L}\right)\left(\frac{c_f}{U_o}\right) \approx \left(\frac{10^3}{2}\right)^2\left(\frac{1}{30}\right)^3(1)\left(\frac{5}{1}\right) \approx 46$$

so that, taking the middle value of B from Eq. (73),

$$\frac{T_h}{T_f} \approx \frac{2.6\times10^{11}}{3.4\times10^{9}} (15)^{2.99} (50)^{4.06} (1)^{10.6} \left(\frac{1}{10^3}\right)^{7.05} [(4.8)10^{-2}(46)]^{1.495}$$

$$\approx 4.6\times10^{-9} \quad .$$

Thus, one generally would expect core shear fatigue failures to occur long before facing sheet failures.* In designing a flap element it thus appears logical first to select a core that has the required fatigue life, and then to verify that the facing sheet will endure at least for the same time span.

Tables III and IV, which have been derived from the parts of Eqs. (92) and (94) that pertain to flap elements with high natural frequencies, indicate the factors by which the facing-sheet and honeycomb-core fatigue lives change as the result of changes in the various structural and jet parameters. Clearly, the one most significant structural parameter is the unsupported span length L; a mere 10% decrease in L may be expected to increase the fatigue life of the skin by a factor of about 4.5, and that of the core by about 3.6.

---

*No comparable experimental data appear to be available. Such data as are available (Ref. 9) pertain to panels, rather than beams, and are affected by stress raisers (e.g., fasteners) that reduce the skin fatigue life.

Equations (90) and (91) exhibit all structural parametric dependences for the low-frequency case, where $\Phi_p(f_1)$ is essentially independent of frequency. But, since $\Phi_p(f_1)$ does vary significantly at the higher frequencies, the aforementioned equations need to be modified. If one substitutes for $\Phi_p(f)$ from Eq. (81) and again uses Eq. (55) with $\alpha_1 = 2.36$, one obtains

$$\frac{T_f}{10^5 \sigma_{ref}^{4.06} B_1} \approx \begin{cases} 31 \left(\frac{\mu^{1.515} B^{2.545} \eta^{2.03}}{L^{6.12} (ecE)^{4.06}} \right) \left(\frac{1}{X^{2.03} \rho_o^{4.06} U_o^{6.09}} \right) & \text{for } f << f_T \\ 1.45 \left(\frac{B^{4.575} \eta^{2.03}}{\mu^{0.515} L^{14.24} (ecE)^{4.06}} \right) \left(\frac{X^{2.03}}{\rho_o^{4.06} U_o^{10.15}} \right) & \text{for } f >> f_T \end{cases} \tag{92}$$

As previously, the first set of parentheses in each expression encloses the structural parameters, the second the jet parameters.

Core. – By substitution of the cycles-to-failure relation of Eq. (76) and the natural frequency expression of Eq. (55), again using $\alpha_1 = 2.36$, into the fatigue life equation, Eq. (77), and by using also the stress expressions of Eqs. (68) and (69), one may find that the honeycomb core fatigue life T_h obeys

$$T_h/9.3 \times 10^{13} \approx L^2 \left(\frac{\mu}{B} \right)^{2.26} \left(\frac{d}{d_{ref}} \right)^{10.6} \left[\frac{A \tau_{ref}}{e} \sqrt{\frac{\eta_1}{\Phi_p(f_1)}} \right]^{7.05} \tag{93}$$

$$\approx \left(\frac{L^2}{c_f r} \right) \left(\frac{d}{d_{ref}} \right)^{10.6} \left(\frac{A}{er} \right)^{7.05} \left(\frac{r \eta_1 \tau_{ref}^2}{c_f \Phi_p(f_1)} \right)^{3.525} .$$

The second form of this expression involves the parameters introduced after Eq. (90) and is presented here in order to demonstrate the dimensional consistency of this result.

given engine also are likely to have only minor significance. On the other hand, the exit velocity U_o is of great importance; a mere 10% increase in this velocity can reduce the panel fatigue life to about one-third of its original value.

Table II is analogous to Table I, but pertains to stringers. From Table II, which is based on the part of Eq. (87) that applies for $f >> f_T$, one may observe, for example, that doubling of the panel edge length a (which is also equal to the spacing between the stringers) increases the stringer fatigue life by a factor of 1.91, whereas doubling the stringer length b reduces the fatigue life to 0.47 of its former value.

By comparing Eqs. (83) and (87) or Tables I and II one finds that the panel fatigue life is much more sensitive to parameter changes than is the stringer fatigue life. It is also evident that increases in h and c_L, as well as decreases in a, serve to increase the panel fatigue life, while they result in reductions in the stringer fatigue life.

From Eqs. (80) and (86) one may determine that the ratio of panel to stringer fatigue life obeys

$$\frac{T}{T_s} \approx 230 \left(\frac{B}{B_s}\right)\left(\frac{h}{a}\right)^{4.60}\left(\frac{Hb^2h}{I}\right)^{0.548}\left(\frac{h\eta\sigma_{ref}^2}{c_L\Phi_p(f)}\right)^{2.026} \tag{88}$$

If one introduces $\Phi_p(f)$ as given by Eq. (81) for $f >> f_m$, if one substitutes for f from Eq. (79), and if one takes $I \approx H^3h/2$ (which corresponds to an I-beam of height and flange width H, with flange thickness h), one finds that one may approximate the above expression by

$$\frac{T}{T_s} = 81 \left(\frac{B}{B_s}\right)\left(\frac{h}{a}\right)^{10.672}\left(\frac{b}{H}\right)^{1.096}\left[\left(\frac{\sigma_{ref}}{q_o}\right)^2\left(\frac{X}{a}\right)\left(\frac{c_L}{U_o}\right)\cdot\eta\right]^{2.026} \tag{89}$$

for the purpose of making order-of-magnitude estimates. Substitution of the middle values of B and B_s given in Eqs. (44) and (53) and of typical orders of magnitude of the various ratios then leads to

$$\sigma_b \approx 0.014 \frac{Hb^2}{I} \sqrt{\frac{hc_L \Phi_p(f)}{\eta}} \quad . \tag{84}$$

The "theoretical" maximum stress given by Eq. (48), however, must be corrected according to Eq. (49), if one desires a better representation of the actual (experimentally observed) maximum stress σ_e. Substitution of Eq. (84) into (49) indicates that that stress obeys

$$\frac{\sigma_e}{\sigma_{ref}} \approx 1.5 \left[\frac{Hb^2}{I \sigma_{ref}} \sqrt{\frac{hc_L \Phi_p(f)}{\eta}} \right]^{1/5} , \tag{85}$$

where $\sigma_{ref} = 10^3$psi, as before.

By combining Eqs. (85), (79), (52) and (54) one obtains the stringer fatigue life T_s as

$$T_s \approx 0.48 B_s \left(\frac{a^2}{hc_L}\right)\left(\frac{I}{Hb^2h}\right)^{0.548} \left(\frac{h\eta\sigma_{ref}^2}{c_L \Phi_p(f)}\right)^{0.274}$$

$$= 0.48 B_s \frac{a^2}{(hc_L)^{1.274} b^{1.096}} \left(\frac{I\sigma_{ref}}{H}\right)^{0.548} \left(\frac{\eta}{\Phi_p(f)}\right)^{0.274} \tag{86}$$

where the first form again groups the parameters to display the dimensionless correctness and the second shows the parametric dependences more clearly.

If one again uses Eq. (81) to account for the dependence of $\Phi_p(f)$ on the panel resonance frequency f, which frequency again may be approximated by Eq. (79), one may find that

DEPENDENCE OF FATIGUE LIFE ON JET AND STRUCTURAL PARAMETERS

Skin-Stringer Flaps

Skin Panels. — In order to display typical parametric dependences conveniently, it is useful to focus on commonly used skin-stringer configurations that have aspect ratios $b/a > 2.5$. For such configurations, the function $F(b/a)$ of Eq. (32) may be approximated by $\sqrt{3}(b/a)$ and the function $G(b/a)$ of Eq. (36) may be taken as equal to 0.69.

If one takes the maximum panel stress to be given by Eq. (39), with the coefficient 1.18 replaced by 0.90 in accordance with the discussion presented after Eq. (41), then one finds by use of the above indicated approximations that

$$\sigma \approx 0.395 \left[\frac{c_L a^2 \Phi_p(f)}{h^3 \eta}\right]^{1/2} \tag{78}$$

and that the fundamental natural frequency of the skin panel obeys

$$f \approx 0.69\, h c_L / a^2 \ . \tag{79}$$

Substitution of Eq. (78) into (45), and substitution of the result and of Eq. (79) into Eq. (47) yields the following expression for the panel fatigue life:

$$\begin{aligned} T &\approx 110\, \frac{Bh}{c_L} \left(\frac{h}{a}\right)^{2.60} \left(\frac{h\eta\sigma_{ref}^2}{c_L \Phi_p(f)}\right)^{2.30} \\ &= 110\, B\, \frac{h^{5.90}}{a^{2.60}\, c_L^{3.30}} \left(\frac{\eta\sigma_{ref}^2}{\Phi_p(f)}\right)^{2.30} \ . \end{aligned} \tag{80}$$

The first form of this equation groups the parameters in a manner that displays its dimensional correctness, whereas the second form indicates the parametric dependences more directly.

Core. — Only very few core shear fatigue failure data points appear to be available; the data do not suffice for regression analysis, and thus one can not establish confidence limits.

Perhaps the best one can do at present is to accept the design data indicated in Fig. 86 of Ref. 9, although the basis for that figure is not indicated. From the curves in that figure one may deduce the following relation between the number of cycles N_h that will induce failure in 5052-H39 aluminum alloy honeycomb core, the maximum rms core shear stress τ, and the core density d:

$$\log N_h = 12.76 - 7.05 \log\left(\frac{\tau}{\tau_{ref}}\right) + 10.58 \log\left(\frac{d}{d_{ref}}\right) \qquad (75)$$

or

$$N_h \approx 5.7 \times 10^{12} \left(\frac{\tau}{\tau_{ref}}\right)^{-7.05} \left(\frac{d}{d_{ref}}\right)^{10.6} . \qquad (76)$$

Here τ_{ref} = 1 psi is a reference value of shear stress and d_{ref} = 1 lb/ft^3 is a reference value of density.

Since not enough data are available for the determination of confidence limits, it appears reasonable to assume that the foregoing expressions pertain to the 0% confidence limit. In order to estimate the numbers of cycles to failure corresponding to the -50% and -95% confidence limits (probably conservatively), one may mutliply the value of N_h obtained from Eqs. (75) or (76) by 0.4 and 0.1, respectively.*

The honeycomb fatigue life T_{hC} corresponding to the confidence limit C, of course, may be calculated from

$$T_{hC} = N_{hC}/f_1 . \qquad (77)$$

---

*These factors correspond approximately to the ratios of the constants in Eq. (53). The factors corresponding to Eqs. (46) and (73) are larger than those given here, hence would lead to less conservative estimates.

If one uses the geometric average (21.7/L) of the above values, in view of the uncertainty of the actual boundary conditions, one may rewrite Eq. (65) as

$$\sigma_1 \approx 0.69 \frac{ecE}{\mu L^2 f_1^{3/2}} \sqrt{\frac{\Phi_p(f_1)}{\eta_1}} \approx 0.19 \frac{ecEL}{(\mu B^3)^{1/4}} \sqrt{\frac{\Phi_p(f_1)}{\eta_1}} \quad , \tag{68}$$

where the latter expression was obtained by substitution of Eq. (55) with $\alpha_1 = 2.36$.

Maximum Root-Mean-Square Shear Stress in Core. – In Appendix B it is shown by means of an analysis that parallels that presented in Ref. 26 that, for a simply supported sandwich beam, the ratio of the maximum shear stress τ in the core to the maximum tensile stress in the skin obeys

$$\frac{\tau}{\sigma_1} = \frac{\pi B}{LAcE} \approx \pi \frac{t_s}{L} \tag{69}$$

where A represents the cross-sectional area of the beam. The approximate equality applies for a beam with a rectangular cross-section, with skin of thickness t_s; this approximate expression may suffice for the evaluation of a rough estimate in cases where not enough information is available to apply the more complete expression.

For beams with other than simply supported boundaries, the simple analytical approach of Appendix B does not work and results like the above cannot be obtained readily. It is therefore suggested that Eq. (69) be used for estimation purposes, regardless of what the boundary conditions are.

Loss Factors. – The available data pertaining to loss factors of honeycomb core sandwich structures are extremely limited. Reference 9 reports test results for about 30 different panels vibrating in their fundamental modes. Their loss factors were found to lie between about 0.03 and 0.05, and to be comparable to a value of about 0.04 measured on panels obtained from aircraft development programs.

In absence of more directly applicable data, an estimate of $\eta_1 = 0.04$ appears to be reasonable.

$$F_1(t) = \int_A p(x,t)\phi(x)dx = ep_0(t) \int_0^L \phi(x)dx \ , \qquad (59)$$

and with a modal stiffness

$$k_1 = (2\pi f_1)^2 M_1 \ . \qquad (60)$$

In the above expressions, $p(x,t)$ represents an arbitrary pressure distribution over the beam, $p_0(t)$ denotes a pressure that is spatially uniform, and e represents the beam width (see Fig. 9). Note that here M_1 is equal to the total mass of the beam.

For a simple spring-mass-dashpot system subject to random excitation, one finds that the root-mean-square displacement U_{rms} obeys (see Refs. 23, 24)

$$U_{rms} = \sqrt{\frac{\pi f_1 \Phi_F(f_1)}{2\eta_1 k_1^2}} \ , \qquad (61)$$

where Φ_F represents the spectral density of the force $F_1(t)$ and η_1 denotes the loss factor of the system, i.e., of the beam in its first mode. Since the spectral density Φ_F of the force is proportional to the mean-square force, Φ_F is related to the spectral density Φ_p of the pressure $p_0(t)$, in view of Eq. (59), as

$$\Phi_F = e^2 J_1^2 \Phi_p \ , \qquad (62)$$

where

$$J_1 = \int_0^L \phi(x)dx \ . \qquad (63)$$

Maximum Root-Mean-Square Stress in Skin. – For a given amount of beam flexure, the greatest skin tensile and compressive stresses occur in those fibers that are farthest from the beam's neutral surface. If c denotes the distance from the neutral surface to the farthest fiber (see Fig. 9), then one may write the maximum

FATIGUE LIFE OF HONEYCOMB-CORE SANDWICH FLAPS

Overview of Estimation Approach

The fatigue of flat, rectangular panels of honeycomb sandwich construction is discussed in Ref. 9 on the basis of classical thin-plate theory. Earlier data cited in that report indicate that this theory yields good approximations to observed vibration and stress responses associated with the fundamental panel mode, and that shearing of the core plays no important role, unless this core is very flimsy.

A flap element, however, may be expected to behave more like an end-supported beam than like an edge-supported panel. The analytical results available for panels thus do not apply to flap elements directly, although one may hope that honeycomb panel fatigue data will also be useful for honeycomb beam fatigue life estimation. The following paragraphs, therefore, first summarize a corresponding beam analysis and then apply related available fatigue data to develop a fatigue life estimation approach.

Beam Response

Resonance Frequency. — In order to simplify the analysis, it is useful as a first approximation to assume the fluctuating excitation pressure to be uniformly distributed over (one surface of) a flap element, and to consider only the response of the first mode of that element modeled as a uniform beam — in a similar manner somewhat analogous to that used in skin-stringer panel analyses or honeycomb sandwich panel analyses (Ref. 9).

The resonance frequency of the first mode of a beam is given (e.g., Ref. 22) by*

$$f_1 = \frac{\alpha_1}{L^2} \sqrt{\frac{B}{\mu}} \quad , \tag{55}$$

*This expression is based on the assumption that shear effects are negligible. As shown in Appendix B, the finite shear stiffness of a beam reduces its natural frequency, but in most practical cases this reduction is insignificant.

of cycles that a stringer survives before failing is related to the experimentally observed maximum rms stress σ_e in it according to

$$\log N_s = -2.74 \log\left(\frac{\sigma_e}{\sigma_{ref}}\right) + \log B_s \qquad (50)$$

where $\sigma_{ref} = 10^3$ psi is a reference stress value as before, and

$$\log B_s = \begin{Bmatrix} 6.98 \\ 7.57 \\ 7.94 \end{Bmatrix} \text{ for the } \begin{Bmatrix} -95\% \\ -50\% \\ 0\% \end{Bmatrix} \text{ Confidence limit .} \qquad (51)$$

Equations (50) and (51) may also be rewritten as

$$N_s = B_s(\sigma_e/\sigma_{ref})^{-2.74} , \qquad (52)$$

$$B_s = \begin{Bmatrix} 9.5 \times 10^6 \\ 3.7 \times 10^7 \\ 8.7 \times 10^7 \end{Bmatrix} \text{ for the } \begin{Bmatrix} -95\% \\ -50\% \\ 0\% \end{Bmatrix} \text{ Confidence limit .} \qquad (53)$$

The discussion and the relation between confidence limits and failure probability presented (in relation to panel failures) in the paragraphs following Eq. (46) apply equally well to stringer failures, as does the discussion of fatigue life. In analogy to Eq. (47), the stringer fatigue life T_{sC} corresponding to the -C% confidence limit obeys

$$T_{sC} = N_{sC}/f , \qquad (54)$$

where N_{sC} is found from Eq. (50) or (52) for the confidence limit of interest and f, it should be recalled, denotes the natural frequency of the *panel*.

4. Calculate N_C from Eq. (45) or (43), and find T_C from Eq. (47).

5. For materials other than 7075-T6 aluminum, multiply T_C by k_m from Appendix C.

Stringers

In typical skin-stringer structures, fatigue failures of stringers usually occur at the clip attachment (where the stringer is joined to the frame or bulkhead), because of the presence of stress raisers in that location. Because of the general complexity of the problem, little analytical work has been done on stringer fatigue, and since stringer failures generally occur in the interior of practical structures, there appears to exist no quantitative field data. Reference 7 contains the most definitive available analytical and experimental information; it is on that report that the following discussion is based.

Analytical estimate of maximum root-mean-square stress. — The analysis of stringer stresses presented in Ref. 7 is based on the following assumptions: (1) The total force acting on a stringer corresponds to the net shear force (integrated distribution minus corner reactions) that acts at the edge of a simply supported panel, which is deflecting in its first mode, in response to a pressure that is uniformly distributed over the panel, but varying randomly in time. (2) The force acting on a stringer is distributed uniformly along its length and acts on the rivet line. (3) The maximum stress in the stringer occurs in flexure at the clip attachment point, where the stringer is taken to be clamped with respect to bending.

With these assumptions one finds that the maximum root-mean-square stress in a stringer obeys*

$$\sigma_b = \frac{2^{3/2}}{3\pi^{7/2}} \frac{Hb_s^3}{I} \sqrt{\frac{f\Phi_p(f)}{\eta}} \left(\frac{b_s}{a_s} + \frac{a_s}{b_s} \right)^{-1} , \qquad (48)$$

where b_s denotes the stringer length (which is usually, but not necessarily always, the longer panel edge length), a_s the distance

*This relation follows from Eq. (67) of Ref. 7. However, there the numerical coefficient, which here is $2^{3/2}/3\pi^{7/2} \approx 0.0171$, was erroneously omitted.

It should be noted, however, that air flow along a panel may extract energy from the panel vibrations, and thus increase the effective structural loss factor — or that this flow may feed energy into panel vibrations (under conditions approaching panel flutter), and thus decrease the effective loss factor. At present there is available no means for estimating this effect, and one can do little better than to evaluate it on the basis of experimental measurements.

Cycles to failure; survival probability. — One may expect that the number of stress reversals a panel can withstand decreases as the stress amplitude increases. Related test data, corresponding to skin-stringer panels of 7075-T6 aluminum alloy exposed to random noise, are given in Fig. 34 of Ref. 9, together with curves representing various statistical confidence limits. Later test data (Ref. 7) were found to fall within these same confidence limits; the design nomographs given in Refs. 7 and 9 are based on these confidence limit curves.

From the curves of the above-mentioned Fig. 34 of Ref. 9 one may determine that the number N of cycles that a panel survives before failing is related to the maximum root-mean-square stress σ according to

$$\log N \approx -4.60 \log\left(\frac{\sigma}{\sigma_{ref}}\right) + \log B \ , \tag{43}$$

where $\sigma_{ref} = 10^3$ psi is a reference stress value, and

$$\log B = \begin{Bmatrix} 9.38 \\ 9.75 \\ 10.04 \end{Bmatrix} \text{ for the } \begin{Bmatrix} -95\% \\ -50\% \\ 0\% \end{Bmatrix} \text{ Confidence limits .} \tag{44}$$

Alternately, one may express the above relation as

$$N = B(\sigma/\sigma_{ref})^{-4.60} \tag{45}$$

with

$$B = \begin{Bmatrix} 2.4 \times 10^9 \\ 5.6 \times 10^9 \\ 10.8 \times 10^9 \end{Bmatrix} \text{ for the } \begin{Bmatrix} -95\% \\ -50\% \\ 0\% \end{Bmatrix} \text{ Confidence limit .} \tag{46}$$

1.18 of Eq. (39) indicates that the stress estimates one obtains by use of Eq. (41) on the average are about 30% lower than those one obtains on the basis of Eq. (39), and, similarly, to be about 20% lower than those one finds from Eq. (40).

It is important to note, however, that Eq. (41) was derived on the basis of experimental data (Ref. 9) on test panels with aspect ratios a/b between 1.0 and 3.0 only, so that the validity of this relation for larger aspect ratios remains uncertain. Furthermore, the test data points (see Fig. 69, p. 138 of Ref. 9) exhibit a good deal of scatter, with a large number of the points deviating considerably from the regression line. It thus is not clear whether the use of the somewhat more complex Eq. (41) is justified instead of Eq. (39) with a reduced coefficient that makes this equation correspond more closely to the available data for $b/a \leq 3.0$.

In view of the fact that Eq. (41) has gained some acceptance, has been reduced to nomograph form, and has been compared with some experimental data (though not well documented) other than that on the basis of which it was derived, it seems logical to retain it for stress estimation purposes. However, for the purpose of studying trends and parametric dependences, the simpler Eq. (39), with the coefficient 1.18 replaced by 0.90, is likely to be advantageous.

Maximum root-mean-square stress in curved panels. — On the basis of analytically developed expressions, in which empirically derived corrections have been included, the maximum root-mean-square stress σ_R (at the middle of the straight edge) in a cylindrically curved panel with radius of curvature R has been found (Ref. 9,7) to be related to the corresponding stress in a similar flat panel as

$$\frac{\sigma_R}{\sigma} = \left[\frac{f_R}{f}\right]^{-3/2}\left[1 + 0.453\left(\frac{b^2}{hR}\right)\left(\frac{A^2 + 0.034}{A^4 + 9.62A^2 + 1}\right)\right] , \qquad (42)$$

where, as before, $A = b/a$ = length of curved edge/length of straight edge and f/f_R is given by Eq. (37).

The applicability of this relation is limited to $0.3 \leq b/a \leq 3.0$, $a/h \geq 100$, and $a/R \leq 0.35$. On the whole, stress estimates for curved panels obtained on the basis of Eq. (42) or corresponding nomographs correlate more poorly with test data than do similar estimates for flat panels (e.g., see

Resonance frequencies of cylindrically curved panels. — The fundamental natural frequency f_R of a cylindrically curved panel with radius of curvature R is related to the natural frequency f of a flat panel with the same thickness h and edge dimensions as*

$$\frac{f_R}{f} \approx \left[1 + \frac{0.006(b^2/hR)^2}{A^4 + 0.61A^2 + 1}\right]^{1/2} , \tag{37}$$

where A = b/a, and a denotes the length of the flat edge of the panel, and b the length of its curved edge. The above relation was developed semi-empirically, on the basis of experimental data on structures with realistic boundary conditions, and is valid only for $h/a \leq 1/100$ and for aspect ratios in the range $0.3 < b/a < 3.0$, and for $a/R \leq 0.35$.

Maximum root-mean-square stress in flat panels. — In a simply supported panel, the maximum flexural stress associated with uniform loading or with the first vibratory mode occurs at the panel center. In a rectangular panel that is clamped on all edges, the corresponding maximum stress occurs at the middle of the longer edge. In practical skin-stringer structures, panel fatigue failures typically occur along the edges, at the rivet line or at the ends of stringer flanges or doublers (Refs. 9, 17); thus, the panel stress associated with fatigue corresponds more closely to the maximum stress in a clamped panel than to that in a simply supported panel.

The maximum flexural stress σ_o induced in a clamped panel with $b \geq a$ by a uniformly distributed static pressure of unit magnitude is given (Ref. 9) by

$$\sigma_{o\ max} = \frac{12}{\pi^2}\left(\frac{b}{h}\right)^2 F^{-2} , \tag{38}$$

where F = F(b/a) is given by Eq. (32).

If one substitutes the foregoing for σ_o into Eq. (29), and if one takes the natural frequency f to be equal to that for a clamped plate, one obtains the maximum rms stress as

$$\sigma = 1.185 \sqrt{\frac{c_L \Phi_p(f)}{a\eta}}\left(\frac{b}{h}\right)^{3/2} F^{-3/2} . \tag{39}$$

---

*This expression results from Ref. 9, if a misprint in that report is corrected (see Ref. 12). Note: The expression appearing in Ref. 7 also is obviously in error.

that they give results whose precision is much greater than necessary, in view of the considerable uncertainty in (1) the estimated pressure spectra, (2) the validity in any practical case of the assumptions involved in the development of Eq. (29), and (3) the boundary conditions operative in practical structures. Furthermore, fatigue data have been accumulated only for the lowest modes, so that application of this data to fatigue prediction for any given structure of a material or configuration different from those for which data is available, or to higher modes, is likely to introduce greater errors than those due to the use of simpler, less precise, resonance frequency estimates.

Many measurements of the random responses of panels (e.g., Refs. 6, 9–12) have shown these responses to be dominated by the fundamental panel mode. Data on realistic aircraft structures (e.g., Refs. 13, 14) and related analyses (summarized in Ref. 8) have indicated that the responses of skin-stringer configurations generally* are dominated by modes in which each panel vibrates in a fundamental mode corresponding to a boundary condition (at each edge) that lies between the fully clamped and the simply supported. It is therefore reasonable to focus on the fundamental panel mode, and to omit the more complex higher modes from consideration.

Reference 9 presents (on p. 224) a curve that summarizes the experimentally observed variation with aspect ratio of the fundamental resonance frequencies of rectangular panels of skin-stringer configurations. Although one may use this curve for estimation purposes, an analytic approximation to it will prove useful for determining how the fatigue life of the panel depends on the various parameters. Inspection of this curve, together with the corresponding curves for panels that are simply supported and for panels that are clamped on all four edges, reveals that the experimentally observed frequencies are very nearly equal to the geometric average of the resonance frequencies for the two ideal boundary condition cases.

The fundamental resonance of a simply supported panel of thickness h and edge lengths a and b is given by

---

*However, some data are available (Refs. 15, 16) which show that the fundamental panel mode response does not always predominate.